

SAMPLING SCHEMES FOR  
MULTIDIMENSIONAL NONBANDLIMITED SIGNALS

by  
PANCHAMKUMAR DILIPKUMAR SHUKLA

A Thesis submitted in fulfilment of requirements for the degree of  
Doctor of Philosophy of University of London and  
Diploma of Imperial College

Communications and Signal Processing Group  
Department of Electrical and Electronic Engineering  
Imperial College London  
University of London

2007

# Declaration

I declare that the content embodied in this thesis is the outcome of my own research work under the guidance of my thesis advisor Dr P. L. Dragotti. Any ideas or quotations from the work of other people, published or otherwise, are fully acknowledged in accordance with the standard referencing practices of the discipline. The material of this thesis has not been submitted for any degree at any other academic or professional institution.

-----  
P. D. Shukla

-----  
Date

# Abstract

Consider the problem of sampling signals that are nonbandlimited but have finite number of degrees of freedom per unit of time and call this number the rate of innovation. Streams of Diracs and piecewise polynomials are the examples of such signals, and thus are known as signals with finite rate of innovation (FRI) [87]. We know that the classical ('bandlimited-sinc') sampling theory does not allow perfect reconstruction of such signals from their samples since they are not bandlimited. However, the recent results on FRI sampling [28, 87] suggest that it is possible to sample and perfectly reconstruct such nonbandlimited signals using a rich class of sampling kernels.

In this thesis, we extend the sampling results of [28] into higher dimensions (i.e. in 2-D and above) using compactly supported kernels that reproduce polynomials (i.e. satisfy Strang-Fix conditions). The polynomial reproduction property of the kernel makes it possible to obtain the continuous-moments of the signal from its samples. By using these moments in the annihilating filter method (Prony's method), the innovative part of the signal, and therefore, the signal itself is perfectly reconstructed. In particular, we present local (directional derivatives based) and global (complex-moments, Radon transform based) sampling schemes for classes of FRI signals such as sets of 2-D Diracs, bilevel and planar polygons, quadrature domains (e.g. circles, ellipses, cardioids), 2-D polynomials with convex polygonal boundaries, and  $n$ -dimensional Diracs and bilevel-convex polytopes.

The sampling results of this thesis have been promisingly explored in super-resolution imaging [2] and distributed compression [31], and might find their applications in photogrammetry, computer graphics, and machine vision.

# Acknowledgment

First and foremost, I earnestly acknowledge my supervisor Pier Luigi Dragotti for his distinct role and unmatched support throughout my research and writing-up. I consider myself as one of the most fortunate PhD students who have received consistent and well planned research guidance through regular weekly meetings for all three years. Even during professional deadlines and personal pressures, Pier Luigi has always greeted me with energetic smiles and motivating dialogues which are hardly possible to forget. I have always felt being a special and important person to him. I am very much thankful to him for listening to me carefully, boosting my self-confidence, and progressively shaping up my research skills. He has provided almost all opportunities a PhD student would dream of. He has gone to great lengths to ensure that my work come to a satisfactory and timely conclusion. In addition to an excellent research advisor, Pier Luigi is one of the most valuable and adorable human beings I have ever met. He has made a noticeable difference to my visualization of the many faceted world around.

Amidst the usual stresses, these research years were quite enjoyable- thanks to many familiar faces and colleagues in the CSP group. In particular, I would like to acknowledge our subgroup members Nicolas Gehrig, Loic Baboulaz, Jesse Berent, Yizhou Wang (Eagle), and Varit Chaisinthop for their help in various ways. I will always remember close interactions with Loic at research as well as personal level. I owe him a great deal for taking care of my PC and data during out-of-campus writing-up and for his genuine concern on my timely completion of the thesis. Moreover, I thank Nikos Mitianoudis for useful technical interactions and reading my draft papers. I would also like to remember John (Yon) for his sense of humor and hilarious outbursts during afternoon tea-breaks. Mazie Paul and Glenys Benson were always there to provide the required administrative and infrastructural help.

The acknowledgement is incomplete without remembering the self-less support of my wife Krupa and my family members. In particular, I am ever indebted to Krupa for sacrificing her personal, social, and emotional privileges in fulfilling my research objectives. In the end, I dedicate this thesis to our baby boy: ‘Dhruv’ born on 17 Jan 2007- within a fortnight after submitting the thesis for viva!

# Contents

<b>Declaration</b>	<b>2</b>
<b>Abstract</b>	<b>3</b>
<b>Acknowledgment</b>	<b>4</b>
<b>Contents</b>	<b>5</b>
<b>List of Figures</b>	<b>8</b>
<b>List of Tables</b>	<b>12</b>
<b>List of Symbols</b>	<b>13</b>
<b>Chapter 1. Introduction</b>	<b>17</b>
1.1 Motivation, Background, and Scope . . . . .	17
1.2 Summary of the problem . . . . .	20
1.3 Thesis outline . . . . .	22
1.4 Original contribution . . . . .	23
<b>Chapter 2. Classical Sampling</b>	<b>26</b>
2.1 Introduction . . . . .	26
2.2 Shannon's sampling theory . . . . .	27
2.3 Extensions and Generalizations . . . . .	32
2.3.1 Papoulis's framework and other extensions . . . . .	32
2.3.2 Approximation for nonbandlimited signals . . . . .	33
2.3.3 Sampling in shift-invariant subspaces . . . . .	35

---

2.4	Summary . . . . .	39
<b>Chapter 3. Sampling Signals with Finite Rate of Innovation (FRI)</b>		<b>40</b>
3.1	Introduction . . . . .	40
3.2	1-D Sampling Framework . . . . .	42
3.2.1	Sampling setup . . . . .	42
3.2.2	FRI signals . . . . .	43
3.2.3	Sampling kernels . . . . .	45
3.2.4	Reconstruction algorithm . . . . .	48
3.2.5	Key results . . . . .	52
3.3	Multidimensional Framework . . . . .	56
3.4	Summary . . . . .	60
<b>Chapter 4. Directional Derivatives based Approach</b>		<b>62</b>
4.1	Introduction . . . . .	62
4.2	Local reconstruction of 2-D Diracs . . . . .	63
4.3	Planar polygons . . . . .	68
4.4	Summary . . . . .	75
<b>Chapter 5. Complex-moments based Approach</b>		<b>76</b>
5.1	Introduction . . . . .	76
5.2	Background and ‘sample-moment’ connection . . . . .	77
5.3	Global reconstruction of bilevel polygons . . . . .	79
5.4	2-D Diracs and Quadrature domains . . . . .	83
5.5	Summary . . . . .	89
<b>Chapter 6. Radon Transform based Approach</b>		<b>90</b>
6.1	Introduction . . . . .	90
6.2	Reconstruction of 2-D polynomials . . . . .	91
6.3	Real image experiment . . . . .	99
6.4	Summary . . . . .	101
<b>Chapter 7. Conclusion</b>		<b>103</b>
7.1	Thesis summary . . . . .	104
7.2	Discussion on practical issues . . . . .	105
7.3	Future scope . . . . .	107

Contents	7
Appendix A. Directional kernel	110
Bibliography	114

---

# List of Figures

- 2.1 Shannon's scheme for sampling and perfect reconstruction of bandlimited signals: The continuous signal  $g(t)$  is multiplied by a stream of Diracs  $\Delta_T(t) = \sum_{k \in \mathbb{Z}} \delta(t - kT)$  leading to a sampled signal  $g_s(t) = \sum_{k \in \mathbb{Z}} g(kT)\delta(t - kT)$ . The block C/D stands for continuous-to-discrete transformation and corresponds to the readout of sample values  $g_k = g(kT)$  from  $g_s(t)$ . The reconstructed signal  $\tilde{g}(t) = g(t)$  is obtained by interpolating the samples  $g_k$  with reconstruction filter  $h_r(t) = \frac{T}{T_c} \text{sinc}(t/T_c)$  which is an ideal lowpass filter with cutoff frequency  $\omega_c = \pi/T_c$  and gain  $T$ . . . . . 28
- 2.2 Sampling and perfect reconstruction in frequency domain: (a)  $\hat{g}(\omega)$  is the Fourier transform (FT) of input signal  $g(t)$ , (b)  $\hat{g}_s(\omega)$  is the FT of sampled signal  $g_s(t)$ , and  $\hat{h}_r(\omega)$  is the FT of reconstruction filter  $h_r(t)$  with cutoff frequency  $\omega_c$  and gain  $T$ , (c)  $\hat{\tilde{g}}(\omega)$  is the FT of reconstructed signal  $\tilde{g}(t) = g(t)$ . . . . . 30
- 2.3 Sampling and reconstruction of nonbandlimited signals in Shannon's framework: The continuous-time signal  $g(t)$  is first filtered by an ideal lowpass filter  $h_a(t)$  followed by the usual sampling and reconstruction scheme of Figure 2.1. However, in this case, the reconstruction is not perfect. . . . . 33
- 2.4 Nesting of subspaces:  $V_{\text{sinc}} \subset V_{\tilde{\varphi}} \subset L_2$ . Notice that the subspace  $V_{\text{sinc}}$  is also a shift-invariant subspace. The sampling procedure is viewed as a projection operator  $P_{\tilde{\varphi}} : L_2 \rightarrow V_{\tilde{\varphi}}$  that computes minimum error approximation  $\tilde{g}(t) = P_{\tilde{\varphi}} g(t)$  of the input signal  $g(t) \in L_2$  onto a shift-invariant subspace  $V_{\tilde{\varphi}}$ . . . . . 35
- 2.5 Three-step paradigm for sampling in shift-invariant subspaces  $V_{\tilde{\varphi}}$ : The prefilter  $h_a(t) = \varphi(-t)$  and postfilter  $h_r(t) = \tilde{\varphi}(t)$  are not necessarily ideal lowpass filters (sinc kernels) and they may or may not be related. However, both kernels span the shift-invariant subspace  $V_{\tilde{\varphi}}$ . The digital correction filter  $q_k$  is optional (e.g. it can be removed when  $g(t) \in V_{\tilde{\varphi}}$ , and  $\varphi(t)$  and  $\tilde{\varphi}(t)$  forms a biorthogonal (or orthogonal) pair). The filter  $q_k$  converts the samples  $s_k$  into the coefficients  $c_k = s_k * q_k$  for reconstructing the output signal  $\tilde{g}(t) = \sum_{k \in \mathbb{Z}} c_k \tilde{\varphi}(t - k)$ . The reconstruction is perfect when  $g(t) \in V_{\tilde{\varphi}}$ . 37

- 3.1 1-D FRI sampling setup: The continuous-time FRI signal  $g(t)$  is pre-filtered by the smoothing filter  $h_a(t) = \varphi(-t/T)$  and then sampled uniformly to obtain the samples  $s_k = \langle g(t), \varphi(t/T - k) \rangle$  (with  $T$  as sampling interval). The samples  $s_k$  are used to retrieve the degrees of freedom of the original signal  $g(t)$  using a nonlinear postfiltering block  $A$  (annihilating filter method). Note that  $g(t)$  is completely characterized by its degrees of freedom. The block  $C/D$  stands for continuous-to-discrete transformation and corresponds to the readout of samples  $s_k, k \in \mathbb{Z}$  from sampled signal  $g_s(t)$ . . . . . 42
- 3.2 Reconstruction algorithm: The samples  $s_k = \langle g(t), \varphi(t - k) \rangle$  are used to compute the useful values  $\sigma_n$  of form  $\sigma_n = \sum_{i=0}^{N-1} (u_i)^n w_i$ , where  $\{w_i, u_i\}$  are the free parameters (not necessarily the degrees of freedom) useful in characterizing the input FRI signal  $g(t)$ . The annihilating filter  $A_n$  is designed in such a way that the convolution  $A_n * \sigma_n = 0$ . The filter coefficients  $A_n$  and the values  $\sigma_n$  are then used to retrieve the parameters  $\{w_i, u_i\}$  by solving the systems of linear equations. . . . . 48
- 3.3 The 2-D FRI sampling setup: Continuous signal  $g(x, y)$  is convolved by a smoothing kernel  $\varphi(x, y)$  and then sampled uniformly by  $\sum_{j \in \mathbb{Z}} \sum_{k \in \mathbb{Z}} \delta(x - jT_x, y - kT_y)$  to obtain the sampled signal  $g_s(x, y)$ . The block  $C/D$  represents continuous to discrete transformation and corresponds to the read-out of sample values  $s_{j,k}, j, k \in \mathbb{Z}$  from  $g_s(x, y)$ . 58
- 4.1 A set of 2-D Diracs:  $g(x, y) = \sum_{i \in \mathbb{Z}} a_i \delta(x - x_i, y - y_i)$  . . . . . 63
- 4.2 Local reconstruction of a 2-D Dirac  $a_p \delta(x - x_p, y - y_p)$ : The B-spline sampling kernel  $\beta^3(x, y)$  that can reproduce polynomials up to degree 3 is given in part (a). The reproduction of polynomial of degree 0 (partition of unity) responsible for the determination of amplitude  $a_p$  is given in part (b), whereas the reproduction of polynomials of degree 1 along  $x$  and  $y$  directions responsible for the determination of coordinates  $x_p$  and  $y_p$  are given in part (c) and part (d) respectively. 64
- 4.3 The continuous model for local reconstruction of polygonal corner points: For a given planar polygon  $g(x, y)$ , a pair of two successive first order directional derivatives  $d_{\theta_1}^{(1)}[\cdot]$  and  $d_{\theta_2}^{(1)}[\cdot]$  decomposes a corner point  $A$  into a 2-D Dirac. . . . . 68
- 4.4 The map for computing two successive differences  $\mathcal{D}_{\theta_1}^{(1)}[\cdot]$  and  $\mathcal{D}_{\theta_2}^{(1)}[\cdot]$  on every pair of samples  $s_{j,k}$  arranged in accordance with the base lattice  $\Lambda$ . The first difference is computed along the lattice direction  $\vec{v}_1$  followed by the second difference along the direction  $\vec{v}_2$ . . . . . 70
- 4.5 Original and directional kernels: (a)  $\varphi(x, y)$  is a Haar scaling function with support  $1 \times 1$ , (b) Directional kernel  $\zeta_{\theta_1, \theta_2}(x, y)$  with support  $4 \times 4$  is related to the corner point of the polygon  $g(x, y)$  formed by the two sides with orientations  $\tan(\theta_1) = 2/1$  and  $\tan(\theta_2) = -1/2$ . . . . . 71

- 4.6 Simulation result for the local reconstruction of planar polygon: The original image of size  $2500 \times 2500$  pixels as given in part (a) consists of a triangle  $g(x, y)$  with three corner points  $A$ ,  $B$ , and  $C$  such that its sides  $AB$ ,  $BC$ , and  $CA$  are oriented at  $\tan(\theta_1) = 2$ ,  $\tan(\theta_3) = -\infty$ , and  $\tan(\theta_2) = -\frac{1}{2}$  respectively. The part (b) consists of the set of  $25 \times 25$  samples  $s_{j,k}$  is obtained by sampling  $g(x, y)$  with the Haar kernel  $\varphi(x, y)$  of size  $100 \times 100$  pixels. The set of new samples  $s'_{j,k}$  as shown in part (c) is obtained by computing two successive directional differences  $\mathcal{D}_{\theta_1}^{(1)}[\cdot]$  and  $\mathcal{D}_{\theta_2}^{(1)}[\cdot]$  (i.e. along the sides  $AB$  and  $AC$ ) on the original set of samples  $s_{j,k}$ . Note that the isolated group of samples in part (c) represents the corner point  $A$ . Similarly, the other two sets of differentiated samples  $s'_{j,k}$  with isolated corner points  $B$  and  $C$  are given in parts (d) and (e) respectively. Using the local reconstruction scheme of (4.9) and (4.10), the reconstructed corner points  $A$ ,  $B$ , and  $C$  (marked with +) are given in part (a). . . . . 74
- 5.1 Simulation result for the global reconstruction of bilevel-convex polygons: (a) The original image  $g(x, y)$  consists of three bilevel polygons: triangle, rectangle, and pentagon. (b) The set of samples  $s_{j,k} = \langle g(x, y), \varphi(x/T_x - j, y/T_y - k) \rangle$  produced by the inner product between  $g(x, y)$  and sampling kernel  $\varphi(x, y)$ . In this case, the sampling kernels is a B-spline  $\beta^7(x, y)$  of order 7 that can reproduce polynomials up to degree seven. (c) The sampled version of the pentagon. (d) Original pentagon and reconstructed corner points (marked with +). . . . . 82
- 5.2 Global reconstruction of 2-D Diracs: (a) The B-spline sampling kernel  $\varphi(x, y) = \beta^5(x, y)$  of support  $379 \times 379$  pixels that can reproduce polynomials up to degree  $2N - 1 = 5$ . (b) The input image  $g(x, y)$  of size  $3711 \times 3711$  pixels contains  $N = 3$  Diracs with amplitudes 10, 20, and 30 located at pixel positions (1100, 1300), (1500, 900), and (1500, 1300) respectively. (c) The low resolution version  $g(x, y) * \varphi(-x/T_x, -y/T_y)$  of the Diracs obtained by the convolution of  $g(x, y)$  with the smoothing kernel  $\varphi(x, y)$ . (d) The set  $50 \times 50$  of samples  $s_{j,k} = \langle g(x, y), \varphi(x/T_x - j, y/T_y - k) \rangle$  obtained by the uniform sampling of the low resolution version of part (c), where the sampling intervals  $T_x = T_y = 63$  pixels. . . . . 85
- 5.3 Reconstruction of the circle: (a) The original circle  $g(x, y)$  with center  $(x_c, y_c)$  and radius  $r$ . (b) The samples  $s_{j,k} = \langle g(x, y), \varphi(x/T_x - j, y/T_y - k) \rangle$  obtained by the kernel  $\varphi(x, y)$  that can reproduce polynomials up to degree one. . . . . 88

- 6.1 AFBP reconstruction: The polynomial  $g(x, y)$  of degree  $R - 1 = 0$  inside a convex polygon with  $N = 5$  corner points (i.e. bilevel pentagon) is shown in part (a). The Radon transform projection  $R_g(t, \theta)$  along an angle  $\theta = 0$  is shown in part (b). Note that  $R_g(t_i, \theta)$  is a single-valued line-integral at an arbitrary  $t = t_i$  within the support of  $R_g(t, \theta)$ . Since this projection  $R_g(t, \theta)$  is a piecewise polynomial of degree  $R = 1$ , the  $R + 1 = 2$ -nd order derivative can decompose it in a stream of differentiated Diracs  $d_t^{(2)} [R_g(t, \theta)]$  as shown in part (d). In this case  $d_t^{(2)} [R_g(t, \theta)]$  represents  $N$  Diracs with  $\hat{N} = N$  weights. . . . . 92
- 6.2 Simulation: The original 2-D polynomial  $g(x, y)$  of degree  $R - 1 = 0$  and the reconstructed corner points  $A$ ,  $B$ , and  $C$  (marked with +) are given in part (a). The set of samples  $s_{j,k}$  produced by the B-spline sampling kernel  $\beta^9(x, y)$  is given in part (b). The  $N + 1 = 4$  sets of differentiated samples  $s'_{j,k} = D_\theta^{(2)} [s_{j,k}]$  along four angles  $\theta = 0, \frac{\pi}{4}, \tan^{-1}(2)$ , and  $\frac{\pi}{2}$  are given in parts (c), (d), (e), and (f). The AFBP reconstruction of the corner points  $A$ ,  $B$ , and  $C$  is illustrated in part (g). . . . . 98
- 6.3 A real image experiment: As shown in part (a), the original 'Remote control' image  $g(x, y)$  of size  $2592 \times 1944$  pixels (along  $x$  and  $y$  directions respectively) is sampled using B-spline kernel  $\beta^3(x, y)$  of order 3 and support  $190 \times 190$  pixels. The raw set of  $41 \times 31$  samples  $s_{j,k}$  shown in part (b) is used to compute the 1st-order difference samples  $s'_{j,k} = \mathcal{D}_\theta^{(1)} [s_{j,k}]$  along  $\theta = 0$  and  $\frac{\pi}{2}$  as given in parts (c) and (d). Parts (e) and (f) contain the modified samples  $s_{j,k}^T = Thresh(s'_{j,k})$  after properly thresholding the raw difference samples  $s'_{j,k}$ . Finally, the back-projection reconstruction of the corner points is given in part (g) and is super-imposed on the original image in part (h). The accuracy of the reconstruction is within  $\pm 5$  pixels. . . . . 100

## List of Tables

7.1	Comparative summary . . . . .	103
-----	-------------------------------	-----

## List of Symbols

The key symbols and notations are defined as follows:

$g(t)$ : Continuous-time input signal in 1-D.

$\hat{g}(\omega)$ : Fourier transform of input signal  $g(t)$ .

$\tilde{g}(t)$ : Reconstructed version of signal  $g(t)$ .

$\hat{\tilde{g}}(\omega)$ : Fourier transform of reconstructed signal  $\tilde{g}(t)$ .

$\varphi(t)$ : Sampling kernel (or analysis function).

$\hat{\varphi}(\omega)$ : Fourier transform of sampling kernel  $\varphi(t)$ .

$\hat{\varphi}^{(R)}(\omega)$ :  $R$ -th order derivative of  $\hat{\varphi}(\omega)$ .

$T$ : Sampling interval.

$*$ : Convolution operator.

$\langle \cdot, \cdot \rangle$ : Inner-product operator.

$C/D$ : Continuous-to-discrete transformation (i.e. readout of sample values at every sampling interval).

$V_{\text{sinc}}$ : Bandlimited sinc space.

$V_{\tilde{\varphi}}$ : Shift-invariant subspace spanned by generating (or synthesis) function  $\tilde{\varphi}(t)$  and its uniform shifts.

$h_a(t)$ : Lowpass antialiasing filter or prefilter (i.e.  $h_a(t) = \varphi(-t/T)$ ).

$h_r(t)$ : Lowpass reconstruction filter.

$g_s(t)$ : Sampled signal (i.e. an impulse-train multiplied filtered (or unfiltered) version of  $g(t)$ ).

$s_k$ : Samples of input signal  $g(t)$  (i.e. the readout values of sampled signal  $g_s(t)$  at every sampling interval  $T$  defined by  $s_k = g_s(kT) = \langle g(t), \varphi(t/T - k) \rangle$ ,  $k \in \mathbb{Z}$ ).

$s_k^{(R)}$ :  $R$ -th order difference of samples  $s_k$ .

$c_k^n$ : Precomputed coefficients useful in reproduction of polynomials  $t^n$ ,  $n \in \mathbb{N}$ .

$\rho$ : Rate of innovation (i.e. number of degrees of freedom per unit time).

$\rho_\tau(t)$ : Local rate of innovation (i.e. number of degrees of freedom over a moving window of length  $\tau$  at time  $t$ ).

$\beta^N(t)$ : B-spline of order  $N$ .

$\mu_n$ : Geometric moments of 1-D signal of form  $\mu_n = \int g(t)t^n dt$ .

$\sigma_n$ : Computed values from samples  $s_k$  of form  $\sigma_n = \sum_{i=0}^N (u_i)^n w_i$ ,  $n = 0, 1, \dots, M-1$ , where  $w_i$  and  $u_i$  are free parameters (not necessarily the degrees of freedom).

$A(z)$ :  $z$ -transform of ‘annihilating filter’  $A_n$ ,  $n = 0, 1, \dots, N$ .

$a_{i,r} \delta^{(r)}(t - t_i)$ :  $r$ -th order differentiated Dirac at location  $t_i$  with weight  $a_{i,r}$ .

$g(x, y)$ : Continuous domain input signal in 2-D. Often used to represent 2-D signals with finite rate of innovation (FRI).

$\hat{g}(\omega_x, \omega_y)$ : Fourier transform of input signal  $g(x, y)$ .

$\rho_{xy}$ : Local rate of innovation in case of 2-D FRI signals (i.e. number of degrees of freedom over the window of size  $\tau_x \times \tau_y$ ).

$\varphi(x, y)$ : 2-D Sampling kernel.

$\hat{\varphi}(\omega_x, \omega_y)$ : Fourier transform of sampling kernel  $\varphi(x, y)$ .

$T_x$ : Sampling interval along  $x$ -axis.

$T_y$ : Sampling interval along  $y$ -axis.

$h_a(x, y)$ : 2-D Antialiasing or prefilter (i.e.  $h_a(x, y) = \varphi(-x/T_x, -y/T_y)$ ).

$s_{j,k}$ : Samples of signal  $g(x, y)$ , that is,  $s_{j,k} = \langle g(x, y), \varphi(x/T_x - j, y/T_y - k) \rangle$ ,  $j, k \in \mathbb{Z}$ .

$c_{j,k}^{\alpha,\beta}$ : Precomputed coefficients useful in reproduction of polynomials  $x^\alpha y^\beta$ ,  $\alpha, \beta \in \mathbb{N}$ .

$\delta(x - x_i, y - y_i)$ : A 2-D Dirac located at coordinate position  $(x_i, y_i)$ .

$d_\theta^{(R)}[\cdot]$ :  $R$ -th order directional derivative operator along the orientation  $\theta$  applied to continuous signal  $g(x, y)$ .

$\mathcal{D}_\theta^{(R)}[\cdot]$ :  $R$ -th order directional difference operator along the orientation  $\theta$  with  $\tan(\theta) \in \mathbb{Q}$  applied to samples  $s_{j,k}$ .

$\Lambda$ : 2-D integer lattice.

$V_\Lambda$ : Sampling matrix of lattice  $\Lambda$ .

$s'_{j,k}$ : Difference samples. In case of directional derivatives based approach (Chapter 4), the samples  $s'_{j,k}$  are computed by a pair of first order directional differences along orientations  $\theta_1$  and  $\theta_2$  in form of  $s'_{j,k} = \mathcal{D}_\theta^{(1)} \left[ \mathcal{D}_\theta^{(1)} [s_{j,k}] \right]$ . Whereas in case of Radon transform based approach (Chapter 6), the difference samples  $s'_{j,k}$  denote the  $(R + 1)$ -th order difference of samples  $s_{j,k}$  along a given orientation  $\theta$ , that is,  $s'_{j,k} = \mathcal{D}_\theta^{(R+1)} [s_{j,k}]$ .

$\beta_\theta^R(x, y)$ : 1-D B-spline of order  $R$  in  $xy$ -plane along orientation  $\theta$ .

$\zeta_{\theta_1, \theta_2}(x, y)$ : Directional kernel of form  $\zeta_{\theta_1, \theta_2}(x, y) = \frac{(\varphi(x, y) * \beta_{\theta_1}^0(x, y)) * \beta_{\theta_2}^0(x, y)}{|\sin(\theta_2 - \theta_1)|}$  in case of directional derivatives based approach (Chapter 4).

$\zeta_\theta(x, y)$ : Directional kernel of form  $\zeta_\theta(x, y) = |v|^{(R+1)} (\varphi(x, y) * \beta_\theta^R(x, y))$  in case of Radon transform based approach (Chapter 6).

$\mu_{\alpha,\beta}$ : Geometric moments of order  $(\alpha + \beta)$  defined by (5.1).

$\tau_{\alpha,\beta}$ : Complex-moments of order  $(\alpha + \beta)$  defined by (5.2).

$\tau_n$ : Simple complex-moments of order  $n$  defined by (5.3).

$\tau_n''$ : Weighted complex-moment with weight  $n(n - 1)$  given by  $\tau_n'' = n(n - 1)\tau_{n-2}$ ,  $\forall n \geq 2$ .

$\varrho_l$ : Complex coefficients in Section 5.3.

$\Omega$ : Closure of bounded planar domains (e.g. bilevel-convex polygons).

$z_l$ : Corner points of the polygon in complex plane  $z = x + iy$ .

$(\cdot)^*$ : complex-conjugate operator.

$R_g(t, \theta)$ : Radon transform projection of signal  $g(x, y)$  at angle  $\theta$ .

$d_t^{(R)}[R_g(t, \theta)]$ :  $R$ -th order derivative of Radon projection  $R_g(t, \theta)$ .

# Chapter 1

## Introduction

### 1.1 Motivation, Background, and Scope

Sampling is one of the fundamental elements of modern signal processing and communication systems. In fact, the problem of sampling is at the heart of the ‘application gamut’ in science, engineering, and technology. Starting from the early commercial and military applications (e.g. speech and radar communication), the process of sampling continues to affect our lives even more personally through personal communication (e.g. mobile phones), entertainment (e.g. MP3 music), new media (digital TV, multimedia, internet), and medical diagnostics (e.g. MRI). Although, the virtue of sampling allows us to monitor, process, store/transmit, or reconstruct the unprecedented amount of data (of real world activities) with increased convenience, the efficient sampling is vital in many applications such as sensor networks [3] and 3-D computed tomography [5]. In the era of data intensive applications (e.g. video streaming) and digitally immersive world (i.e. ubiquitous and pervasive communication), the research in sampling is even more relevant, rewarding, and challenging than before. In particular, the advances in sampling have demonstrated the important role played by sophisticated mathematics such

as harmonic analysis, approximation and optimization theory, wavelets and splines, spectral estimation, and sparse representations. An extensive tutorial on classical sampling theory and its various aspects is given in [41]. For a comprehensive account on modern sampling developments, we refer to [78, 84].

Formally, sampling is the process of representing a continuous-time signal  $g(t)$  by a discrete set of values  $g_k$ ,  $k \in \mathbb{Z}$ . If the time instances at which these values (samples) are taken are equidistant, that is,  $g_k = g(kT)$  for every  $T$  seconds, then the signal is uniformly sampled [63, 93]. Often, in practice, rather than having an access to the original signal  $g(t)$ , one has only access to its filtered (lowpass) version  $g(t) * h_a(t)$ , where  $h_a(t) = \varphi(-t/T)$  is an antialiasing filter or a sampling kernel. The filtered signal  $g(t) * \varphi(-t/T)$  is then uniformly sampled to obtain the samples  $s_k = g_s(kT)$  as given by:

$$s_k = g_s(kT) = \langle g(t), \varphi(t/T - k) \rangle = \int_{-\infty}^{\infty} g(t) \varphi(t/T - k) dt.$$

The key questions that arise with the sampling are:

- Is it possible to perfectly reconstruct the original signal  $g(t)$  from the set of samples  $s_k = g_s(kT)$ ?
- What should be the reconstruction algorithm?
- What type of sampling kernel  $\varphi(t)$  should be used?

The classical answer to these questions are given by the well known Shannon's sampling theorem [67, 68] which considers sampling and perfect reconstruction of bandlimited signals using 'sinc' kernel. In practice, the signals being sampled come from various sources and are often nonbandlimited. It is therefore customary to prefilter such signals using lowpass filter and make them bandlimited before being sampled. Shannon's sampling theory [67, 68] and its extensions [41] are very pow-

erful and have been extensively utilized in reconstructing bandlimited signals (or approximating nonbandlimited signals) from their samples. Moreover, Shannon's sampling theory is also extended to the classes of nonbandlimited signals that reside in a shift-invariant subspace- a space spanned by a generating function and its uniform shifts [78, 80] (see Section 2.3.3 for formal definition).

Recently, novel sampling schemes have been presented for larger classes of signals that are neither bandlimited nor reside in a fixed subspace. In particular, these signals are parametric nonbandlimited signals and are characterized by a finite number of parameters per unit of time. Such finite complexity signals enjoy a finite number of degrees of freedom per unit of time (or a finite rate of innovation) and thus are classified as signals with Finite Rate of Innovation (FRI)<sup>1</sup> [87]. Streams of Diracs, nonuniform splines, and piecewise polynomials are examples of such signals. The new schemes [87] consider sampling and perfect reconstruction of FRI signals from a finite number of samples using annihilating filter method (Prony's method). Subsequently, the schemes of [87] are extended to the classes of 2-D FRI signals such as sets of 2-D Diracs, and polygons in [56] and [54]. The schemes of [56] rely on global algorithms in Fourier domain, and can be unstable at times. Most importantly, all these schemes [54, 56, 87] use infinite support sinc and Gaussian kernels, and therefore, are not convenient in practice. However, the results of [27, 28] show that many 1-D FRI signals with local finite rate of innovation can be sampled and perfectly reconstructed using compactly supported kernels that can reproduce polynomials. In particular, any kernel  $\varphi(t)$  that satisfies Strang-Fix conditions (Equation (3.6)) can reproduce polynomials  $t^n$ . In other words, it follows that

$$\sum_{k \in \mathbb{Z}} c_k^n \varphi(t - k) = t^n, \quad n = 0, 1, \dots, N,$$

---

<sup>1</sup>Formal definition of FRI signals is given in Section 3.2.2. The terms 'degrees of freedom' or 'innovations' refer to the free parameters that characterize a given FRI signal.

for a proper choice of coefficients  $c_k^n$ . The sampling kernel  $\varphi(t)$  includes B-splines and wavelet type scaling functions (refer to Section 3.2.3 for further details).

In this thesis, we extend the 1-D FRI sampling results of [27, 28] to the multidimensional FRI signals using local (or compactly supported) kernels that reproduce polynomials. It is important to remember that the polynomial reproduction property of the sampling kernels plays a pivotal role in our sampling schemes. In particular, it allows us to obtain the ‘continuous moments’ of the signals from their samples. Using these moments in the annihilating filter method, the degrees of freedom and therefore, the FRI signals themselves are reconstructed. However, the exact reconstruction algorithms are quite sophisticated and make use of various tools such as directional derivatives, complex-moments, and Radon transform together with the annihilating filter method. In particular, we propose local (Directional derivatives based) and global (Complex-moments, and Radon transform based) reconstruction approaches with varying complexities for sampling classes of multidimensional FRI signals.<sup>2</sup> Note that we concentrate on sampling and perfect reconstruction theory, and therefore, throughout the thesis we consider noiseless signals and measurements.

## 1.2 Summary of the problem

Summarizing the ‘motivation, background, and scope’, we reiterate that the problem of efficient sampling is relevant and important in modern data intensive applications. Many applications deal with real life signals that are nonbandlimited, and in some situations, it might be desirable to achieve perfect reconstruction of these signals from their samples. In order to progress towards the ultimate objective- ‘perfect reconstruction of real life signals’, it is reasonable to investigate whether it is possible

---

<sup>2</sup>The signals we consider include sets of 2-D Diracs, planar and bilevel-convex polygons, quadrature domains (e.g. circles, ellipses, cardioids), 2-D polynomial with convex polygonal boundaries, and higher dimensional Diracs and bilevel-convex polytopes.

achieve perfect reconstruction of certain nonbandlimited signals, at least some synthetic ones (e.g. Diracs and piecewise polynomials) to begin with.

As discussed in Section 1.1, neither Shannon's sampling theory [67, 68] nor modern extensions (e.g. sampling in shift-invariant subspaces [78, 80]) allow perfect reconstruction of nonbandlimited signals. Moreover, most of the classical solutions employ frequency domain approach and consider infinite support sinc kernel- often inconvenient in practice while working with finite length signals. The initial results in sampling signals with finite rate of innovations (FRI) [54, 56, 87] demonstrate that one can perfectly reconstruct many nonbandlimited signals from a finite number of samples, continuing with infinite support sinc and Gaussian kernels and frequency domain processing. However, the recent work on FRI sampling [27, 28] considers a spatial domain approach and shows that one can perfectly reconstruct 1-D FRI signals (e.g. Diracs and piecewise polynomials) from a finite number of samples by employing local (or compactly supported) kernels that reproduce polynomials (e.g. B-splines).

The aim of this work is to extend the 1-D FRI sampling schemes of [27, 28] into higher dimensions (e.g. 2-D and above) in providing precise answer to the problem of perfect reconstruction for classes of multidimensional nonbandlimited signals. The other implicit objective is to understand the link between continuous and discrete domains- central to modern data acquisition and rendering architectures that affect applications such as vectored graphics, computer animation, and machine vision. In terms of realization, the proposed sampling schemes have been promisingly explored for image super-resolution algorithms [2] and distributed compression [31] within the group.<sup>3</sup>

Finally, the structure of the thesis is given in the following section and the original contribution is highlighted in Section 1.4.

---

<sup>3</sup>The group research profile is available at: <http://www.commsp.ee.ic.ac.uk/~pld/group/>

## 1.3 Thesis outline

In the following chapter, we provide a background on sampling and perfect reconstruction. In particular, we refer to the classical results in sampling theory. First, we review the famous Shannon’s sampling theorem (with its historical connections) for sampling and perfect reconstruction of bandlimited signals. We then recall important extensions and generalizations of the Shannon’s theorem. Finally, we close the chapter on classical sampling by reviewing a modern and more general interpretation to sampling, namely, sampling in shift-invariant subspaces.

In Chapter 3, we concentrate on sampling signals with finite rate of innovation (FRI) [28, 87]. We begin with the fundamentals of FRI sampling. We discuss in detail the 1-D sampling framework (i.e. sampling setup, sampling kernel, and reconstruction algorithm), and summarize the key sampling results considering the kernels that reproduce polynomials [28]. We then establish a multidimensional FRI framework, which we recall frequently in the subsequent chapters.

In Chapters 4, 5, and 6, we utilize the multidimensional framework of Chapter 3 and propose local (Directional derivatives based) and global (Complex-moments, and Radon transform based) approaches for reconstructing higher dimensional FRI signals from their samples. To be more precise:

In Chapter 4, we present local reconstruction algorithms for 2-D Diracs and planar polygons. First, we show that a set of 2-D Diracs can be reconstructed locally (i.e. one Dirac per time) from its samples. We then extend this result for a planar polygon by retrieving its corner points using correct pairs of directional derivatives. The directional derivatives based approach relies on a novel link between ‘continuous domain directional derivatives’ and ‘discrete domain directional differences’, which exploits the fundamentals of lattice theory [20, 44, 85].

In Chapter 5, we employ complex-moments for global reconstruction of

bilevel-convex polygons, 2-D Diracs, and quadrature domains (e.g. circles, ellipses, and cardioids). First, we compute the moments of these signals from their samples. We then use these moments in the annihilating filter method for retrieving the free parameters (or degrees of freedom) which uniquely determine the given signals. Implicitly, we also derive a sampling perspective to the ‘shape from moments method’ of [30, 60].

In Chapter 6, we propose a Radon transform based approach for sampling more general signals such as 2-D polynomials with polygonal boundaries, and higher dimensional Diracs and bilevel-convex polytopes. The key feature of this approach is ‘Annihilating Filter based Back-Projection’ (AFBP) algorithm, which integrates the moment property of Radon transform [61] in the framework of FRI sampling [28, 54]. We also highlight a real image experiment to demonstrate the potential of AFBP algorithm for corner reconstruction.

Finally, we present the concluding remarks and an outline for the future work in Chapter 7.

## 1.4 Original contribution

The main contribution of the thesis is multidimensional extensions to the 1-D sampling schemes for signals with finite rate of innovation (FRI) [28, 87], particularly focusing on sampling kernels that reproduce polynomials [28]. First, we establish a multidimensional FRI framework in Section 3.3. Second, by utilizing the multidimensional framework, we propose local (Directional derivatives based) and global (Complex-moments, and Radon transform based) approaches for reconstructing higher dimensional FRI signals from their samples in Chapters 4, 5, and 6 respectively. In particular, in Chapter 4, we present local reconstruction algorithm for 2-D Diracs and then extend it for planar polygons by employing directional derivatives

based approach. In Chapter 5, we use complex-moments for global reconstruction of bilevel-convex polygons, 2-D Diracs, and quadrature domains (e.g. circles, ellipses, and cardioids). Finally, in Chapter 6, we propose a Radon transform based approach for sampling more general signals such as 2-D polynomials with polygonal boundaries, and  $n$ -dimensional Diracs and bilevel-convex polytopes. To the best of our knowledge, Chapters 4, 5, and 6 of the thesis contain the original research work which has culminated into the following publications:

- P. Shukla and P. L. Dragotti. Sampling schemes for multidimensional signals with finite rate of innovation. *IEEE Transactions on Signal Processing*, accepted in November 2006, will appear in July 2007.<sup>4</sup>
- P. Shukla and P. L. Dragotti. Tomographic approach for sampling multidimensional signals with finite rate of innovation. In *Proc. of IEEE International Conference on Image Processing (ICIP)*, Atlanta, USA, October 2006.<sup>5</sup>
- P. Shukla and P. L. Dragotti. Sampling schemes for 2-D signals with finite rate of innovation using kernels that reproduce polynomials. In *Proc. of IEEE International Conference on Image Processing (ICIP)*, Genova, Italy, September 2005.<sup>6</sup>
- P. Shukla and P. L. Dragotti. Shapes from samples using moments and Radon projections. In *Proc. of WavE 2006: International Conference on Wavelets and Applications at EPFL*, Lausanne, Switzerland, July 2006.<sup>7</sup>
- P. L. Dragotti, M. Vetterli, P. Shukla, and T. Blu. Sampling moments and reconstructing signals with finite rate of innovation: Shannon meets Strang-

---

<sup>4</sup>The journal paper consolidates almost entire work of the thesis from Section 3.3.

<sup>5</sup>The ICIP06 paper includes the initial results on the ‘Radon transform based approach’ of Chapter 6.

<sup>6</sup>The ICIP05 paper covers the ‘Directional derivatives based approach’ of Chapter 4 and some results on the ‘Complex-moments based approach’ of Chapter 5.

<sup>7</sup>The WavE 2006 poster showcased the results on the ‘Radon transform based approach’.

Fix. In *Proc. of SIAM Conference on Imaging Science*, Minneapolis, USA, May 2006.<sup>8</sup>

---

<sup>8</sup>The SIAM talk projected the key results of [28] and that of ‘Complex-moments based approach’.

# Chapter 2

## Classical Sampling

### 2.1 Introduction

The term ‘sampling’ belongs to the fundamental vocabulary of electrical and computer engineers. Sampling is the process of representing a continuous-time signal  $g(t), t \in \mathbb{R}$  by a discrete set of values  $g_k, k \in \mathbb{Z}$  [63]. If the time instances at which these samples are taken are equidistant, that is,  $g_k = g(kT)$  for every  $T$  seconds, then the signal is uniformly (or regularly) sampled. If the time instances are not equidistant, that is, if the samples  $g_k = g(t_k)$  are taken at arbitrary points  $t_k \in \mathbb{R}$ , then we have nonuniform or irregular sampling [52]. Throughout the thesis, we focus on uniform sampling- the situation most commonly encountered in practice.

Given that one only observes the uniform samples  $g_k = g(kT)$  of the continuous-time signal  $g(t)$ , the natural questions are:

- 1) What is the optimal way of sampling  $g(t)$ ?
- 2) Is it possible to retrieve the original signal  $g(t)$  from its samples  $g_k = g(kT)$ ?

The classical answer to these questions is given by the well known Shannon’s sampling theorem, which is discussed in detail in Section 2.2.

Since decades, Shannon’s sampling theory has been extensively utilized in

many areas of science and technology, including scientific measurements, medical and biological signal processing, and analog-to-digital convertors. For instance, telephone systems and audio CD players are typical examples. Over the years, Shannon's sampling theory has been extended in many directions. This includes nonuniform and derivative sampling of bandlimited signals [41], and more general multichannel (generalized) sampling [64]. In recent years many of these results have been extended to the case of nonbandlimited signals. These recent extensions have been found to be useful in applications such as image interpolation, equalization of communication channels, and in multiresolution computation [84]. For instance, recent applications of generalized sampling include motion-compensated deinterlacing of television images [76], and super-resolution [83].

A detailed tutorial review on Shannon's sampling theory and its extensions up to mid-1970's is given by Jerry in [41]. In depth treatment on basic theory as well as recent advancements in sampling can be found in various books such as by Marks [57], Zayed [93], and Benedetto [5]. For a comprehensive account on modern sampling developments, we refer to Unser [78] and Vaidyanathan [84].

In this chapter, we focus on the classical sampling and its extensions. In the following section, we review Shannon's theorem for sampling and perfect reconstruction of bandlimited signals [67, 68]. We then discuss extensions and generalizations of Shannon's sampling theory in Section 2.3. In particular, we highlight the case of sampling in shift-invariant subspaces [78, 80] which allows sampling of more general signals that are not necessarily bandlimited.

## 2.2 Shannon's sampling theory

The fundamental result in sampling theory is the well-known Shannon's sampling theorem [67, 68], which states that a continuous time signal  $g(t)$  is uniquely defined

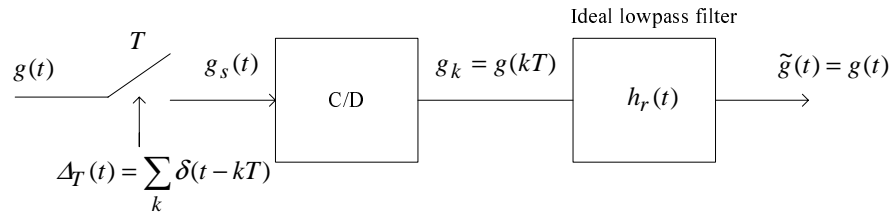


**Figure 2.1: Shannon's scheme for sampling and perfect reconstruction of bandlimited signals:** The continuous signal  $g(t)$  is multiplied by a stream of Diracs  $\Delta_T(t) = \sum_{k \in \mathbb{Z}} \delta(t - kT)$  leading to a sampled signal  $g_s(t) = \sum_{k \in \mathbb{Z}} g(kT) \delta(t - kT)$ . The block **C/D** stands for **continuous-to-discrete transformation and corresponds to the readout of sample values  $g_k = g(kT)$  from  $g_s(t)$** . The reconstructed signal  $\tilde{g}(t) = g(t)$  is obtained by interpolating the samples  $g_k$  with reconstruction filter  $h_r(t) = \frac{T}{T_c} \text{sinc}(t/T_c)$  which is an ideal lowpass filter with cutoff frequency  $\omega_c = \pi/T_c$  and gain  $T$ .

by its samples  $g_k = g(kT)$ , if the sampling frequency  $\omega_s = 2\pi/T$  radians/seconds is greater than two times the maximum frequency<sup>1</sup> component  $\omega_m$  of signal  $g(t)$ , that is,

$$\omega_s \geq 2\omega_m \quad \text{or} \quad \omega_m \leq \pi/T. \quad (2.1)$$

The reconstructed signal  $\tilde{g}(t)$  is obtained by interpolating the samples  $g_k = g(kT)$  using appropriate shifting and scaling of the sinc interpolator:

$$\tilde{g}(t) = \frac{T}{T_c} \sum_{k \in \mathbb{Z}} g(kT) \text{sinc}(t/T_c - k), \quad (2.2)$$

where  $\text{sinc}(t) = \sin(\pi t)/(\pi t)$ .

The interpolating function or the reconstruction filter  $h_r(t) = \frac{T}{T_c} \text{sinc}(t/T_c)$  is an ideal lowpass filter with gain  $T$  and cutoff frequency  $\omega_c = \pi/T_c$ , that is, its Fourier transform  $\hat{h}_r(\omega) = T \Pi\left(\frac{\omega}{2\omega_c}\right)$  is equal to zero outside the frequency band  $[-\omega_c, \omega_c]$ . In order to perfectly recover the original signal  $g(t)$ , the cutoff frequency  $\omega_c$  of the

---

<sup>1</sup>The maximum frequency component  $\omega_m$  is the bandlimit of the signal  $g(t)$ , that is, the Fourier transform  $\hat{g}(\omega) = 0$  for  $|\omega| \geq \omega_m$ .

lowpass filter  $\hat{h}_r(\omega)$  must satisfy

$$\omega_m \leq \omega_c \leq \omega_s - \omega_m. \quad (2.3)$$

where  $\omega_m$  is the maximum frequency of  $g(t)$  and  $\omega_s$  is the sampling frequency.

Shannon's scheme for sampling and perfect reconstruction of bandlimited signals is illustrated in Figure 2.1, where the continuous signal  $g(t)$  is assumed to be bandlimited. The signal  $g(t)$  is sampled by multiplying it with the periodic train of Diracs  $\Delta_T(t) = \sum_{k \in \mathbb{Z}} \delta(t - kT)$  which leads to the sampled signal  $g_s(t) = g(t)\Delta_T(t) = \sum_{k \in \mathbb{Z}} g(kT)\delta(t - kT)$ . The block C/D stands for continuous-to-discrete transformation and corresponds to the readout of sample values  $g_k = g(kT)$  from  $g_s(t)$ . The reconstructed signal  $\tilde{g}(t) = g(t)$  is obtained by interpolating the samples  $g_k$  with the reconstruction filter  $h_r(t) = \frac{T}{T_c} \text{sinc}(t/T_c)$  using Equation (2.2), where  $h_r(t)$  is an ideal lowpass (or reconstruction) filter with cutoff frequency  $\omega_c = \pi/T_c$  and gain  $T$ .

A frequency domain interpretation of the Shannon's scheme is given in Figure 2.2. The Fourier transform  $\hat{g}(\omega)$  of signal  $g(t)$  is assumed to be bandlimited up to  $\omega_m$  as shown in part (a). Note that the Fourier transform  $\Delta_{\omega_s}(\omega)$  of the periodic train of Diracs  $\Delta_T(t) = \sum_{k \in \mathbb{Z}} \delta(t - kT)$  is also a periodic train of Diracs  $\Delta_{\omega_s}(\omega) = \frac{2\pi}{T} \sum_{k \in \mathbb{Z}} \delta(\omega - k\omega_s)$ . Therefore, the Fourier transform  $\hat{g}_s(\omega)$  of the sampled signal  $g_s(t) = g(t)\Delta_T(t)$  is given by

$$\hat{g}_s(\omega) = \frac{1}{2\pi} (\hat{g}(\omega) * \Delta_{\omega_s}(\omega)) = \frac{1}{T} \sum_{k \in \mathbb{Z}} \hat{g}(\omega - k\omega_s),$$

where  $\hat{g}_s(\omega)$  is periodic with period  $\omega_s = 2\pi/T$ , and is obtained by the periodic copies of  $\hat{g}(\omega)$  at every integer multiples of  $\omega_s$  as shown in Figure 2.2(b). Recall that the reconstruction filter  $\hat{h}_r(\omega) = T \Pi\left(\frac{\omega}{2\omega_c}\right)$  is an ideal lowpass filter with gain  $T$  and cutoff frequency  $\omega_c$  satisfying (2.3). This means that one can extract one instance of

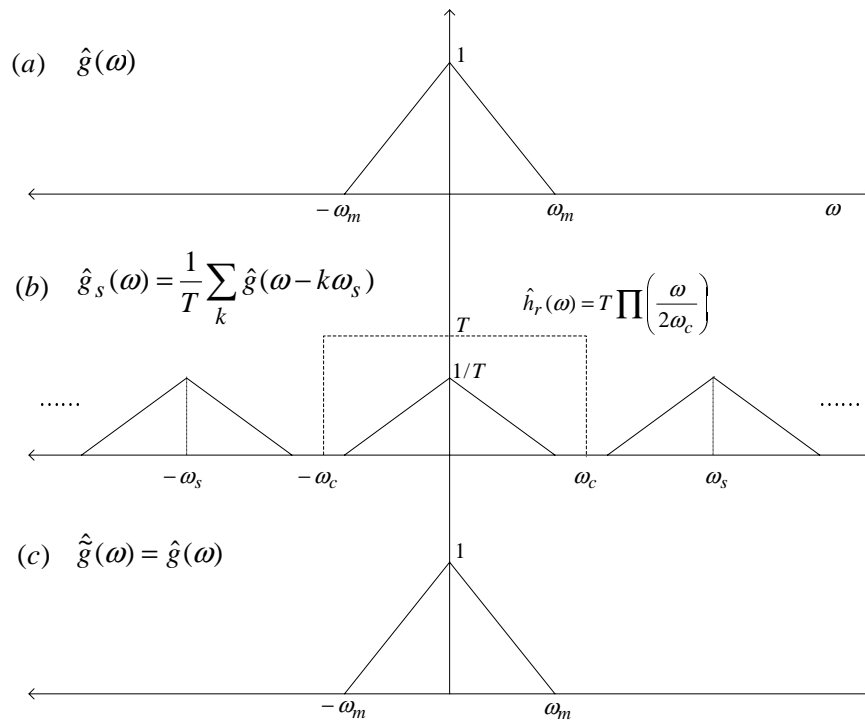


**Figure 2.2: Sampling and perfect reconstruction in frequency domain:** (a)  $\hat{g}(\omega)$  is the Fourier transform (FT) of input signal  $g(t)$ , (b)  $\hat{g}_s(\omega)$  is the FT of sampled signal  $g_s(t)$ , and  $\hat{h}_r(\omega)$  is the FT of reconstruction filter  $h_r(t)$  with cutoff frequency  $\omega_c$  and gain  $T$ , (c)  $\hat{\tilde{g}}(\omega)$  is the FT of reconstructed signal  $\tilde{g}(t) = g(t)$ .

the spectrum  $\hat{\tilde{g}}(\omega)$  from the periodic spectra  $\hat{g}_s(\omega)$  without any overlap (or aliasing) by multiplying  $\hat{g}_s(\omega)$  with  $\hat{h}_r(\omega)$  as shown in part (b). In fact, the spectrum of the reconstructed signal  $\hat{\tilde{g}}(\omega)$  is identical to the spectrum of the original signal  $\hat{g}(\omega)$  as given in part (c). This clearly illustrates that it is possible to perfectly recover a continuous-time bandlimited signal  $g(t)$  from its samples  $g_k = g(kT)$  using the sinc interpolator of (2.2).

Recall that the reconstruction in (2.2) is exact if  $g(t)$  is bandlimited to  $\omega_m$ . This highest frequency  $\omega_m$  is the Nyquist frequency,<sup>2</sup> a term coined by Shannon in recognition of Nyquist (1928) for his contribution in communication theory [62]. In fact, Shannon was well aware of equivalent forms of the sampling theorem that

<sup>2</sup> The Nyquist rate is twice the the Nyquist frequency and is commonly known as the minimum sampling rate  $\omega_{s(\min)} = 2\omega_m = 2\pi/T$  that avoids aliasing.

had appeared in mathematical literature, in particular, the work of J. M. Whittaker (1929) [91]. While Shannon must get full credit for formalizing this result and realizing its potential for communication theory and signal processing, it is important to remember that in Russian literature, this theorem was independently introduced to the communication theory by Kotel'nikov (1933) [45, 46], similarly in German literature by Raabe (1939) and in Japanese literature by Someya (1949) [50]. Interestingly, the formulation of (2.2) is known as 'cardinal series expansion' in mathematical literature—often attributed to E. T. Whittaker (1915) [16, 90] but has also been traced back much further [4, 38]. An extensive chronology of interpolation from ancient astronomy to modern signal/image processing is given by Meijering in [59].

While Shannon's theory is very elegant and has profoundly influenced the ways of analog to digital conversions, there are few problems associated with it [78]: First, the theorem allows perfect reconstruction of bandlimited signals only. Clearly, real world signals or images are never exactly bandlimited, and therefore, one cannot perfectly reconstruct such signals. However, we notice that Shannon's theorem cannot be generalized for perfect reconstruction of even synthetic cases of nonbandlimited signals (e.g. Diracs and piecewise polynomials) from their samples taken at any finite sampling rate. Nonetheless, one can reconstruct a minimum error approximations of a nonbandlimited signal as discussed in Section 2.3.2. Second, it requires a unique reconstruction filter— an ideal lowpass filter for perfect reconstruction. Although, the ideal lowpass filter (i.e. infinite support sinc kernel) cannot be realized in practice, it does not offer any choice of other reconstruction kernel. Third, Shannon's original reconstruction formula is rarely used in practice because of the infinite support and slow decay of the sinc function. Instead, it is common to use a zero-order hold followed by a reconstruction filter which sometimes includes compensation for the zero-order hold. Increasingly, the signal is first upsampled. In general, perfect reconstruction is hardly achieved in practice.

Finally, Shannon's theory and its extensions (discussed in the following sections) are mainly frequency domain formulations. However, we notice that some signals are better described in other domains (e.g. Joint time-frequency representations or wavelet transform for non-stationary signals).

## 2.3 Extensions and Generalizations

There are many extensions and generalizations of the Shannon's sampling theory and reviewing them all is beyond the scope of this thesis. However, in this section, first we quickly review Papoulis's multichannel (generalized) sampling and other extensions [64, 78, 84], mainly for bandlimited signals. We then highlight the case of approximate reconstruction of nonbandlimited signals in Shannon's framework [13, 67], where we highlight the subspace based interpretation to the sampling. Finally, we focus on the modern sampling approach of Unser et al.– known as sampling in shift-invariant subspaces [78, 80]. The shift-invariant approach explicitly considers the shortcomings of Shannon's scheme and allows for sampling of more general classes of signals that are not necessarily bandlimited.

### 2.3.1 Papoulis's framework and other extensions

In 1977, Papoulis introduced a powerful extension of Shannon's sampling theory, known as multichannel (or generalized) sampling [64]. It shows that a bandlimited signal could be reconstructed exactly from the samples of the response of  $m$  linear shift-invariant systems sampled at  $1/m$  the reconstruction rate. This suggests that there are many different ways of extracting information from a signal, and the reconstruction is generally possible provided there are as many measurements as there are degrees of freedom in the signal representation. If the measurements are taken in a structured manner, then the reconstruction process is simplified.

For example, in the Papoulis framework, reconstruction is achieved by multivariate filtering [12, 57]. Typical instances of generalized sampling are interlaced and derivative sampling [48, 92], both of which are special cases of Papoulis's framework. While the generalized sampling concept is relatively straightforward, the reconstruction is not always possible due to potential instabilities [14].

In the last two decades, Papoulis's theory has been generalized in several directions [78, 84]. Although, remaining bandlimited, it was extended for multidimensional and multicomponent signals [15, 66]. Djokovic and Vaidyanathan [25, 84] applied similar ideas for reconstruction of functions in certain wavelet spaces: they concentrated on the special cases of interlaced sampling, sampling of a functions and its derivatives, and reconstruction from local averages. A further step was taken by Unser and Zerubia [78, 82], who showed the reconstruction in shift-invariant subspaces without any constraint on the input signal (i.e. signal may be nonbandlimited). Instead of perfect reconstruction, they obtain a consistent approximation such that the it yields exactly the same measurements (samples) if the reconstructed signal is reinjected into the system.

### 2.3.2 Approximation for nonbandlimited signals

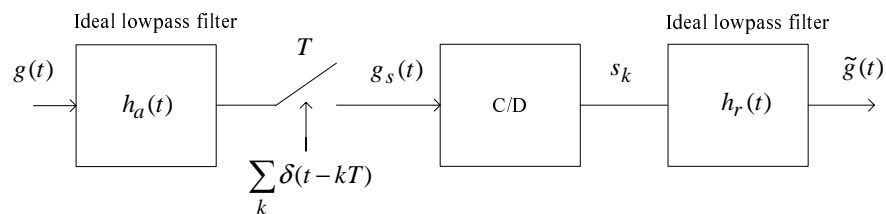


**Figure 2.3: Sampling and reconstruction of nonbandlimited signals in Shannon's framework:** The continuous-time signal  $g(t)$  is first filtered by an ideal lowpass filter  $h_a(t)$  followed by the usual sampling and reconstruction scheme of Figure 2.1. However, in this case, the reconstruction is not perfect.

Recall that the Shannon's perfect reconstruction scheme (as shown in

Figure 2.1) relies on the fact that the input signal  $g(t)$  is bandlimited. However, it is possible to reconstruct a nonbandlimited signal  $g(t)$  in Shannon's framework by making it bandlimited before sampling [13, 67]. This is illustrated in Figure 2.3.

A nonbandlimited signal  $g(t)$  is first prefiltered by an ideal lowpass filter  $h_a(t) = \text{sinc}(-t/T)$  (or antialiasing filter) such that the frequency spectrum of the filtered signal  $g(t) * h_a(t)$  is restricted to  $[-\omega_m, \omega_m]$ . The filtered signal  $g(t) * h_a(t)$  is then sampled uniformly at every  $T$  seconds (with  $\omega_s = 2\pi/T$ ) to obtain the samples  $s_k = g_s(kT)$ :

$$\begin{aligned} s_k &= g(t) * h_a(t)|_{t=kT} \\ &= \int_{-\infty}^{\infty} g(t) \text{sinc}(t/T - k) dt \\ &= \langle g(t), \text{sinc}(t/T - k) \rangle, \end{aligned} \tag{2.4}$$

where  $\langle \cdot, \cdot \rangle$  is the inner-product operator. Note that, now the samples are denoted by symbol  $s_k$  rather than  $g_k = g(kT)$  since the original signal  $g(t)$  is modified by the antialiasing filter  $h_a(t)$ .

Similar to (2.2), the reconstructed signal  $\tilde{g}(t)$  is obtained by interpolating the samples  $s_k$  with appropriate scaling and shifting of the sinc kernel (or ideal lowpass filter  $h_r(t) = \text{sinc}(t/T)$ ), leading to the signal

$$\begin{aligned} \tilde{g}(t) &= \sum_{k \in \mathbb{Z}} s_k \text{sinc}(t/T - k) \\ &= \sum_{k \in \mathbb{Z}} \langle g(t), \text{sinc}(t/T - k) \rangle \text{sinc}(t/T - k). \end{aligned} \tag{2.5}$$

Since the sinc basis functions  $\{\text{sinc}(t/T - k)\}_{k \in \mathbb{Z}}$  form an orthogonal set in  $L_2(\mathbb{R})$ , the interpolation formula (2.5) can be viewed as an orthogonal projection of the input signal  $g(t)$  onto the subspace of bandlimited signals spanned by sinc function.

This means that the reconstructed signal  $\tilde{g}(t)$  is a least square (or minimum-

error) approximation of  $g(t)$  onto the sinc subspace [78]. For more details on the reconstruction of nonbandlimited signals from their lowpass approximations, we refer to [17].

### 2.3.3 Sampling in shift-invariant subspaces

Recently, sampling theory has experienced a strong research revival, mainly due to increased interest around wavelets [22,51,86]. Researchers found that the mathematics of wavelets were also applicable to sampling but with more freedom since multiresolution is not mandatory. This led researchers to reexamine some of the foundations of classical theory and develop more general formulations [78]. In particular, in [78, 80] Unser et al. addressed the shortcomings of Shannon's framework, and provided a more general Hilbert-space formulation for sampling and reconstruction of signals  $g(t)$  that are not necessarily bandlimited (i.e.  $g(t) \in L_2$ ).<sup>3</sup> This new sampling formulation is termed as sampling in shift-invariant subspaces (i.e. subspaces spanned by generating functions and their uniform shifts). The following summary of the principal results is based on that of [78, 80].

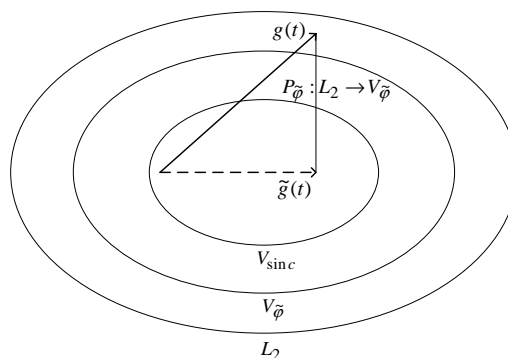


**Figure 2.4: Nesting of subspaces:**  $V_{\text{sinc}} \subset V_{\tilde{\varphi}} \subset L_2$ . Notice that the subspace  $V_{\text{sinc}}$  is also a shift-invariant subspace. The sampling procedure is viewed as a projection operator  $P_{\tilde{\varphi}} : L_2 \rightarrow V_{\tilde{\varphi}}$  that computes minimum error approximation  $\tilde{g}(t) = P_{\tilde{\varphi}} g(t)$  of the input signal  $g(t) \in L_2$  onto a shift-invariant subspace  $V_{\tilde{\varphi}}$

<sup>3</sup>Here,  $L_2$  is the space of all functions that are square-integrable in Lebesgue's sense.

In this formulation, the sampling procedure is viewed as a projection operator  $P_{\tilde{\varphi}} : L_2 \rightarrow V_{\tilde{\varphi}}$  that computes minimum error approximation  $\tilde{g}(t) = P_{\tilde{\varphi}} g(t)$  of the input signal  $g(t) \in L_2$  onto a shift-invariant subspace  $V_{\tilde{\varphi}}$  spanned by a generating (synthesis) function  $\tilde{\varphi}(t)$  and its uniform shifts. The shift-invariant subspace  $V_{\tilde{\varphi}}$  is more general than the bandlimited sinc space  $V_{\text{sinc}}$ . The nesting of the subspaces  $V_{\text{sinc}} \subset V_{\tilde{\varphi}} \subset L_2$  is shown in Figure 2.4.

The shift-invariant or approximation space  $V_{\tilde{\varphi}}$  is given by

$$V_{\tilde{\varphi}} = \left\{ g(t) = \sum_{k \in \mathbb{Z}} c_k \tilde{\varphi}(t - k) \right\}, \quad (2.6)$$

where coefficients  $c_k$  are square-summable, i.e.  $c_k \in l_2$ , and the family of functions  $\{\tilde{\varphi}_k = \tilde{\varphi}(t - k)\}_{k \in \mathbb{Z}}$  form a Riesz basis of  $V_{\tilde{\varphi}}$ . The definition of Riesz basis is that there exists two positive constants  $A$  and  $B$  satisfying  $0 < A \leq B < \infty$  such that

$$A \cdot \|c_k\|_{l_2}^2 \leq \left\| \sum_{k \in \mathbb{Z}} c_k \tilde{\varphi}(t - k) \right\|^2 \leq B \cdot \|c_k\|_{l_2}^2, \quad (2.7)$$

where  $\|c_k\|_{l_2}^2 = \sum_k |c_k|^2$  is the squared  $l_2$ -norm (or energy) of  $c_k$ .

If the reconstruction kernel  $\tilde{\varphi}(t)$  satisfies inequality (2.7), it is an admissible (valid) shift-invariant kernel. For every admissible kernel  $\tilde{\varphi}(t)$ , there exists a unique dual kernel  $\hat{\varphi}(t)$  which can be determined by the biorthogonal constraint:  $\langle \tilde{\varphi}(t - m), \hat{\varphi}(t - n) \rangle = \delta_{m-n}$ ,  $m, n \in \mathbb{Z}$ . In fact,  $\varphi(t) = \hat{\varphi}(t)$  is an optimal analysis kernel for the given synthesis kernel  $\tilde{\varphi}(t)$ . Moreover, the family of dual functions  $\{\hat{\varphi}_k = \hat{\varphi}(t - k)\}_{k \in \mathbb{Z}}$  belongs to the shift-invariant space  $V_{\tilde{\varphi}}$  as well.

For the special case of  $A = B = 1$  in (2.7), the synthesis functions  $\tilde{\varphi}_k$  are orthonormal, i.e.,  $\forall m, n \in \mathbb{Z}$ ,  $\langle \tilde{\varphi}_m, \tilde{\varphi}_n \rangle = \delta_{m-n}$ , and in this case the optimal analysis kernel  $\varphi(t) = \hat{\varphi}(t) = \tilde{\varphi}(t)$ .

In this case, the standard sampling scheme of Figure 2.3 is seen as a three-

step paradigm: prefiltering, sampling, and postfiltering, where the input (analysis) filter  $h_a(t) = \varphi(-t)$  and output (synthesis) filter  $h_r(t) = \tilde{\varphi}(t)$  may not necessarily be ideal (i.e. sinc kernels) and the input signal is not necessarily bandlimited, i.e.  $g(t) \in L_2$ . Additionally, the kernels  $\varphi(t)$  and  $\tilde{\varphi}(t)$  may not be related. The three-step shift-invariant scheme is depicted in Figure 2.5. The samples  $s_k$  of the signal  $g(t)$  are given by the inner products:  $s_k = \langle g(t), \varphi(t/T - k) \rangle$ , where for simplicity, one can assume the sampling interval  $T = 1$ .

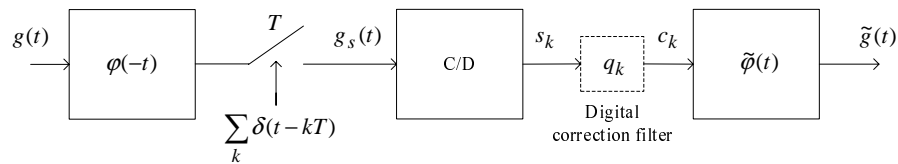


**Figure 2.5: Three-step paradigm for sampling in shift-invariant subspaces  $V_{\tilde{\varphi}}$ : The prefilter  $h_a(t) = \varphi(-t)$  and postfilter  $h_r(t) = \tilde{\varphi}(t)$  are not necessarily ideal lowpass filters (sinc kernels) and they may or may not be related. However, both kernels span the shift-invariant subspace  $V_{\tilde{\varphi}}$ . The digital correction filter  $q_k$  is optional (e.g. it can be removed when  $g(t) \in V_{\tilde{\varphi}}$ , and  $\varphi(t)$  and  $\tilde{\varphi}(t)$  forms a biorthogonal (or orthogonal) pair). The filter  $q_k$  converts the samples  $s_k$  into the coefficients  $c_k = s_k * q_k$  for reconstructing the output signal  $\tilde{g}(t) = \sum_{k \in \mathbb{Z}} c_k \tilde{\varphi}(t - k)$ . The reconstruction is perfect when  $g(t) \in V_{\tilde{\varphi}}$ .**

The shift-invariant formulation of (2.6) suggests that any continuous signal  $g(t) \in V_{\tilde{\varphi}}$  is characterized by a sequence of coefficients  $c_k = \langle g(t), \tilde{\varphi}(t - k) \rangle$ . However, these coefficients are not necessarily the samples  $s_k = \langle g(t), \varphi(t - k) \rangle$  of signal  $g(t)$ . This is explained with the following examples [78] (also see Figure 2.5):

1. Assume that signal  $g(t) \in V_{\tilde{\varphi}}$  and that the analysis kernel  $\varphi(t)$  and synthesis kernel  $\tilde{\varphi}(t)$  form a biorthogonal pair. In this case, one can perfectly reconstruct  $g(t) = \tilde{g}(t) = \sum_{k \in \mathbb{Z}} c_k \tilde{\varphi}(t - k)$  from a sequence of coefficients  $c_k = \langle g(t), \tilde{\varphi}(t - k) \rangle$  which are, in fact, the samples  $s_k = \langle g(t), \varphi(t - k) \rangle$ . In this case there is no need of digital correction filter  $q_k$ .
2. Now consider the case when  $g(t) \in V_{\tilde{\varphi}}$  but the shift-invariant kernels  $\varphi(t)$

and  $\tilde{\varphi}(t)$  do not form a biorthogonal pair. In this situation, the dual  $\mathring{\varphi}(t)$  of the synthesis kernel  $\tilde{\varphi}(t)$  is not the same as the analysis kernel  $\varphi(t)$ . Therefore, the samples  $s_k = \langle g(t), \varphi(t - k) \rangle$  are not equal to the coefficients  $c_k = \langle g(t), \mathring{\varphi}(t - k) \rangle$  required for perfect reconstruction. However, it is possible to show that one can recover the correct coefficients  $c_k$  from the samples  $s_k$  by inserting a digital correction filter  $q_k$  between the sampling and postfiltering stages as shown in Figure 2.5. The filter  $q_k$  is determined by the cross-correlation  $\sigma_k = \langle \varphi(t - k), \tilde{\varphi}(t) \rangle$  between the analysis filter  $\varphi(t)$  and the synthesis filter  $\tilde{\varphi}(t)$ . In particular, the digital correction filter  $q_k$  is characterized by its z-transform  $Q(z) = \frac{1}{\sum_{k \in \mathbb{Z}} \sigma_k z^{-k}}$  and the correct coefficients  $c_k$  are given by  $c_k = s_k * q_k$ .

3. Finally, if  $g(t) \in L_2$  but  $g(t) \notin V_{\tilde{\varphi}}$ , then one cannot achieve perfect reconstruction of  $g(t)$ . This is due to the fact that the shift-invariant reconstruction acts as the projector operator  $P_{\tilde{\varphi}} : L_2 \rightarrow V_{\tilde{\varphi}}$  that computes the minimum-error approximation  $\tilde{g}(t)$  of  $g(t)$  onto the subspace  $V_{\tilde{\varphi}}$ . That is  $\tilde{g}(t) = P_{\tilde{\varphi}} g(t) = \arg \min_{f(t) \in V_{\tilde{\varphi}}} \|g(t) - f(t)\|^2$ . Clearly,  $\tilde{g}(t) \neq g(t)$  when  $g(t) \notin V_{\tilde{\varphi}}$ . Alternative reconstruction algorithms try to obtain an approximation  $\tilde{g}(t)$  that would yield exactly the same measurements if injected back into the system. This is the case of consistent sampling or reconstruction [78, 80].

Thus, the shift-invariant formulation generalizes the classical framework for nonideal acquisition devices. The projection property allows perfect reconstruction of any signal  $g(t)$  that is included in a more general reconstruction space  $V_{\tilde{\varphi}}$ . This is not only true for bandlimited signals but also for any signal (e.g. polynomial spline) that resides in the shift-invariant space. However, this formulation cannot be applied to an arbitrary nonbandlimited signal  $g(t) \in L_2$ , and typically, only a projection (or approximation)  $\tilde{g}(t)$  of  $g(t)$  onto a specific subspace  $V_{\tilde{\varphi}}$  can be recovered.

## 2.4 Summary

In this chapter, we introduced the fundamentals of sampling and reviewed classical sampling theories. In particular, we started with Shannon's sampling scheme for bandlimited signals, and then highlighted various extensions to this scheme. Finally, we presented a modern subspace-based interpretation to the sampling of more general signals. Throughout the chapter, we focused on 1-D sampling framework. However, we note that the classical schemes have been extended and utilized for multidimensional sampling as well [15, 64, 78].

In the following chapter, we introduce the state-of-the-art developments in sampling parametric nonbandlimited signals known as signals with finite rate of innovations (FRI) [28, 87].

## Chapter 3

# Sampling Signals with Finite Rate of Innovation (FRI)

### 3.1 Introduction

In 2002, Vetterli, Marziliano, and Blu [87] showed that it is possible to sample and perfectly reconstruct a large class of signals that are neither bandlimited nor reside in a fixed subspace. However, these nonbandlimited signals are finite complexity parametric signals. A common feature of such signals is that they are characterized by a finite number of degrees of freedom per unit of time. The number of degrees of freedom per unit of time is defined as rate of innovation, and therefore, such signals are termed as signals with finite rate of innovation (FRI)<sup>1</sup> [87]. Vetterli et al. showed that it is possible to sample and perfectly reconstruct 1-D FRI signals such as streams of Diracs, nonuniform splines, and piecewise polynomials from a finite number of uniform samples using infinite support sinc and Gaussian kernels. The reconstruction is based on annihilating or locator filter, a tool widely used in spectral estimation [73] and error-correction coding [7]. The results of [87] provide theorems

---

<sup>1</sup>Formal definition of FRI signals is given in Section 3.2.2.

for sampling and perfect reconstruction of 1-D FRI signals without considering the effect of noise. However, the presence of noise in 1-D FRI sampling is considered in [28, 56]. Moreover, the results of [87] are extended further for 2-D FRI signals such as sets of 2-D Diracs and polygons (again using sinc and Gaussian kernels) by Maravic and Vetterli in [54, 55]. A detailed treatment on 1-D and 2-D FRI sampling is given in the PhD theses of Maziliano [58] and Maravic [53] respectively. A geometrical approach for sampling FRI signals can be found in [49].

Later, Dragotti et al. [27, 28] realized that the sampling schemes of [54, 55, 87] are limited by the use of infinite support (global) kernels, and such kernels make the reconstruction algorithm unstable and complex. In fact, the complexity is influenced by the global rate of innovation of the input signal. The results of [27, 28] show that many 1-D FRI signals<sup>2</sup> with local finite rate of innovation can be sampled and perfectly reconstructed using a wide range of sampling kernels and local reconstruction algorithm (again based on annihilating filter). In particular, it was shown that the local kernels that reproduce polynomials (i.e. satisfy Strang-Fix conditions [74]) are more convenient in practice.

In a very short span, the theory of 1-D and 2-D FRI sampling has been explored in number of signal processing applications. The initial results are promising in applications such as:

- ◊ Resolution enhancement of signals and images [28, 58, 70, 71].
- ◊ Image super-resolution algorithms [2] and in distributed compression [31].
- ◊ High-resolution synchronization and channel estimation [53] and in economic and successive approximation based architecture [47] for ultra-wideband systems.
- ◊ Compression of ECG signals [37].
- ◊ A/D conversions [42].

This chapter is organized as follows: In the following section, we review

---

<sup>2</sup> This includes streams of Diracs, piecewise polynomials [27, 28], and piecewise sinusoidals [6].

the basics of 1-D FRI sampling. We then focus onto the multidimensional FRI framework in Section 3.3. Finally, we summarize in Section 3.4.

## 3.2 1-D Sampling Framework

In the following discussion, we describe the core elements of 1-D FRI sampling, namely, 1) Sampling setup, 2) FRI signals, 3) Sampling kernels, and 4) Reconstruction algorithm.

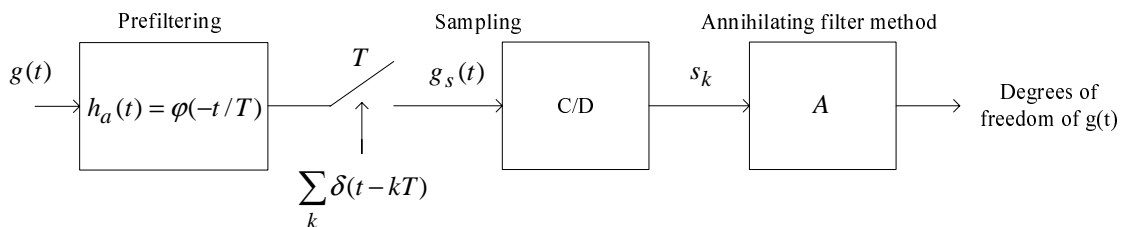


**Figure 3.1: 1-D FRI sampling setup:** The continuous-time FRI signal  $g(t)$  is prefiltered by the smoothing filter  $h_a(t) = \varphi(-t/T)$  and then sampled uniformly to obtain the samples  $s_k = \langle g(t), \varphi(t/T - k) \rangle$  (with  $T$  as sampling interval). The samples  $s_k$  are used to retrieve the degrees of freedom of the original signal  $g(t)$  using a nonlinear postfiltering block  $A$  (annihilating filter method). Note that  $g(t)$  is completely characterized by its degrees of freedom. The block  $C/D$  stands for continuous-to-discrete transformation and corresponds to the readout of samples  $s_k, k \in \mathbb{Z}$  from sampled signal  $g_s(t)$ .

### 3.2.1 Sampling setup

The setup for sampling 1-D FRI signals is given in Figure 3.1. It consists of three standard elements: prefiltering, sampling, and postfiltering. However, as opposed to the classical and shift-invariant schemes, the postfiltering block  $A$ , in this case, is not a kernel based interpolator but a nonlinear reconstruction algorithm known as annihilating filter method (discussed in Section 3.2.4).

The original continuous-time FRI signal  $g(t)$  is filtered with  $h_a(t) = \varphi(-t/T)$

and the filtered version  $g(t) * h_a(t)$  is sampled uniformly to obtain the set of samples  $s_k = g_s(kT), k \in \mathbb{Z}$  given by

$$\begin{aligned} s_k &= g(t) * h_a(t)|_{t=kT} \\ &= \int_{-\infty}^{\infty} g(t) \varphi(t/T - k) dt \\ &= \langle g(t), \varphi(t/T - k) \rangle, \end{aligned} \quad (3.1)$$

where  $\varphi(t)$  is the sampling kernel and  $T$  is the sampling interval. For simplicity, assume that  $T = 1$  when not specified. The filter  $h_a(t)$  represents an impulse response of the acquisition device.

The aim of this framework is to achieve the perfect reconstruction of the input FRI signal  $g(t)$  from a finite number of samples  $s_k$ . The key questions, in this case, are: (i) What exactly is an FRI signal  $g(t)$ ? (ii) What classes of sampling kernels  $\varphi(t)$  can be employed? (iii) What kind of reconstruction algorithm is required?

The answers to these questions are presented in the following subsections. Note that we are considering a framework for developing perfect reconstruction sampling schemes, and therefore, the signal  $g(t)$  and its samples  $s_k$  are assumed to be noiseless [87]. As mentioned earlier, the reconstruction of 1-D FRI signals in the presence of noise is treated in [28, 56].

### 3.2.2 FRI signals

Consider a 1-D signal of the form

$$g(t) = \sum_{i=0}^N \sum_{n \in \mathbb{Z}} \lambda_{i,n} \phi_i(t - t_n), \quad (3.2)$$

where the set of functions  $\{\phi_i(t)\}, i = 0, 1, \dots, N$  is known. Notice that the degrees of freedom of  $g(t)$  are the time instants  $t_n$  and coefficients  $\lambda_{i,n}$ .

It is therefore natural to introduce a counting function  $C_g(t_a, t_b)$  that counts the number of free parameters of  $g(t)$  over an interval  $\tau = [t_a, t_b]$ . The rate of innovation of  $g(t)$  is then defined as

$$\rho = \lim_{\tau \rightarrow \infty} \frac{1}{\tau} C_g \left( -\frac{\tau}{2}, \frac{\tau}{2} \right). \quad (3.3)$$

**Definition 1** (Vetterli, Marziliano, and Blu, [87]). *A signal with a finite rate of innovation is a signal that is characterized by (3.2) and with a finite  $\rho$  as given in (3.3).*

It is of interest to note that shift-invariant signals, including bandlimited signals, fall under Definition 1. For instance, if we call  $f_m$  the maximum non-zero frequency in a bandlimited real signal, then it is straightforward to compute the rate of innovation  $\rho = 1/T = f_s = 2f_m$ , where  $T$  is a sampling interval and  $f_s$  is a sampling frequency. Therefore, one possible interpretation is that it is possible to sample bandlimited signals because they have finite rate of innovation (rather than because they are bandlimited) [28, 87].

In some case, it is more convenient to consider a local rate of innovation with respect to a moving window of size  $\tau$ . The local rate of innovation at time  $t$  is thus given by [87]

$$\rho_\tau(t) = \frac{1}{\tau} C_g \left( t - \frac{\tau}{2}, t + \frac{\tau}{2} \right). \quad (3.4)$$

Clearly,  $\rho_\tau(t)$  tends to  $\rho$  as  $\tau \rightarrow \infty$ . In particular, the local rate of innovation plays a more important role than the global rate of innovation when local reconstruction is desired [28].

Examples of signals with finite rate of innovation include streams of Diracs, nonuniform splines, and piecewise polynomials and sinusoidals.

### 3.2.3 Sampling kernels

As shown in the sampling setup of Figure 3.1, the signal  $g(t)$  is filtered before being sampled. The samples  $s_k$  are given by  $s_k = \langle g(t), \varphi(t - k) \rangle$ , where the sampling kernel  $\varphi(t)$  is the time reversed version of the filter's impulse response  $h_a(t)$ .

It is desirable to have a freedom in selecting or designing the sampling kernel  $\varphi(t)$  of choice. However, in practice, the kernel is characterized by the physical properties of the acquisition device (or processing algorithm), and in most cases, it is specified a-priori and cannot be modified. In general, it is useful to develop sampling schemes that do not require non-realizable or very specific kernels.

In comparison with the classical framework, the FRI framework provides a larger choice of kernels that allow perfect reconstruction. In particular, the initial results on FRI sampling concentrate on sinc and Gaussian kernels [55, 87]. While, more recent results on 1-D FRI sampling [28] show that one can use a wide range of kernels that can reproduce polynomials (e.g. B-splines [77]) or exponentials (e.g. E-splines [81]), or can be characterized by rational Fourier transforms. To be more precise, these kernels are classified into three families [28]:

1. *Polynomial reproducing kernels*: Any kernel  $\varphi(t)$  that together with its uniform shifts  $\varphi(t - k)$  can reproduce polynomials  $t^n$  up to certain degree  $N$ . That is, any kernel that satisfies

$$\sum_{k \in \mathbb{Z}} c_k^n \varphi(t - k) = t^n, \quad n = 0, 1, \dots, N \quad (3.5)$$

for a proper choice of coefficients  $c_k^n$  (with subscript  $k$  as an index along  $t$  and superscript  $n$  deciding the degree of the polynomial  $t^n$ ).

Note that the kernels of this family include any function that satisfy so-called Strang-Fix conditions [74]. To be more precise, any kernel  $\varphi(t)$  follows Equ-

tion (3.5) if and only if, its Fourier transform  $\hat{\varphi}(\omega)$  satisfies:

$$\hat{\varphi}(0) \neq 0 \text{ and } \hat{\varphi}^{(n)}(2m\pi) = 0 \text{ for } m \neq 0 \text{ and } n = 0, 1, \dots, N, \quad (3.6)$$

where  $\hat{\varphi}^{(n)}(\omega)$  denotes  $n$ -th order derivative of  $\hat{\varphi}(\omega)$ . Note that the functions that satisfy Strang-Fix conditions can either be of compact support or of infinite support [8]. However, the case of kernels with compact support is more relevant in sampling of FRI signals, since it allows local reconstruction with local complexity.

One important example of kernels that satisfy Strang-Fix conditions is given by the family of B-splines [77]. For example, a B-spline of order zero  $\beta^0(t)$  (or a box function) is given by

$$\begin{aligned} \beta^0(t) &= 1, & 0 \leq t < 1; \\ &= 0, & \text{otherwise,} \end{aligned}$$

with its Fourier transform  $\hat{\beta}^0(\omega) = \frac{1-e^{-i\omega}}{i\omega}$ . Similarly, a B-spline  $\beta^N(t)$  of order  $N$  is obtained from the  $(N+1)$ -fold convolution of the box function  $\beta^0(t)$ , that is,  $\beta^N(t) = \underbrace{\beta^0(t) * \beta^0(t) \dots * \beta^0(t)}_{N+1 \text{ times}}$ . The B-spline of order  $N$  has support size  $N+1$  and can reproduce polynomials up to degree  $N$ . Interestingly, B-splines are the shortest support kernels known for a given order of polynomial approximation. Moreover, any kernel  $\varphi(t)$  that reproduces polynomial up to degree  $N$  can be decomposed into a B-spline and a distribution  $u(t)$  with  $\int u(t)dt \neq 0$ , that is,  $\varphi(t) = u(t) * \beta^N(t)$  [77].

Strang-Fix conditions are used extensively in wavelet theory as well. In particular, any wavelet with  $N+1$  vanishing moments is generated by a scaling function that can reproduce polynomials up to degree  $N$ . This means that such a scaling function is also a valid sampling kernel  $\varphi(t)$  [28].

2. *Exponential reproducing kernels*: Any kernel  $\varphi(t)$  that together with its shifted versions can reproduce exponentials of the form  $e^{\alpha_n t}$  with  $\alpha_n = \alpha_0 + n\lambda$ , where  $\lambda \in \mathbb{C}$ , and  $n = 0, 1, \dots, N$ . That is, any kernel satisfying

$$\sum_{k \in \mathbb{Z}} c_k^n \varphi(t - k) = e^{\alpha_n t}, \quad \text{with } \alpha_n = \alpha_0 + n\lambda \text{ and } n = 0, 1, \dots, N \quad (3.7)$$

for a proper choice of the coefficients  $c_k^n$ .

For example, the kernels that reproduce exponentials are exponential splines (E-splines) [81]. The higher order E-splines are obtained by successive convolution of lower-order ones, and are of compact support. The immediate advantage of compact support property is that it makes the reconstruction algorithm local.

3. *Rational kernels*: Any stable kernel  $\varphi(t)$  with rational Fourier transform of the form

$$\hat{\varphi}(\omega) = \frac{\prod_{m=0}^M (i\omega - b_m)}{\prod_{n=0}^N (i\omega - \alpha_n)} \quad \text{with } M < N, \alpha_n = \alpha_0 + n\lambda \text{ and } \lambda \in \mathbb{C}, \quad (3.8)$$

where  $\hat{\varphi}(\omega)$  is the Fourier transform of  $\varphi(t)$ , and  $i = \sqrt{-1}$ .

This family of kernels include any linear differential acquisition device. That is, any linear device or system for which the input and output are related by a linear differential equation. This includes most of the commonly used electrical or mechanical systems. Again the rational kernels can be converted into compactly supported kernels that reproduce exponentials (e.g. E-splines [81] or generalized E-splines [79]), which in turn, allow reconstruction algorithm to be local and easier to implement [28].

In all cases, the choice of  $N$  depends on the local rate of innovation of the original FRI signal  $g(t)$ . This means that a signal with a higher number of degrees of freedom in a given interval would require a higher order sampling kernel. Nonetheless, in all

cases, the reconstruction algorithm is local, and therefore, more stable [28].

Note that in this thesis we concentrate on compactly supported kernels that satisfy Strang-Fix conditions and thus reproduce polynomials (i.e. the first family of kernels).

### 3.2.4 Reconstruction algorithm

Consider the sampling setup of Figure 3.1. Recall that the reconstruction of FRI signals  $g(t)$  is based on a nonlinear parameter estimation algorithm known as the annihilating filter method [87]. The central theme of the reconstruction algorithm is illustrated in Figure 3.2.

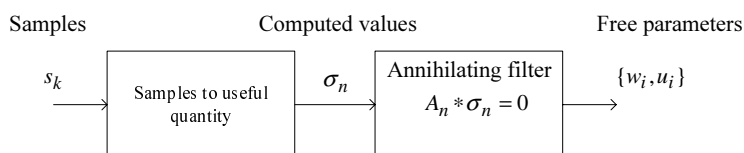


**Figure 3.2: Reconstruction algorithm:** The samples  $s_k = \langle g(t), \varphi(t - k) \rangle$  are used to compute the useful values  $\sigma_n$  of form  $\sigma_n = \sum_{i=0}^{N-1} (u_i)^n w_i$ , where  $\{w_i, u_i\}$  are the free parameters (not necessarily the degrees of freedom) useful in characterizing the input FRI signal  $g(t)$ . The annihilating filter  $A_n$  is designed in such a way that the convolution  $A_n * \sigma_n = 0$ . The filter coefficients  $A_n$  and the values  $\sigma_n$  are then used to retrieve the parameters  $\{w_i, u_i\}$  by solving the systems of linear equations.

The samples  $s_k$  are used to compute a finite number of useful values  $\sigma_n$  of form  $\sigma_n = \sum_{i=0}^{N-1} (u_i)^n w_i$ , where  $\{w_i, u_i\}$  are the free parameters (not necessarily the degrees of freedom) useful in characterizing the input FRI signal  $g(t)$ . Depending on the type of the sampling kernel involved (e.g. sinc/Gaussian [87] or B-splines/scaling functions [28]), the computed values  $\sigma_n$  are either the Fourier coefficients (DFT) or the geometric moments of the original signal  $g(t)$  [28, 87]. In particular, the computed values  $\sigma_n$  are the Fourier coefficients (DFT) in the schemes that use sinc

and Gaussian kernels [87], whereas  $\sigma_n$  are the moments<sup>3</sup> of  $g(t)$  in the schemes that use polynomial reproducing kernels [28].

In both cases, the values  $\sigma_n$  are in form of a powersum series (or linear combinations of exponentials) [47]:

**Definition 2** (Powersum series). *A Powersum series of  $N$  components is given by*

$$\sigma_n = \sum_{i=0}^N (u_i)^n w_i, n = 0, 1, \dots, M - 1, \quad (3.9)$$

where  $\{w_i, u_i\}$  are the  $N$  pairs of parameters to be estimated from  $M$  values of  $\sigma_n$ .

A sequence of form (3.9) was first studied by Baron de Prony in 1795 in finding the decay rates of chemical processes. De Prony showed that in the noiseless case it is possible to find the  $N$  pairs  $\{w_i, u_i\}$  exactly from only  $M = 2N$  values of  $\sigma_n$ . The Prony's method is sometimes called 'real exponential fitting' or 'exponential analysis' in the natural sciences literature [21, 40]. Note that the the values  $\sigma_n$  and the parameters  $\{w_i, u_i\}$  were real-valued in the original formulation. However, they can be complex-valued as well.

Prony's method is known as the annihilating filter method in signal processing literature [73, 87]. It involves locator or annihilating filter- a tool widely used in spectral estimation [73], error-control coding [7] but also for sampling-interpolation [88], array processing [89], and shape reconstruction [30, 61]. In particular, in spectral estimation, it is common to obtain the values of form  $\sigma_n = \sum_{i=0}^{N-1} (u_i)^n w_i$ ,  $w_i \in \mathbb{C}, u_i \in \mathbb{C}, n \in \mathbb{N}$ , where  $w_i$  denotes weights, and  $u_i$  denotes locations of the spectral components.

In such case, the annihilating method consists of two steps:

---

<sup>3</sup>The computation of the moments from samples is given in Equation (3.15).

1. The design of an FIR filter  $A_n, n = 0, 1, \dots, N$  with z-transform

$$A(z) = \sum_{n=0}^N A_n z^{-n} = \prod_{i=0}^{N-1} (1 - u_i z^{-1}) \quad (3.10)$$

that annihilates the quantity  $\sigma_n$ , that is  $A_n * \sigma_n = 0$ , where  $u_i$ 's are distinct.

2. Determination of the locations  $u_i$  and weights  $w_i$  using filter  $A_n$  and finite number of known values  $\sigma_n$ .

Given that one has access to at least  $2N$  values of  $\sigma_n, n = 0, 1, \dots, 2N - 1$ , one can show that for  $\forall n = N + 1, \dots, 2N - 1$ , the convolution

$$\begin{aligned} A_n * \sigma_n &= \sum_{l=0}^N A_l \sigma_{n-l} & (3.11) \\ &= \sum_{l=0}^N \sum_{i=0}^{N-1} w_i A_l (u_i)^{n-l} \\ &= \sum_{i=0}^{N-1} w_i \underbrace{\left( \sum_{l=0}^N A_l (u_i)^{-l} \right)}_{=0 \text{ from (3.10)}} (u_i)^n \\ &= 0. & (3.12) \end{aligned}$$

Since the filter  $A_n$  annihilates the given quantity  $\sigma_n$ , it is known annihilating filter. In case of spectral estimation, the locations  $u_i$  are usually distinct, and hence there exists a unique filter  $A_n$  for the given values  $\sigma_n$ . Moreover, the knowledge of the filter  $A_n$  is sufficient to retrieve the locations  $u_0, u_1, \dots, u_{N-1}$  from the fact that these locations are the roots of the filter  $A(z)$  as shown in (3.10).

Recall that the filter  $A(z)$  consists of  $N$  unknown coefficients  $A_n$  (since  $A_0 = 1$ ). In order to determine the  $N$  unknowns  $A_n$ , we need to solve a system of  $N$  linear equations, and therefore, we require at least  $2N$  values of  $\sigma_n$ . Using the values  $\sigma_0, \sigma_1, \dots, \sigma_{2N-1}$ , the convolution  $\sigma_n * A_n$  can be described by the matrix/vector

form:

$$\begin{bmatrix} \sigma_{N-1} & \sigma_{N-2} & \cdots & \sigma_0 \\ \sigma_N & \sigma_{N-1} & \cdots & \sigma_1 \\ \vdots & \vdots & \ddots & \vdots \\ \sigma_{2N-2} & \sigma_{2N-3} & \cdots & \sigma_{N-1} \end{bmatrix} \begin{bmatrix} A_1 \\ A_2 \\ \vdots \\ A_N \end{bmatrix} = - \begin{bmatrix} \sigma_N \\ \sigma_{N+1} \\ \vdots \\ \sigma_{2N-1} \end{bmatrix}. \quad (3.13)$$

The solution of this Yule-Walker system gives the filter coefficients  $A_n$ . From (3.10), it is straightforward to see that the roots of filter  $A(z)$  are the locations  $u_i$ .

Once the locations  $u_i$  are known, the weights  $w_i$  are determined by solving Equation (3.9) as follows

$$\begin{bmatrix} 1 & 1 & \cdots & 1 \\ u_0 & u_1 & \cdots & u_{N-1} \\ \vdots & \vdots & \ddots & \vdots \\ (u_0)^{N-1} & (u_1)^{N-1} & \cdots & (u_{N-1})^{N-1} \end{bmatrix} \begin{bmatrix} w_0 \\ w_1 \\ \vdots \\ w_{N-1} \end{bmatrix} = \begin{bmatrix} \sigma_0 \\ \sigma_1 \\ \vdots \\ \sigma_{N-1} \end{bmatrix}. \quad (3.14)$$

Given that all locations  $u_i$  are distinct, the Vandermonde system of (3.14) is invertible and yields a unique solution for the weights  $w_i$ .

In a similar manner, one can also show that signals of form  $\sigma_n = \sum_{i=0}^{N-1} (u_i)^n w_i n^R$  are annihilated by the filter  $A(z) = \prod_{i=0}^{N-1} (1 - u_i z^{-1})^{R+1}$ , where  $n, R \in \mathbb{N}$  [87].

The annihilating filter method plays an important role in determining the degrees of freedom (or innovations) in FRI sampling. For example, a stream of  $N$  Diracs  $g(t) = \sum_{i=0}^{N-1} a_i \delta(t - t_i)$  with  $N$  pairs of free parameters  $\{a_i, t_i\}$  (i.e. amplitudes  $a_i$  and locations  $t_i$ ) can be determined from  $M = 2N$  values of  $\sigma_n$  as discussed above. Moreover, the annihilating filter method has been successfully utilized for sampling streams of differentiated Diracs, and piecewise polynomial and sinusoidal signals [6, 28, 87].

### 3.2.5 Key results

Given the important role played by kernels that reproduce polynomials in this thesis, and for the sake of completeness, we now present in more detail the reconstruction schemes of [28]. In particular, we highlight the reconstruction of streams of Diracs, differentiated Diracs, and piecewise polynomial signals. We will recall some of these results in the Radon transform based approach discussed in Chapter 6.

#### Stream of Diracs:

Consider a finite length stream of  $N$  Diracs, that is,  $g(t) = \sum_{i=0}^{N-1} a_i \delta(t - t_i)$ ,  $t \in \mathbb{R}$ . The observed samples  $s_k = \langle g(t), \varphi(t - k) \rangle = \sum_{i=0}^{N-1} a_i \varphi(t_i - k)$ , where for simplicity, we assume that  $T = 1$  and that the sampling kernel  $\varphi(t)$  can reproduce polynomials up to degree  $2N - 1$ . Under these hypotheses, one can retrieve the locations  $t_i$  and amplitudes  $a_i$  of the stream of Diracs  $g(t)$  from its samples  $s_k$ . The reconstruction algorithm operates in three steps [28]:

1. Compute  $2N$  moments  $\mu_n$  of the stream of Diracs  $g(t)$  using the observed samples  $s_k$  and the coefficients  $c_k^n$  identified from Equation (3.5).<sup>4</sup> In fact, it follows that

$$\begin{aligned}
 \mu_n &= \sum_k c_k^n s_k \\
 &\stackrel{(a)}{=} \left\langle g(t), \sum_k c_k^n \varphi(t - k) \right\rangle \\
 &\stackrel{(b)}{=} \left\langle \sum_{i=0}^{N-1} a_i \delta(t - t_i), \sum_k c_k^n \varphi(t - k) \right\rangle \\
 &\stackrel{(c)}{=} \int_{-\infty}^{\infty} \sum_{i=0}^{N-1} a_i \delta(t - t_i) t^n dt \\
 &= \sum_{i=0}^{N-1} a_i t_i^n, \quad n = 0, 1, \dots, 2N - 1, \tag{3.15}
 \end{aligned}$$

---

<sup>4</sup>The coefficients  $c_k^n$  are bounded for a finite interval and can be accurate to the machine precision.

where (a) follows from the linearity of the inner product, (b) from the fact that  $g(t) = \sum_{i=0}^{N-1} a_i \delta(t - t_i)$ , and (c) from the polynomial reproduction property of (3.5). Note that the integral in (c) is the  $n$ -th order moment of the original signal  $g(t)$ .

2. Since the computed moments  $\mu_n = \sum_{i=0}^{N-1} a_i t_i^n$  are in the form of powersum series defined in (3.9), retrieve the locations  $t_i$  and amplitudes  $a_i$  of the  $N$  Diracs from the  $2N$  moments  $\mu_n$  by solving the Yule-Walker system given in (3.13).
3. Once the locations  $t_i$  are known, find the amplitudes  $a_i$  by solving the Vandermonde system given in (3.14).

Following the three steps shown above, it is indeed possible to uniquely reconstruct a stream of  $N$  Diracs from its samples using annihilating filter method. It is also possible to extend this algorithm for an infinite stream of Diracs with finite local rate of innovation using a sequential, local reconstruction algorithm. In particular, this involves grouping of finite number of consecutive Diracs, allowing sufficient empty interval between any two groups. In this situation, each group of Diracs is reconstructed independently and sequentially by using the local reconstruction algorithm discussed above [28].

#### Stream of differentiated Diracs:

In second case, assume that  $g(t)$  is a stream of differentiated Diracs, that is,

$$g(t) = \sum_{i=0}^{N-1} \sum_{r=0}^{R_i-1} a_{i,r} \delta^{(r)}(t - t_i). \quad (3.16)$$

Note that this signal has  $N$  Diracs with  $\hat{N} = \sum_{i=0}^{N-1} R_i$  weights. Moreover, recall that the  $r$ -th derivative of a Dirac is a distribution that satisfies the property  $\int f(t) \delta^{(r)}(t - t_0) dt = (-1)^r f^{(r)}(t_0)$ .

In this case,  $g(t)$  is sampled with a kernel  $\varphi(t)$  that can reproduce polynomials

up to degree  $2\hat{N} - 1$ , and the observed samples  $s_k = \langle g(t), \varphi(t - k) \rangle = \sum_{i=0}^{N-1} \sum_{r=0}^{R_i-1} (-1)^r a_{i,r} \varphi^{(r)}(t_i - k)$  are used for computing the moments  $\mu_n$  of differentiated Diracs. The moments are then used to retrieve the locations  $t_i$  and the weights  $a_{i,r}$  of differentiated Diracs  $g(t)$  by employing the annihilating filter  $A_n$  with the z-transform  $A(z) = \prod_{i=0}^{N-1} (1 - t_i z^{-1})^{R_i}$ . The annihilating filter method, in this case, involves solution of  $\hat{N}$  equations using  $2\hat{N}$  moments  $\mu_n$ .

### Piecewise polynomial signals:

Finally, consider a piecewise polynomial signal  $g(t)$  with pieces of maximum degree  $R - 1$  ( $R \geq 0$ ). That is,

$$g(t) = \sum_{i \in \mathbb{Z}} \sum_{r=0}^{R-1} a_{i,r} (t - t_i)_+^r, \quad (3.17)$$

where  $t_+^r = \max(t, 0)^r$ . Clearly, the  $R$ -th order derivative of  $g(t)$  is a stream of differentiated Diracs given by  $g^{(R)}(t) = \sum_{i \in \mathbb{Z}} \sum_{r=0}^{R-1} r! a_{i,r} \delta^{(R-r-1)}(t - t_i)$ . This means that if one can relate the samples of  $g(t)$  to those of  $g^{(R)}(t)$  then one can use the results of differentiated Diracs in sampling piecewise polynomial signals. This is indeed shown in [28] by recalling the link between discrete differences and continuous derivatives. More precisely, consider a function  $\varphi(t)$  with Fourier transform  $\hat{\varphi}(\omega)$  and consider the difference:  $\varphi(t) - \varphi(t - 1)$ . The Fourier transform of  $\varphi(t) - \varphi(t - 1)$  is

$$\varphi(t) - \varphi(t - 1) \Leftrightarrow \hat{\varphi}(\omega) (1 - e^{-i\omega}) = i\omega \hat{\varphi}(\omega) \frac{(1 - e^{-i\omega})}{i\omega} = i\omega \hat{\varphi}(\omega) \hat{\beta}^0(\omega).$$

It thus follows that

$$\varphi(t) - \varphi(t - 1) = \frac{d}{dt} [\varphi(t) * \beta^0(t)]. \quad (3.18)$$

The above formula can be used in the sampling formulation as follows: Consider the samples  $s_k = \langle g(t), \varphi(t - k) \rangle$  where  $\varphi(t)$  is a generic sampling kernel. Let  $s_k^{(1)}$

denote the first order finite difference  $s_{k+1} - s_k$ . It then follows that

$$\begin{aligned} s_k^{(1)} = s_{k+1} - s_k &= \langle g(t), \varphi(t - k - 1) - \varphi(t - k) \rangle \\ &\stackrel{(a)}{=} \left\langle g(t), -\frac{d}{dt} [\varphi(t - k) * \beta^0(t - k)] \right\rangle \\ &\stackrel{(b)}{=} \left\langle \frac{d}{dt} g(t), \varphi(t - k) * \beta^0(t - k) \right\rangle, \end{aligned}$$

where equality (a) is obtained using Equation (3.18) and (b) follows from integration by parts. Thus, the samples  $s_k^{(1)}$  are equivalent to those given by the inner products between the derivative of  $g(t)$  and the new kernel  $\varphi(t) * \beta^0(t)$ . In a similar manner, it is straightforward to show that the  $R$ -th order finite difference  $s_k^{(R)}$  represents the samples obtained by sampling  $g^{(R)}(t)$  with the kernel  $\varphi(t) * \beta^{R-1}(t)$ , where  $\beta^{R-1}(t)$  is the B-spline of degree  $R-1$ . Moreover, if we assume that  $\varphi(t)$  is of compact support  $L$  and that it can reproduce polynomials of maximum degree  $n$  then the new kernel  $\varphi(t) * \beta^{R-1}(t)$  has support  $L + R$  and can reproduce polynomials of maximum degree  $n + R$ .

Now, assume that we observe the samples  $s_k = \langle g(t), \varphi(t/T - k) \rangle$  of an infinite-length piecewise polynomial signal  $g(t)$ , where  $\varphi(t)$  is the sampling kernel of support  $L$  that can reproduce polynomials up to certain degree  $n$ , and  $T$  is the sampling interval. Also assume that  $g(t)$  has pieces of maximum degree  $R-1$  ( $R \geq 0$ ) with at most  $N$  polynomial discontinuities in an interval of size  $2N(L + R)T$ .

Given the samples  $s_k$ , it is possible to compute the  $R$ -th order finite difference  $s_k^{(R)}$  given by:  $s_k^{(R)} = \mathcal{D}^{(R)}[s_k] = \langle g^{(R)}(t), \varphi(t/T - k) * \beta^{R-1}(t/T - k) \rangle$ . In fact, the difference samples  $s_k^{(R)}$  are equivalent to the inner products between differentiated Diracs  $g^{(R)}(t)$  and new kernel  $\varphi(t/T) * \beta^{R-1}(t/T)$ , where  $\beta^{R-1}(t)$  is the B-spline of degree  $R-1$ . The new kernel is of compact support  $L + R$  that can reproduce polynomials up to degree  $n + R$ . Since by hypothesis,  $g(t)$  has at most  $N$  polynomial discontinuities in an interval of size  $2N(L + R)T$ , the signal  $g^{(R)}(t)$  consists of at

most  $N$  differentiated Diracs at locations  $t_i$  with  $\hat{N} = NR$  number of weights  $a_{i,r}$  in the same interval. Now recalling back the case of differentiated Diracs, one can uniquely retrieve the weights  $a_{i,r}$  and the locations  $t_i$  from the  $2\hat{N} = 2NR$  moments of  $g^{(R)}(t)$ . However, to be able to obtain the  $2\hat{N} = 2NR$  moments, the new sampling kernel must be able to reproduce polynomials at least up to degree  $2NR - 1$ , that is, the condition  $n + R \geq 2NR - 1$  must be satisfied. This means that the original sampling kernel  $\varphi(t)$  must be able to reproduce polynomials of maximum degree  $n \geq 2NR - R - 1$ .

Thus, it shows that by computing the finite differences of the samples  $s_k$  of the polynomial signal  $g(t)$ , one can obtain a new set of samples  $s_k^{(R)}$  which is sufficient for retrieving the the weights  $a_{i,r}$  and the locations  $t_i$  of the differentiated Diracs  $g^{(R)}(t)$ , and therefore, for reconstructing the original polynomial signal  $g(t)$ .

With this, we complete the review of 1-D FRI sampling. We now formulate the multidimensional FRI framework.

### 3.3 Multidimensional Framework

Note that the sampling of 2-D FRI signals (e.g. Diracs and bilevel polygons) has been considered by Maravic et al. [54,55]. The schemes of [54,55] first compute the Fourier coefficients from the samples and then use these coefficients in the annihilating filter method for retrieving the degrees of freedom of FRI signals. In particular, in [54], it was shown that a set of  $N$  2-D Diracs or a bilevel-convex polygon with  $N$  corner points can also be reconstructed by sampling its  $N + 1$  Radon projections. However, the schemes of [54,55] are complex and unstable since they employ infinite support sinc and Gaussian sampling kernels. In the proposed work, we consider the kernels with compact support that reproduce polynomials.

Recalling the existing background and the scope of our work, we now

present the multidimensional FRI framework in detail. In the following discussion, we describe the FRI signals, the sampling setup, the sampling kernels, and the reconstruction algorithms. Mainly, we concentrate on the 2-D case.

### FRI signals

It is possible to extend the notion of FRI in 2-D (or in higher dimension). In particular, a 2-D FRI signal  $g(x, y)$  is given by

$$g(x, y) = \sum_{i=0}^N \sum_{j \in \mathbb{Z}} \sum_{k \in \mathbb{Z}} \lambda_{i,j,k} \phi_i(x - x_j, y - y_k), \quad (3.19)$$

where  $\{\phi_i(x, y)\}$  is the set of known functions. The free parameters, in this case, are the shifts  $x_j$  and  $y_k$  and the coefficients  $\lambda_{i,j,k}$ , where  $x, y, \lambda_{i,j,k} \in \mathbb{R}$ . The local rate of innovation is then given by  $\rho_{xy} = \frac{1}{\tau_x \tau_y} C_g \left[ \left(-\frac{\tau_x}{2}, \frac{\tau_x}{2}\right), \left(-\frac{\tau_y}{2}, \frac{\tau_y}{2}\right) \right]$  determined over the window of size  $\tau_x \times \tau_y$ .

For instance, when  $\phi_i(x, y) = \delta(x, y)$ , and both  $x_j - x_{j-1}$  and  $y_k - y_{k-1}$  are i.i.d. random variables with exponential density, then  $g(x, y)$  describes a separable 2-D Poisson process. A set of 2-D Diracs is one particular realization of the 2-D Poisson process. Other examples of 2-D FRI signals include lines in 2-D, polygonal lines, convex and bilevel polygons, and classes of algebraic curves (e.g. ellipses, cardioids, and lemniscates) [55, 60].

### Sampling setup

The 2-D FRI sampling setup is shown in Figure 3.3, where a continuous 2-D FRI signal  $g(x, y)$  is prefiltered by a smoothing (sampling) kernel  $h_a(x, y) = \varphi(-x/T_x, -y/T_y)$ , and the filtered version  $g(x, y) * \varphi(-x/T_x, -y/T_y)$  is sampled

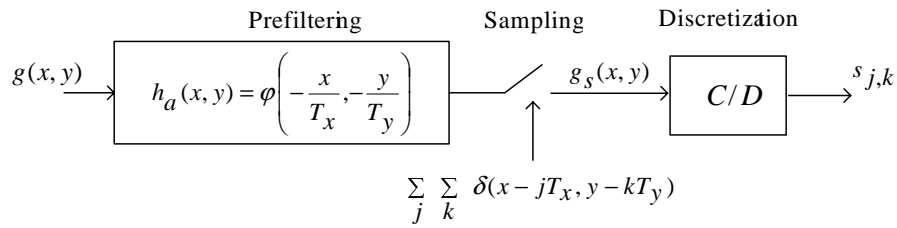


**Figure 3.3: The 2-D FRI sampling setup:** Continuous signal  $g(x, y)$  is convolved by a smoothing kernel  $\varphi(x, y)$  and then sampled uniformly by  $\sum_{j \in \mathbb{Z}} \sum_{k \in \mathbb{Z}} \delta(x - jT_x, y - kT_y)$  to obtain the sampled signal  $g_s(x, y)$ . The block  $C/D$  represents continuous to discrete transformation and corresponds to the read-out of sample values  $s_{j,k}$ ,  $j, k \in \mathbb{Z}$  from  $g_s(x, y)$ .

uniformly to obtain the set of samples  $s_{j,k} = g_s(jT_x, kT_y)$  given by

$$\begin{aligned}
 s_{j,k} &= g(x, y) * h_a(x, y) |_{x=jT_x, y=kT_y} \\
 &= \int \int_{\mathbb{R}^2} g(x, y) \varphi(x/T_x - j, y/T_y - k) dx dy \\
 &= \langle g(x, y), \varphi(x/T_x - j, y/T_y - k) \rangle,
 \end{aligned} \tag{3.20}$$

where  $T_x, T_y \in \mathbb{R}^+$  are sampling intervals along  $x$  and  $y$  directions respectively. For simplicity, we assume  $T_x = T_y = 1$  unless explicitly specified. Note that the setup of Figure 3.3 is typical for acquisition devices and processing algorithms, and can be extended to higher dimensions [78].

### Sampling kernels

In this thesis, we consider any compactly supported kernel that satisfies Strang-Fix conditions [74] and therefore reproduce polynomials up to certain degree  $n$ . To be more precise, the 2-D sampling kernel  $\varphi(x, y)$ , in our case, is given by the tensor product of two 1-D functions  $\varphi(x)$  and  $\varphi(y)$  that reproduce polynomials  $x^\alpha$  and  $y^\beta$  respectively, where  $\alpha, \beta \in \{0, 1, \dots, n\}$  and  $x, y \in \mathbb{R}$ . In particular, there exists real

coefficients  $c_{j,k}^{\alpha,\beta}$  such that the kernel  $\varphi(x, y)$  satisfies:

$$\sum_{j=-\infty}^{\infty} \sum_{k=-\infty}^{\infty} c_{j,k}^{\alpha,\beta} \varphi(x-j, y-k) = x^\alpha y^\beta, \quad (3.21)$$

where  $\alpha, \beta$  specify the degrees of polynomials that the kernel  $\varphi(x, y)$  can reproduce along  $x$  and  $y$  directions respectively. For instance, B-spline of order  $n$  can reproduce polynomial up to degree  $n$ , i.e.  $\alpha, \beta \in \{0, 1, \dots, n\}$ . Note that  $c_{j,k}^{\alpha,0}$  is responsible for the reproduction of a polynomial of degree  $\alpha$  along  $x$ -axis, while  $c_{j,k}^{0,\beta}$  is responsible for the reproduction of a polynomial of degree  $\beta$  along  $y$ -axis.

Furthermore, for  $\alpha = \beta = 0$ , if the kernel  $\varphi(x, y)$  allows  $c_{j,k}^{\alpha,\beta} = c_{j,k}^{0,0} = 1$ , then (3.21) reduces to

$$\sum_{j=-\infty}^{\infty} \sum_{k=-\infty}^{\infty} \varphi(x-j, y-k) = 1. \quad (3.22)$$

The above equation states that the sum of shifted versions of sampling kernel produces unit amplitude polynomial of degree zero, and is often termed as ‘partition of unity’ in wavelet community. For instance, orthogonal Daubechies scaling functions [22] and biorthogonal B-splines [77] are included in the class of kernels that satisfy the property of (3.21).

## Reconstruction algorithms

The polynomial reproduction property of the sampling kernel allows us to compute the moments of FRI signal from its samples. To be more precise, assume that we observe the samples  $s_{j,k} = \langle g(x, y), \varphi(x/T_x - j, y/T_y - k) \rangle$  of the FRI signal  $g(x, y)$ , where  $\varphi(x, y)$  the sampling kernel of compact support that reproduce polynomials up to certain degree  $n$  along both  $x$  and  $y$  directions, and  $T_x, T_y$  are the sampling intervals along these directions. Moreover, from (3.21), we know that there exists

coefficients  $c_{j,k}^{\alpha,\beta}$ ,  $\alpha, \beta \in \{0, 1, \dots, n\}$  such that the weighted sum of samples (for  $T_x = T_y = 1$ ) follows

$$\begin{aligned}
\sum_j \sum_k c_{j,k}^{\alpha,\beta} s_{j,k} &\stackrel{(a)}{=} \sum_j \sum_k c_{j,k}^{\alpha,\beta} \langle g(x, y), \varphi(x - j, y - k) \rangle \\
&= \sum_j \sum_k c_{j,k}^{\alpha,\beta} \int \int_{\mathbb{R}^2} g(x, y) \varphi(x - j, y - k) dx dy \\
&= \int \int_{\mathbb{R}^2} g(x, y) \sum_j \sum_k c_{j,k}^{\alpha,\beta} \varphi(x - j, y - k) dx dy \\
&\stackrel{(b)}{=} \int \int_{\mathbb{R}^2} g(x, y) x^\alpha y^\beta dx dy \\
&= \mu_{\alpha,\beta}, \tag{3.23}
\end{aligned}$$

where  $\mu_{\alpha,\beta}$  are the (geometric) moments of signal  $g(x, y)$  by definition [39, 75]. The equalities (a) and (b) are obtained from (3.20) and (3.21) respectively.

In theory, these moments are then used in the annihilating filter method for retrieving the degrees of freedom of  $g(x, y)$  and thus for reconstructing the signal  $g(x, y)$  uniquely. However, as opposed to 1-D FRI sampling, the reconstruction algorithms for the multidimensional case are more intricate. In particular, depending on the classes of FRI signals, the reconstruction algorithms also involve various tools such as directional derivatives (Chapter 4), complex-moments (Chapter 5) and Radon transform (Chapter 6).

### 3.4 Summary

In this chapter, we reviewed the recent developments in sampling (and perfect reconstruction) of signals with finite rate of innovation (FRI) [28, 87]. In particular, we described the key elements of 1-D and multidimensional FRI framework.

In the following chapters, we employ the multidimensional framework and present novel approaches for sampling higher dimensional FRI signals.

# Chapter 4

## Directional Derivatives based Approach

### 4.1 Introduction

We have presented multidimensional FRI framework in the previous chapter. We are now ready to propose novel sampling schemes for higher dimensional FRI signals. In this chapter, we consider sampling of 2-D Diracs and planar polygons.

In order to introduce the essential role of polynomial reproducing kernels in our sampling schemes, we begin with a ‘warm up’ example, that is, local reconstruction of 2-D Diracs. In fact, the example of Diracs serves as a comprehensive model for understanding various sampling approaches of this thesis, including the directional derivatives based approach presented in the second part of this chapter. In directional derivatives based approach, we discover a link between ‘continuous domain directional derivatives’ and ‘discrete domain directional difference’ using the fundamentals of lattice theory [20]. We then show that this link together with the local reconstruction scheme of 2-D Diracs can be utilized for local reconstruction of planar polygons.

In the following section, we begin with a local reconstruction scheme for 2-D Diracs. We then extend the reconstruction of 2-D Diracs for planar polygons in Section 4.3. Finally, in Section 4.4, we summarize the contribution of this chapter.

## 4.2 Local reconstruction of 2-D Diracs

Consider a simple class of FRI signals, that is, a set of 2-D Diracs  $g(x, y) = \sum_{i \in \mathbb{Z}} a_i \delta(x - x_i, y - y_i)$ ,  $a, x, y \in \mathbb{R}$  as shown in Figure 4.1. Note that each 2-D Dirac can be parameterized by an amplitude  $a_i$  and a coordinate position  $(x_i, y_i)$ , and thus has a finite number of degrees of freedom (or rate of innovation) which equals three.

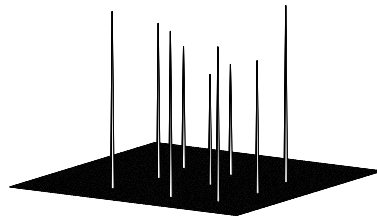


**Figure 4.1: A set of 2-D Diracs:**  $g(x, y) = \sum_{i \in \mathbb{Z}} a_i \delta(x - x_i, y - y_i)$

Now recall the 2-D sampling setup given in Figure 3.3. For the given set of 2-D Diracs  $g(x, y)$ , we observe the samples  $s_{j,k} = \langle g(x, y), \varphi(x/T_x - j, y/T_y - k) \rangle$ , where  $T_x, T_y$  are the sampling intervals and  $\varphi(x, y)$  is the sampling kernel with compact support  $L_x \times L_y$ .

We assume that the Diracs in signal  $g(x, y)$  are distributed in such a way that there is at most one Dirac in any given window of size  $(L_x + 1)T_x \times (L_y + 1)T_y$ . The kernel  $\varphi(x, y)$ , we consider, satisfies partition of unity (3.22) and can reproduce polynomials up to degree one, i.e.  $\alpha, \beta \in \{0, 1\}$  in (3.21). Since the kernel satisfies partition of unity (3.22), an algebraic sum of shifted kernels is constant and is equal to unity. This is illustrated in Figure 4.2 (b). Moreover, from (3.21), the linear

combinations of shifted kernels with coefficients  $c_{j,k}^{1,0}$  and  $c_{j,k}^{0,1}$  produce unit-slope linear functions along  $x$  and  $y$  directions (see Figures 4.2 (c) and (d)).

Since there is at most one Dirac in any given window of size  $(L_x + 1)T_x \times (L_y + 1)T_y$ , we are sure that only  $L_x \times L_y$  samples  $s_{j,k} = \langle g(x, y), \varphi(x/T_x - j, y/T_y - k) \rangle$  are influenced by a unique Dirac  $a_p \delta(x - x_p, y - y_p)$ ,  $p \in \mathbb{Z}$ .

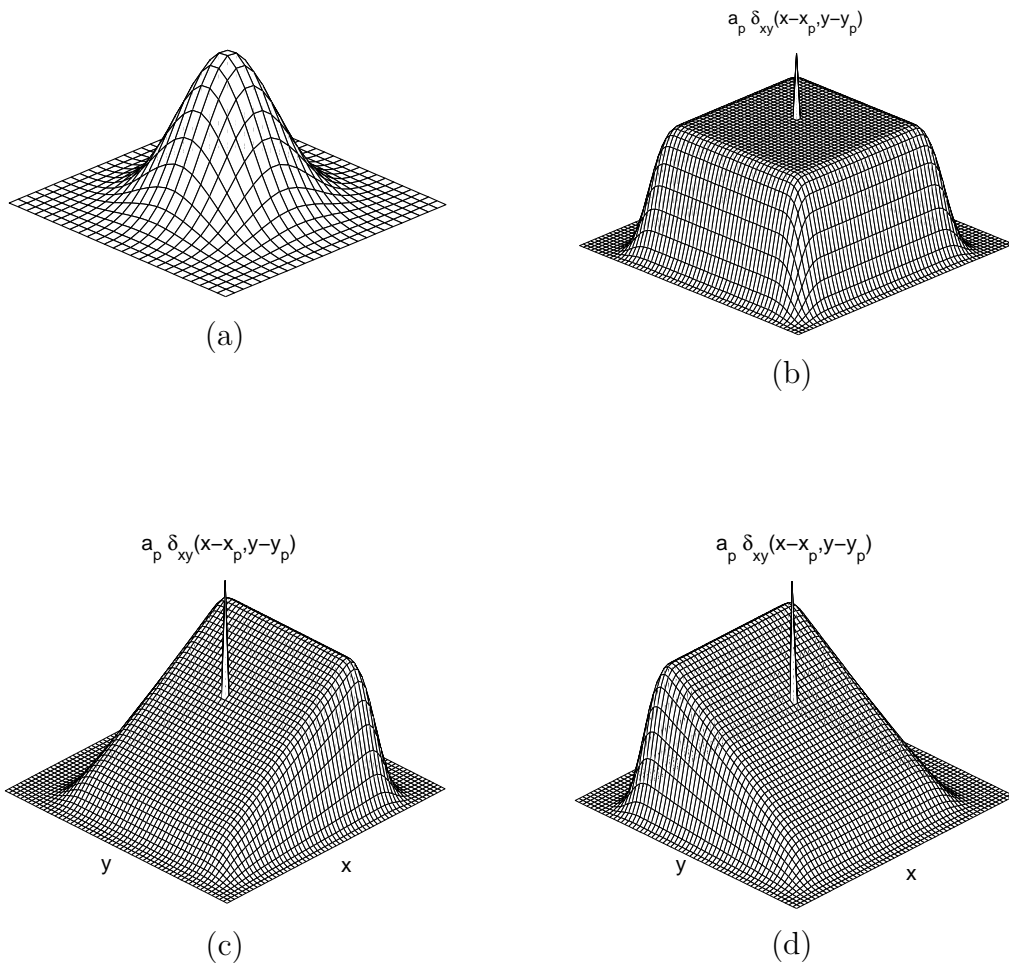


**Figure 4.2: Local reconstruction of a 2-D Dirac  $a_p \delta(x - x_p, y - y_p)$ :** The B-spline sampling kernel  $\beta^3(x, y)$  that can reproduce polynomials up to degree 3 is given in part (a). The reproduction of polynomial of degree 0 (partition of unity) responsible for the determination of amplitude  $a_p$  is given in part (b), whereas the reproduction of polynomials of degree 1 along  $x$  and  $y$  directions responsible for the determination of coordinates  $x_p$  and  $y_p$  are given in part (c) and part (d) respectively.

Therefore, for a given Dirac (assuming  $T_x = T_y = 1$ ), we have that

$$\begin{aligned}
\sum_{j=1}^{L_x} \sum_{k=1}^{L_y} s_{j,k} &= \left\langle a_p \delta(x - x_p, y - y_p), \sum_{j=1}^{L_x} \sum_{k=1}^{L_y} \varphi(x - j, y - k) \right\rangle \\
&= \int_{-\infty}^{\infty} \int_{-\infty}^{\infty} a_p \delta(x - x_p, y - y_p) \left( \sum_{j=1}^{L_x} \sum_{k=1}^{L_y} \varphi(x - j, y - k) \right) dx dy \\
&= a_p \sum_{j=1}^{L_x} \sum_{k=1}^{L_y} \varphi(x_p - j, y_p - k) \\
&= a_p \quad (\text{from Equation (3.22)})
\end{aligned} \tag{4.1}$$

and

$$\begin{aligned}
\sum_{j=1}^{L_x} \sum_{k=1}^{L_y} c_{j,k}^{1,0} s_{j,k} &= \left\langle a_p \delta(x - x_p, y - y_p), \sum_{j=1}^{L_x} \sum_{k=1}^{L_y} c_{j,k}^{1,0} \varphi(x - j, y - k) \right\rangle \\
&= \int_{-\infty}^{\infty} \int_{-\infty}^{\infty} a_p \delta(x - x_p, y - y_p) \left( \sum_{j=1}^{L_x} \sum_{k=1}^{L_y} c_{j,k}^{1,0} \varphi(x - j, y - k) \right) dx dy \\
&= a_p \sum_{j=1}^{L_x} \sum_{k=1}^{L_y} c_{j,k}^{1,0} \varphi(x_p - j, y_p - k) \\
&= a_p x_p. \quad (\text{from Equation (3.21)})
\end{aligned} \tag{4.2}$$

Similarly, it is straightforward to arrive at  $\sum_{j=1}^{L_x} \sum_{k=1}^{L_y} c_{j,k}^{0,1} s_{j,k} = a_p y_p$  in the line of above derivation.

Hence, the amplitude  $a_p$  of a given Dirac is retrieved using

$$a_p = \sum_{j=1}^{L_x} \sum_{k=1}^{L_y} s_{j,k}, \tag{4.3}$$

and the position  $(x_p, y_p)$  is retrieved using

$$x_p = \frac{\sum_{j=1}^{L_x} \sum_{k=1}^{L_y} c_{j,k}^{1,0} s_{j,k}}{a_p}, \quad y_p = \frac{\sum_{j=1}^{L_x} \sum_{k=1}^{L_y} c_{j,k}^{0,1} s_{j,k}}{a_p}, \tag{4.4}$$

where the coefficients  $c_{j,k}^{1,0}$  and  $c_{j,k}^{0,1}$  are identified from Equation (3.21).

The above equations allow us to reconstruct one Dirac per time from the set of samples  $s_{j,k} = \langle g(x, y), \varphi(x/T_x - j, y/T_y - k) \rangle$ . To be more precise, since the samples of an arbitrary Dirac do not overlap with the samples of any other Dirac, each Dirac is completely characterized by a distinct group of only  $L_x \times L_y$  samples. In such condition, the observed samples  $s_{j,k}$  (with precomputed coefficients  $c_{j,k}^{1,0}$  and  $c_{j,k}^{0,1}$ ) are used to reconstruct the Diracs as follows:

**Algorithm 1. Local reconstruction of 2-D Diracs**

1. Start with a hypothetical window of  $L_x \times L_y$  points overlayed at the top-left corner<sup>1</sup> of the set of samples  $s_{j,k}$ .
2. If all  $L_x \times L_y$  elements of  $s_{j,k}$  within the window are non zero, compute the amplitude  $a_p$  and the position  $(x_p, y_p)$  of the detected Dirac  $a_p \delta(x - x_p, y - y_p)$  using (4.3) and (4.4).
3. Shift the window by one sample (from left to right and then from top to bottom) and repeat the Step 2 for all possible shifts (i.e. until the window arrives at the bottom-right corner of  $s_{j,k}$ ).

Thus, the local reconstruction scheme of 2-D Diracs follows

**Proposition 1.** Assume a sampling kernel  $\varphi(x, y)$  with support  $L_x \times L_y$  that can reproduce polynomials of degree zero and one along the Cartesian axes  $x$  and  $y$ . A set of finite amplitude 2-D Diracs  $g(x, y) = \sum_{i \in \mathbb{Z}} a_i \delta(x - x_i, y - y_i)$  is uniquely determined from its samples  $s_{j,k} = \langle g(x, y), \varphi(x/T_x - j, y/T_y - k) \rangle$ , if there is at most one Dirac in any distinct window of size  $(L_x + 1)T_x \times (L_y + 1)T_y$ .

Essentially, this proposition concludes the local reconstruction of 2-D Diracs. However, in the following paragraphs, we introduce a moment based interpretation to the local reconstruction of 2-D Diracs and initiate a background for the global and higher dimensional extensions discussed in the following chapters.

---

<sup>1</sup>Here, we assume that the samples  $s_{j,k}$  are stored in matrix form, that is, the top-left corner corresponds to sample  $s_{0,0}$ .

Recall that the polynomial reproduction property of the sampling kernel  $\varphi(x, y)$  makes it possible to obtain the (geometric) moments  $\mu_{\alpha, \beta}$  of the original signal  $g(x, y)$  from its samples  $s_{j,k}$ , that is,  $\mu_{\alpha, \beta} = \sum_j \sum_k c_{j,k}^{\alpha, \beta} s_{j,k}$  (see Equation (3.23)). In case of Diracs, we assume that the Diracs are sufficiently apart, and that the kernel  $\varphi(x, y)$  can reproduce polynomials of degree zero and one. These assumptions enable us to obtain the first order moments  $\mu_{\alpha, \beta}$ ,  $\alpha, \beta \in \{0, 1\}$  of each 2-D Dirac locally. Therefore, the Equations (4.3) and (4.4) can also be written in the following form:

$$a_p = \sum_{j=1}^{L_x} \sum_{k=1}^{L_y} s_{j,k} = \mu_{0,0}, \quad (4.5)$$

and

$$x_p = \frac{\sum_{j=1}^{L_x} \sum_{k=1}^{L_y} c_{j,k}^{1,0} s_{j,k}}{a_p} = \frac{\mu_{1,0}}{\mu_{0,0}}, \quad y_p = \frac{\sum_{j=1}^{L_x} \sum_{k=1}^{L_y} c_{j,k}^{0,1} s_{j,k}}{a_p} = \frac{\mu_{0,1}}{\mu_{0,0}}, \quad (4.6)$$

where  $\mu_{\alpha, \beta}$ ,  $\alpha, \beta \in \{0, 1\}$  are the local moments of a given 2-D Dirac  $a_p \delta(x - x_p, y - y_p)$ .

Note that in the local reconstruction scheme we only need to determine three unknown parameters:  $a_p$ ,  $x_p$  and  $y_p$  per time. However, the reconstruction of two or more 2-D Diracs at a time (i.e. the global scheme) requires a higher number of unknowns to be determined. This in turn involves the solution of a large system of equations, which uses the higher order moments and the annihilating filter method. This scenario is treated in the following chapter using complex-moments.

Moreover, it is possible to show that the local reconstruction scheme of 2-D Diracs can be extended to higher dimensions (i.e. in 3-D and above) using the multidimensional FRI framework of Chapter 3. For instance, a set of 3-D Diracs  $g(x, y, z) = \sum_{i \in \mathbb{Z}} a_i \delta(x - x_i, y - y_i, z - z_i)$ , spaced sufficiently apart, can be sampled by a 3-D kernel  $\varphi(x, y, z) = \varphi(x)\varphi(y)\varphi(z)$  of support  $L_x \times L_y \times L_z$  that can reproduce polynomials of degree zero and one along the Cartesian axes  $x$ ,  $y$  and  $z$ . The observed samples  $s_{j,k,l} = \langle g(x, y, z), \varphi(x/T_x - j, y/T_y - k, z/T_z - l) \rangle$  with pre-

computed coefficients  $c_{j,k,l}^{\alpha,\beta,\gamma}$ ,  $\alpha, \beta, \gamma \in \{0, 1\}$  can be used to retrieve the amplitude  $a_p$  and the position  $(x_p, y_p, z_p)$  of an arbitrary Dirac locally by extending Equations (4.3) and (4.4) for the 3-D case. Again, the reconstruction of two or more multidimensional Diracs per time (i.e. the global reconstruction) is more intricate and involves ‘annihilating filter based back-projection’ (AFBP) algorithm discussed in Chapter 6.

### 4.3 Planar polygons

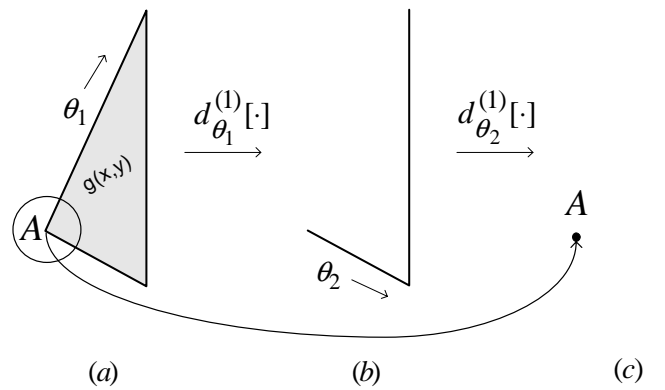


**Figure 4.3: The continuous model for local reconstruction of polygonal corner points: For a given planar polygon  $g(x, y)$ , a pair of two successive first order directional derivatives  $d_{\theta_1}^{(1)}[\cdot]$  and  $d_{\theta_2}^{(1)}[\cdot]$  decomposes a corner point  $A$  into a 2-D Dirac.**

Consider a planar polygon  $g(x, y)$  with  $N$  corner points as shown in Figure 4.3(a). The sides of the polygon are identified by the 2-D lines:

$$y_i = \tan(\theta_i) x_i + b_i, \quad i = 1, 2, \dots, N,$$

where  $b_i$  are the shifts and  $\theta_i$  are the orientations.

For this  $N$  sided polygon, consider an arbitrary corner point (e.g. point  $A$  in Figure 4.3) formed by two sides with orientations  $\theta_1$  and  $\theta_2$ . A pair of first or-

der directional derivatives  $d_{\theta_1}^{(1)}[\cdot]$  and  $d_{\theta_2}^{(1)}[\cdot]$  on  $g(x, y)$  can be written as

$$\begin{aligned} d_{\theta_2}^{(1)} \left[ d_{\theta_1}^{(1)} [g(x, y)] \right] &= \cos(\theta_1) \cos(\theta_2) \frac{\partial^2}{\partial x^2} (g(x, y)) + \sin(\theta_1 + \theta_2) \frac{\partial}{\partial y} \left( \frac{\partial}{\partial x} (g(x, y)) \right) + \\ &\quad \sin(\theta_1) \sin(\theta_2) \frac{\partial^2}{\partial y^2} (g(x, y)). \end{aligned} \quad (4.7)$$

Clearly, this pair of directional derivatives produces a 2-D Dirac at the corner point  $A$  (see Figures 4.3(b) and (c)). Likewise, we can ‘turn’ other corner points into Diracs by selecting proper pairs of derivatives. This suggests that the local reconstruction scheme of 2-D Diracs, described in the previous section, can be tailored for reconstructing the corner points of planar polygons.

However, the practical difficulty is that, instead of a direct access to the polygon  $g(x, y)$ , we only have access to its samples  $s_{j,k} = \langle g(x, y), \varphi(x/T_x - j, y/T_y - k) \rangle$ , where  $\varphi(x, y)$  is a sampling kernel that can reproduce a polynomial of degree zero. Fortunately, discrete equivalent to the directional derivatives is directional differences, and directional differences can be connected to the corresponding continuous derivatives. The connection between them is based on the fundamentals of lattice theory, and in particular, involves subsampling over rectangular lattices. Since we are dealing with a finite number of samples  $s_{j,k}$ ,  $j, k \in \mathbb{Z}$  over a uniform rectangular grid, we focus onto the 2-D integer lattices. For further details on lattice theory, we refer to [20, 44, 85].

For a given corner point (e.g. point  $A$ ), assume that the orientations  $\theta_1$  and  $\theta_2$  of the two adjacent polygonal sides are such that  $\theta_1 = \tan^{-1} \left( \frac{v_{1,2}}{v_{1,1}} \right)$  and  $\theta_2 = \tan^{-1} \left( \frac{v_{2,2}}{v_{2,1}} \right)$  where  $v_{1,1}, v_{1,2}, v_{2,1}, v_{2,2} \in \mathbb{Z}$ . Let the corresponding base lattice  $\Lambda$  be given by  $\Lambda = \{ \lambda : \lambda = n_1 \vec{v}_1 + n_2 \vec{v}_2 \}$ , where  $\vec{v}_i = [v_{i,1}, v_{i,2}]$ ,  $i = 1, 2$  are its basis vectors and  $n_1, n_2 \in \mathbb{N}$ . The lattice  $\Lambda$  is characterized by a sampling matrix  $V_\Lambda = \begin{bmatrix} v_{1,1} & v_{1,2} \\ v_{2,1} & v_{2,2} \end{bmatrix}$  with determinant  $\det(V_\Lambda)$ .

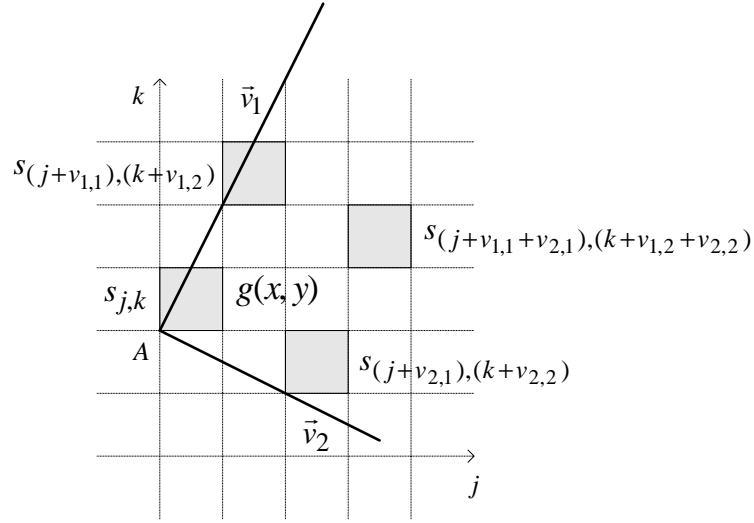


**Figure 4.4:** The map for computing two successive differences  $\mathcal{D}_{\theta_1}^{(1)}[\cdot]$  and  $\mathcal{D}_{\theta_2}^{(1)}[\cdot]$  on every pair of samples  $s_{j,k}$  arranged in accordance with the base lattice  $\Lambda$ . The first difference is computed along the lattice direction  $\vec{v}_1$  followed by the second difference along the direction  $\vec{v}_2$ .

Now, as illustrated in Figure 4.4, we compute the finite differences of the samples  $s_{j,k}$ , first along the lattice direction  $\vec{v}_1$  and then along  $\vec{v}_2$ . Assuming  $T_x = T_y = 1$ , a pair of directional differences  $\mathcal{D}_{\theta_1}^{(1)}[\cdot]$  and  $\mathcal{D}_{\theta_2}^{(1)}[\cdot]$  modifies the samples  $s_{j,k}$  into a new set of samples  $s'_{j,k}$  as given by

$$\begin{aligned}
 s'_{j,k} &= \mathcal{D}_{\theta_2}^{(1)} \left[ \mathcal{D}_{\theta_1}^{(1)} [s_{j,k}] \right] \\
 &= \left\{ s_{(j+v_{2,1}+v_{1,1}), (k+v_{2,2}+v_{1,2})} - s_{(j+v_{2,1}), (k+v_{2,2})} \right\} - \left\{ s_{(j+v_{1,1}), (k+v_{1,2})} - s_{j,k} \right\} \\
 &= \left\langle g(x, y), \right. \\
 &\quad \left. \left\{ \varphi(x - (j + v_{2,1} + v_{1,1}), y - (k + v_{2,2} + v_{1,2})) - \varphi(x - (j + v_{2,1}), y - (k + v_{2,2})) \right\} \right. \\
 &\quad \left. - \left\{ \varphi(x - (j + v_{1,1}), y - (k + v_{1,2})) - \varphi(x - j, y - k) \right\} \right\rangle.
 \end{aligned}$$

By using Parseval's identities, and after certain manipulations (refer to Appendix A),

we derive that

$$\begin{aligned} \frac{s'_{j,k}}{|\det(V_\Lambda)|} &= \frac{\mathcal{D}_{\theta_2}^{(1)} \left[ \mathcal{D}_{\theta_1}^{(1)} [s_{j,k}] \right]}{|\det(V_\Lambda)|} \\ &= \left\langle \frac{\partial}{\partial \theta_2} \left( \frac{\partial}{\partial \theta_1} (g(x, y)) \right), \zeta_{\theta_1, \theta_2}(x - j, y - k) \right\rangle, \end{aligned} \quad (4.8)$$

where  $\zeta_{\theta_1, \theta_2}(x, y) = \frac{(\varphi(x, y) * \beta_{\theta_1}^0(x, y)) * \beta_{\theta_2}^0(x, y)}{|\sin(\theta_2 - \theta_1)|}$  is a modified kernel, and  $\beta_{\theta_1}^0(x, y)$  and  $\beta_{\theta_2}^0(x, y)$  are the 1-D B-splines of order zero in  $xy$ -plane along orientations  $\theta_1$  and  $\theta_2$  respectively. The skewness of the modified kernel depends on the orientations  $\theta_1$  and  $\theta_2$ , and therefore, we denote the modified kernel as ‘directional kernel’. For instance, assuming that the original kernel  $\varphi(x, y)$  is a Haar scaling function (see Figure 4.5(a)), the directional kernel  $\zeta_{\theta_1, \theta_2}(x, y)$  is shown in Figure 4.5(b).

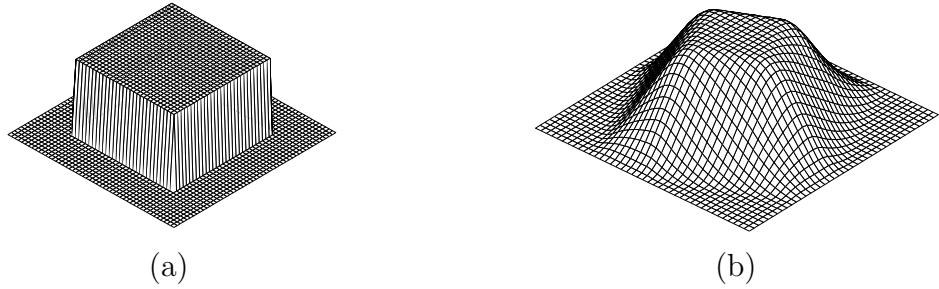


**Figure 4.5: Original and directional kernels: (a)  $\varphi(x, y)$  is a Haar scaling function with support  $1 \times 1$ , (b) Directional kernel  $\zeta_{\theta_1, \theta_2}(x, y)$  with support  $4 \times 4$  is related to the corner point of the polygon  $g(x, y)$  formed by the two sides with orientations  $\tan(\theta_1) = 2/1$  and  $\tan(\theta_2) = -1/2$ .**

The kernel  $\zeta_{\theta_1, \theta_2}(x, y)$  is of compact support  $(|v_{1,1}| + |v_{2,1}| + L_x) \times (|v_{1,2}| + |v_{2,2}| + L_y)$ , where  $L_x \times L_y$  is the support of the original sampling kernel  $\varphi(x, y)$ . The skewed shape of kernel  $\zeta_{\theta_1, \theta_2}(x, y)$ , and the factors  $\frac{1}{|\det(V_\Lambda)|}$  and  $\frac{1}{|\sin(\theta_2 - \theta_1)|}$  in Equation (4.8) are due to subsampling over integer lattices. It is important to note that there exists an independent directional kernel  $\zeta_{\theta_1, \theta_2}(x, y)$  for each independent corner point of the polygon  $g(x, y)$ .

Equation (4.8) states that the new samples  $s'_{j,k}$  given by the finite differences

along  $\vec{v}_1$  and  $\vec{v}_2$  are equivalent to those obtained by sampling  $d_{\theta_2}^{(1)} \left[ d_{\theta_1}^{(1)} [g(x, y)] \right]$  with the directional kernel  $\zeta_{\theta_1, \theta_2}(x, y)$ . Moreover, if all the corner points of the polygon  $g(x, y)$  are sufficiently apart such that there is only one corner point (e.g. point  $A$ ) in the support of its associated directional kernel  $\zeta_{\theta_1, \theta_2}(x, y)$ , then it is possible to reconstruct the corner points using the local reconstruction scheme of 2-D Diracs as discussed in Section 4.2.

Assuming that the kernel  $\varphi(x, y)$  satisfies partition of unity (3.22), the directional kernel  $\zeta_{\theta_1, \theta_2}(x, y)$  always satisfies partition of unity (3.22) but also reproduces polynomials up to degree one (3.21) along both  $x$  and  $y$  directions. The polynomial reproduction property of the directional kernel  $\zeta_{\theta_1, \theta_2}(x, y)$  enables us to determine the amplitude  $a_p$  and the coordinate position  $(x_p, y_p)$  of the resultant 2-D Dirac  $a_p \delta(x - x_p, y - y_p)$  at the given corner point from the new set of samples  $s'_{j,k}$ . In fact, we only need an isolated group of samples (i.e.  $(|v_{1,1}| + |v_{2,1}| + L_x) \times (|v_{1,2}| + |v_{2,2}| + L_y)$  samples) in the vicinity of the given corner point. In particular, the local reconstruction scheme of (4.3) and (4.4) for the case of polygonal corner point (e.g. point  $A$ ) leads to the following identities

$$a_p = \frac{\sum_j \sum_k s'_{j,k}}{|\det(V_\Lambda)|}, \quad (4.9)$$

$$x_p = \frac{\sum_j \sum_k c_{j,k}^{1,0} s'_{j,k}}{a_p |\det(V_\Lambda)|}, \quad y_p = \frac{\sum_j \sum_k c_{j,k}^{0,1} s'_{j,k}}{a_p |\det(V_\Lambda)|}, \quad (4.10)$$

where  $c_{j,k}^{1,0}$  and  $c_{j,k}^{0,1}$  are the coefficients of kernel  $\zeta_{\theta_1, \theta_2}(x, y)$ , identified from Equation (3.21).

Clearly, the coordinate pair  $(x_p, y_p)$  gives the position of the given corner point (e.g. point  $A$ ), whereas  $a_p$  gives the amplitude of the planar polygon  $g(x, y)$ . It is straightforward to see that this reconstruction scheme applies equally to all

the corner points of  $g(x, y)$  using their associated directional kernels. From the knowledge of the corner points and associated directions, it is possible to perfectly reconstruct the polygon  $g(x, y)$ . Finally, to summarize the local reconstruction of planar polygons, we have

**Proposition 2.** *Assume an  $N$  sided planar polygon  $g(x, y)$  with the orientations  $\theta_i, i = 1, 2, \dots, N$  of its sides satisfying  $\tan(\theta_i) \in \mathbb{Q}$ , and the sampling kernel  $\varphi(x, y)$  that can reproduce polynomial of at least degree zero. A set of samples  $s_{j,k} = \langle g(x, y), \varphi(x/T_x - j, y/T_y - k) \rangle$  is sufficient to reconstruct the polygon  $g(x, y)$  provided that there is at most one corner point in the support of each directional kernel  $\zeta_{\theta_i, \theta_{i+1}}(x, y)$ , where  $\theta_{i+N} = \theta_i$ .*

In practice, the orientations of the polygonal sides are not known in advance. However, if we assume that the sides of the  $N$  sided planar polygon  $g(x, y)$  take only a finite number of orientations  $\theta_i$ , where  $\tan(\theta_i) \in \mathbb{Q}$ , then by trying all possible orientations we can retrieve the correct ones. More precisely, given a sufficiently large set of samples  $s_{j,k} = \langle g(x, y), \varphi(x/T_x - j, y/T_y - k) \rangle$ , the reconstruction of  $g(x, y)$  is realized by the following steps:

**Algorithm 2. Local reconstruction of planar polygon**

1. Apply a distinct pair of finite differences  $\mathcal{D}_{\theta_1}^{(1)}[\cdot]$  and  $\mathcal{D}_{\theta_2}^{(1)}[\cdot]$  over the set of samples  $s_{j,k}$  and obtain a new set of samples  $s'_{j,k} = \mathcal{D}_{\theta_2}^{(1)} \left[ \mathcal{D}_{\theta_1}^{(1)} [s_{j,k}] \right]$ .
2. Check whether at least one isolated group of samples in  $s_{j,k}$  is segmented. If yes, then using the local reconstruction scheme of (4.9) and (4.10), determine the amplitude  $a_p$  and the position  $(x_p, y_p)$  of the Dirac, and therefore, the corner point.
3. Reiterate from step 1 (with a new pair) until all  $N$  corner points are determined.
4. Using the recovered corner points and the successful pairs of orientations, reconstruct the polygon  $g(x, y)$ .

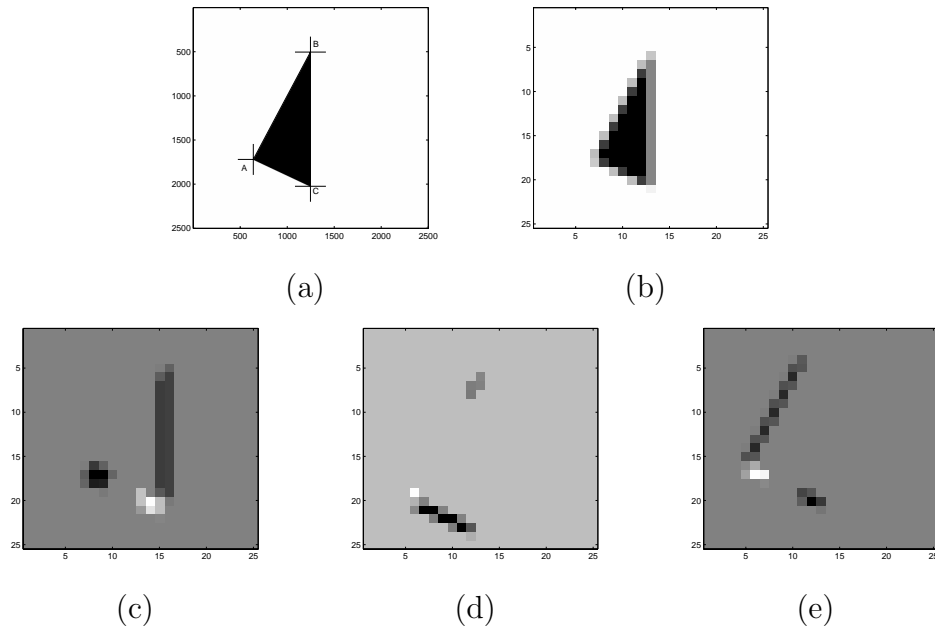


**Figure 4.6: Simulation result for the local reconstruction of planar polygon:** The original image of size  $2500 \times 2500$  pixels as given in part (a) consists of a triangle  $g(x, y)$  with three corner points  $A$ ,  $B$ , and  $C$  such that its sides  $AB$ ,  $BC$ , and  $CA$  are oriented at  $\tan(\theta_1) = 2$ ,  $\tan(\theta_3) = -\infty$ , and  $\tan(\theta_2) = -\frac{1}{2}$  respectively. The part (b) consists of the set of  $25 \times 25$  samples  $s_{j,k}$  is obtained by sampling  $g(x, y)$  with the Haar kernel  $\varphi(x, y)$  of size  $100 \times 100$  pixels. The set of new samples  $s'_{j,k}$  as shown in part (c) is obtained by computing two successive directional differences  $\mathcal{D}_{\theta_1}^{(1)}[\cdot]$  and  $\mathcal{D}_{\theta_2}^{(1)}[\cdot]$  (i.e. along the sides  $AB$  and  $AC$ ) on the original set of samples  $s_{j,k}$ . Note that the isolated group of samples in part (c) represents the corner point  $A$ . Similarly, the other two sets of differentiated samples  $s'_{j,k}$  with isolated corner points  $B$  and  $C$  are given in parts (d) and (e) respectively. Using the local reconstruction scheme of (4.9) and (4.10), the reconstructed corner points  $A, B$ , and  $C$  (marked with  $+$ ) are given in part (a).

We conclude this section with a simple numerical example. The simulation result is shown in Figure 4.6. As shown in Figure 4.6(a), consider a planar polygon  $g(x, y)$  (i.e. a planar triangle  $ABC$ ) with three corner points  $A$ ,  $B$ , and  $C$  such that its sides  $AB$ ,  $BC$ , and  $CA$  are oriented at  $\tan(\theta_1) = 2$ ,  $\tan(\theta_3) = -\infty$ , and  $\tan(\theta_2) = -\frac{1}{2}$  respectively. The set of samples  $s_{j,k} = \langle g(x, y), \varphi(x - j, y - k) \rangle$  given in part (b) is obtained by sampling the polygon  $g(x, y)$  with the Haar kernel  $\varphi(x, y)$ . The new set of samples  $s'_{j,k} = \mathcal{D}_{\theta_2}^{(1)} \left[ \mathcal{D}_{\theta_1}^{(1)} [s_{j,k}] \right]$  as shown in part (c) is derived from the original set of samples  $s_{j,k}$  using two successive differences  $\mathcal{D}_{\theta_1}^{(1)}[\cdot]$  and  $\mathcal{D}_{\theta_2}^{(1)}[\cdot]$

along the orientations  $AB$  and  $AC$ . In a similar manner, the other two sets of differentiated samples  $s'_{j,k}$  are obtained using the difference pairs  $\mathcal{D}_{\theta_3}^{(1)} \left[ \mathcal{D}_{\theta_1}^{(1)} [s_{j,k}] \right]$  and  $\mathcal{D}_{\theta_3}^{(1)} \left[ \mathcal{D}_{\theta_2}^{(1)} [s_{j,k}] \right]$  as given in parts (d) and (e) respectively. Note that the small isolated groups of samples in parts (c), (d), and (e) represent three 2-D Diracs located at the corner points  $A$ ,  $B$ , and  $C$  respectively. These corner points are retrieved using the local reconstruction scheme of (4.9) and (4.10) and are marked with  $+$  in Figure 4.6(a). The reconstruction of the corner points is exact to machine precision. The computational cost of this local reconstruction algorithm is linear with the number  $N$  of the corner points, that is, of the order  $\mathcal{O}(N)$ .

In the case of an image with two or more polygons, each polygon is reconstructed independently assuming that the polygons are sufficiently apart and that the samples of one polygon do not influence the samples of any other polygon.

## 4.4 Summary

In this chapter, we have proposed local schemes for sampling and perfect reconstruction of Diracs and planar polygons. The contribution of this chapter is three-fold: 1) In the first part of the chapter, we have shown that it is possible to perfectly reconstruct Diracs in 2-D (and above) from their samples locally (i.e. one Diracs per time); 2) In the second part of the chapter, we extended the local reconstruction scheme of 2-D Diracs for planar polygons and proposed an algorithm useful for super-resolution corner reconstruction; 3) The algorithm, we developed, exploits a novel link between directional derivatives and differences based on the fundamentals of lattice theory. This new link provides a background for the Radon transform based approach discussed in Chapter 6.

# Chapter 5

## Complex-moments based Approach

### 5.1 Introduction

In the previous chapter, we have shown that planar polygons can be reconstructed locally if the corner points are sufficiently apart. In this chapter, we present a global scheme for reconstructing bilevel and convex polygons with close corner points. In particular, we consider simultaneous recovery of all the corner points using complex-moments and annihilating filter method. In addition to bilevel and convex polygons, we show that sets of 2-D Diracs and quadrature domains (e.g. circles, ellipses, and cardioids) are perfectly reconstructed from their samples. Implicitly, we provide a sampling perspective to the ‘shape from moments method’ of [30, 60].

In the following section, we provide a background on moments and draw a useful connection to obtain the moments of a signal from its samples. In Sections 5.3, we use this ‘sample-moment’ connection for global reconstruction of bilevel-convex polygons. We then extend the reconstruction scheme of bilevel polygons for 2-D Diracs and quadrature domains in Section 5.4. Finally, in Section 5.5, we summarize

the contribution of this chapter.

## 5.2 Background and ‘sample-moment’ connection

The relationship between shapes and moments finds its application in many diverse fields such as computer tomography, geophysical inversion, thermal imaging, and pattern recognition [29, 30, 39, 60]. In fact, the general formulation of recovering shapes from their moments is a highly ill-posed problem [30, 60]. However, it has been shown that certain classes of shapes such as binary polygons and quadrature domains are uniquely determined by a finite number of moments [23, 60].

Formally, the geometric moments  $\mu_{\alpha,\beta}$  of order  $n = (\alpha + \beta)$  of a square-integrable function  $g(x, y)$  in the closure  $\Omega \in \mathbb{R}^2$  are defined as [39, 75]

$$\mu_{\alpha,\beta} = \int \int_{\Omega} g(x, y) x^{\alpha} y^{\beta} dx dy, \quad (5.1)$$

where  $\alpha, \beta \in \{0, 1, \dots, n\}$ .

Similarly, the complex-moments  $\tau_{\alpha,\beta}$  of order  $n = (\alpha + \beta)$  of  $g(x, y)$  are defined as [1]

$$\tau_{\alpha,\beta} = \int \int_{\Omega} g(x, y) (x + iy)^{\alpha} (x - iy)^{\beta} dx dy, \quad (5.2)$$

where  $i = \sqrt{-1}$ .

Sometimes, it is convenient to use simple complex-moment  $\tau_n$  of order  $n = (\alpha + \beta)$  as given by [61]

$$\tau_n = \int \int_{\Omega} g(x, y) (x + iy)^n dx dy. \quad (5.3)$$

Note that the binomial expansion of  $(x + iy)^n$  in (5.3) makes it possible to retrieve

an  $n$ th order complex-moment  $\tau_n$  from the geometric moments  $\mu_{\alpha,\beta}$  of order  $n$  using:

$$\tau_n = \sum_{\beta=0}^n \binom{n}{\beta} i^\beta \mu_{\alpha,\beta}, \quad \text{with } \alpha = n - \beta. \quad (5.4)$$

Moreover, one can also compute weighted complex-moments  $\tau_n''$  from the simple complex-moment  $\tau_n$  [61]. For instance, the complex-moment with weight  $n(n-1)$  is given by  $\tau_n'' = n(n-1)\tau_{n-2}$ ,  $\forall n \geq 2$ , where  $\tau_0'' = \tau_1'' = 0$ .

Now going back to the 2-D sampling setup of Figure 3.3, assume that we observe a sampled version of  $g(x, y)$ , that is, we observe samples  $s_{j,k} = \langle g(x, y), \varphi(x/T_x - j, y/T_y - k) \rangle$ , where the kernel  $\varphi(x, y)$  can reproduce polynomials up to degree  $n$  along  $x$  and  $y$  directions. From the polynomial reproduction property of kernel  $\varphi(x, y)$ , we know that it is possible to retrieve the moments  $\mu_{\alpha,\beta}$  of  $g(x, y)$  from its samples  $s_{j,k}$  (recall Equation (3.23)). In fact, we have that

$$\begin{aligned} \mu_{\alpha,\beta} &= \int \int_{\Omega} g(x, y) x^\alpha y^\beta dx dy \\ &\stackrel{(a)}{=} \int \int_{\Omega} g(x, y) \sum_j \sum_k c_{j,k}^{\alpha,\beta} \varphi(x - j, y - k) dx dy \\ &= \sum_j \sum_k c_{j,k}^{\alpha,\beta} \int \int_{\Omega} g(x, y) \varphi(x - j, y - k) dx dy \\ &\stackrel{(b)}{=} \sum_j \sum_k c_{j,k}^{\alpha,\beta} s_{j,k}, \quad \forall \alpha, \beta \in \{0, 1, \dots, n\}, \end{aligned} \quad (5.5)$$

where the equalities (a) and (b) are obtained from (3.21) and (3.20) respectively. Note that  $c_{j,k}^{\alpha,\beta}$  are the pre-computed coefficients associated with the kernel  $\varphi(x, y)$ .

This result is at the heart of our sampling schemes. With the ‘sample-moment’ connection (5.5) at our disposal, we now begin with the global reconstruction of bilevel-convex polygons.

### 5.3 Global reconstruction of bilevel polygons

Assume that  $g(x, y)$  is a bilevel, simply connected, and non-degenerate polygon with  $N$  corner points (vertices)  $z_l$ ,  $l = 1, 2, \dots, N$  in the complex plane  $z = x + iy$ . Moreover, the polygon  $g(x, y)$  is regular and resides in a bounded closure  $\Omega$ . For such a polygon, Davis's theorem [23] states that

$$\int \int_{\Omega} g(x, y) h^{(2)}(z) dx dy = \sum_{l=1}^N \varrho_l h(z_l), \quad (5.6)$$

where  $h(z)$  is an analytic function with  $h^{(2)}(z)$  being its second order derivative, and  $\varrho_l$  are complex coefficients.

The above result suggests that the integral of the second derivative of any analytic function  $h(z)$  over a bilevel polygonal region  $g(x, y)$  (enclosed within the closure  $\Omega$ ) in the complex plane depends on the values of  $h(z)$  at the corner points  $z_l$ . This means that the double integral in (5.6) is accurately determined by a finite number of complex values. In particular, Davis showed that any triangular region in the complex plane is uniquely determined by its complex-moments  $\tau_n$  up to order 3 [23, 61].

Later, Milanfar et al. [61] re-examined Davis's result (5.6) by employing a specific analytic function  $h(z) = z^n$ . To be more precise, assuming that the corner points  $z_l$  (with  $z_l^*$  as their complex conjugates) are arranged in counter-clockwise direction in order of increasing index and satisfy modulo operation  $z_l = z_{l+N}$ , it was shown that the complex coefficients  $\varrho_l$  are given by [61]:

$$\varrho_l = \frac{i}{2} \left( \frac{z_{l-1}^* - z_l^*}{z_{l-1} - z_l} - \frac{z_l^* - z_{l+1}^*}{z_l - z_{l+1}} \right), \quad l = 1, 2, \dots, N,$$

and that

$$\begin{aligned}
\sum_{l=1}^N \varrho_l (z_l)^n &= \int \int_{\Omega} g(x, y) h^{(2)}(z) dx dy \\
&= \int \int_{\Omega} g(x, y) (z^n)^{(2)} dx dy \\
&= n(n-1) \int \int_{\Omega} g(x, y) (x + iy)^{n-2} dx dy \\
&= n(n-1) \tau_{n-2} \\
&= \tau_n'' \quad \forall n \geq 2,
\end{aligned} \tag{5.7}$$

where  $\tau_n''$  is the complex-moment with weight  $n(n-1)$ , and is related to the simple complex-moment  $\tau_n$  of (5.3) by  $\tau_n'' = n(n-1)\tau_{n-2}$ . Note that  $\tau_0'' = \tau_1'' = 0$  by definition.

It is clear to see that the weighted complex-moments  $\tau_n'' = \sum_{l=1}^N (z_l)^n \varrho_l$  are represented by the linear combinations of exponentials  $(z_l)^n$ . Since the moments  $\tau_n'' = \sum_{l=1}^N (z_l)^n \varrho_l$  are in the form of powersum series (3.9), one can employ the annihilating filter method for retrieving the  $N$  corner points  $z_l$  of  $g(x, y)$  using the  $2N$  complex-moments  $\tau_n''$ ,  $n = 0, 1, \dots, 2N-1$  (recall Section 3.2.4 for annihilating filter method). Moreover, if the bilevel polygon  $g(x, y)$  is convex, it can be uniquely reconstructed from the retrieved corner points  $z_l$  [61]. Hence, it follows that a bilevel and convex polygon with  $N$  corner points is uniquely reconstructed from the weighted complex-moments  $\tau_n''$  up to order  $2N-1$  or from the simple complex-moments  $\tau_n$  up to order  $2N-3$  [61]. In fact, it is straightforward to compute the simple complex-moments  $\tau_n$  up to order  $2N-3$  from the geometric moments  $\mu_{\alpha, \beta}$  of order  $2N-3$  by using (5.4).

Let us now return to the sampling setup of Figure 3.3, where the input signal  $g(x, y)$  is a bilevel and convex polygon with  $N$  corner points  $z_l = (x_l + iy_l)$ ,  $l = 1, 2, \dots, N$ . Clearly,  $g(x, y)$  is an FRI signal with degrees of freedom equal to  $2N$ . For this setup, what we observe is a set of samples  $s_{j,k} = \langle g(x, y), \varphi(x/T_x - j, y/T_y - k) \rangle$  produced by the kernel  $\varphi(x, y)$  that can reproduce polynomials up to degree  $2N-3$

along  $x$  and  $y$  directions. The polynomial reproduction property of the kernel  $\varphi(x, y)$  allows us to obtain the moments  $\mu_{\alpha, \beta}$  of the polygon  $g(x, y)$  from its samples  $s_{j, k}$  (recall the ‘sample-moment’ connection given in (5.5)). In particular, since the kernel can reproduce polynomials up to degree  $2N - 3$ , it allows us to obtain the geometric moments  $\mu_{\alpha, \beta}$  of order  $2N - 3$  using:  $\mu_{\alpha, \beta} = \sum_j \sum_k c_{j, k}^{\alpha, \beta} s_{j, k}$ , where  $\alpha, \beta = \{0, 1, \dots, 2N - 3\}$ . The knowledge of  $\mu_{\alpha, \beta}$  then allows us to retrieve the simple complex-moments  $\tau_n$  up to order  $2N - 3$  using:  $\tau_n = \sum_{\beta=0}^n \binom{n}{\beta} i^\beta \mu_{\alpha, \beta}$  with  $\alpha = n - \beta$  and  $n = 0, 1, \dots, 2N - 3$ . Finally, we obtain the weighted complex-moments  $\tau_n''$  of (5.7) using:  $\tau_n'' = n(n - 1)\tau_{n-2}$  for all  $n = 2, 3, \dots, 2N - 1$  and  $\tau_0'' = \tau_1'' = 0$ .

We use these  $2N$  complex-moments  $\tau_n''$  in the annihilating filter method to retrieve the corner points  $z_l$  of the polygon  $g(x, y)$ . To be more precise, we design a filter  $A_n$  such that the convolution  $\tau_n'' * A_n = 0$ . The  $N$  complex roots of the annihilating filter  $A(z)$  give the positions of the  $N$  corner points  $z_l$  (in  $x + iy$  form). The assumption of convexity and bilevelness<sup>1</sup> guarantees a unique reconstruction of the polygon  $g(x, y)$ . Consequently, the global scheme for sampling bilevel-convex polygon is summarized as follows

**Proposition 3.** *A bilevel and convex polygon  $g(x, y)$  with  $N$  corner points is uniquely determined from the samples  $s_{j, k} = \langle g(x, y), \varphi(x/T_x - j, y/T_y - k) \rangle$  provided that the sampling kernel  $\varphi(x, y)$  can reproduce polynomials up to degree  $2N - 3$  along both the Cartesian axes  $x$  and  $y$ .*

The simulation result, for a simple scenario, is shown in Figure 5.1. The original bilevel image  $g(x, y)$  with three convex polygons: triangle, rectangle, and pentagon is shown in Figure 5.1(a). We observe the set of samples  $s_{j, k} = \langle g(x, y), \varphi(x/T_x - j, y/T_y - k) \rangle$  produced by the inner product between  $g(x, y)$  and sampling kernel  $\varphi(x, y)$  as shown in part (b). In this case, the sampling kernel is a B-spline  $\beta^7(x, y)$  of order 7 that can reproduce polynomials up to degree seven.

---

<sup>1</sup>If the convex polygon is large enough such that there is at least one sample enclosed within the polygonal boundary then we can reconstruct its amplitude as well.

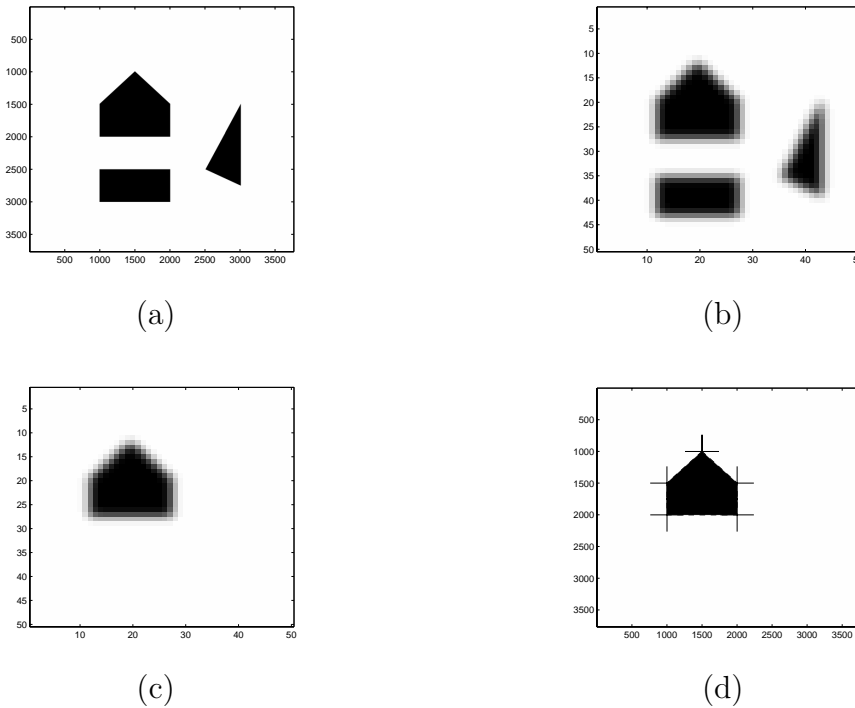


**Figure 5.1: Simulation result for the global reconstruction of bilevel-convex polygons:** (a) The original image  $g(x,y)$  consists of three bilevel polygons: triangle, rectangle, and pentagon. (b) The set of samples  $s_{j,k} = \langle g(x,y), \varphi(x/T_x - j, y/T_y - k) \rangle$  produced by the inner product between  $g(x,y)$  and sampling kernel  $\varphi(x,y)$ . In this case, the sampling kernels is a B-spline  $\beta^7(x,y)$  of order 7 that can reproduce polynomials up to degree seven. (c) The sampled version of the pentagon. (d) Original pentagon and reconstructed corner points (marked with +).

Moreover, we assume that the polygons are sufficiently apart, and for that reason, the samples of one polygon do not overlap with the samples of the other polygons. This makes it possible to reconstruct each polygon independently. In fact, for each set of polygonal samples, we first compute the complex-moments  $\tau_n''$  of appropriate order (i.e.  $2N$  moments for  $N$  corner points) and then run the annihilating filter method to retrieve the corner points. For instance, a set of samples around the pentagon is given in part (c). The reconstructed corner points of the pentagon are indicated with + in part (d) and the reconstruction is exact to machine precision.

The computational cost of this global reconstruction is influenced by the cost

of root finding and is of the order of  $\mathcal{O}(N^3)$ , where  $N$  is the number of corner points.

## 5.4 2-D Diracs and Quadrature domains

In addition to bilevel polygons, there are other 2-D signals that are uniquely determined from a finite number of moments. We now investigate sampling of such signals.

### 2-D Diracs:

Assume that  $g(x, y)$  is a set of  $N$  2-D Diracs in the compact closure  $\Omega$ , that is,  $g(x, y) = \sum_{l=1}^N a_l \delta(x - x_l, y - y_l)$ , where  $a_l$  denotes amplitudes and  $z_l = x_l + iy_l$  denotes positions. Notice that  $g(x, y)$  is not regular in  $\Omega$ , and therefore, in this case, we cannot apply Davis's theorem. However, it is straightforward to obtain the simple complex-moments  $\tau_n$  of  $g(x, y)$  as given by

$$\begin{aligned} \tau_n &= \int \int_{\Omega} g(x, y) (x + iy)^n dx dy \\ &= \int \int_{\Omega} \sum_{l=1}^N a_l \delta(x - x_l, y - y_l) (x + iy)^n dx dy \\ &= \sum_{l=1}^N a_l (z_l)^n, \quad \text{where } z_l = x_l + iy_l. \end{aligned} \quad (5.8)$$

Note that the moments  $\tau_n = \sum_{l=1}^N a_l (z_l)^n$  in above formulation are in form of powersum series (3.9). Therefore, by using the annihilating filter method, one can accurately retrieve the amplitudes  $a_l$  and positions  $z_l$  of  $N$  Diracs from the  $2N$  complex-moments  $\tau_n, n = 0, 1, \dots, 2N - 1$ . The knowledge of degrees of freedom (i.e. amplitudes  $a_l$  and positions  $z_l$ ) is sufficient for the unique reconstruction of  $g(x, y)$ .

From the sampling point of view, we observe the Diracs  $g(x, y)$  in form of its

samples  $s_{j,k} = \langle g(x, y), \varphi(x/T_x - j, y/T_y - k) \rangle$ , where  $\varphi(x, y)$  is the sampling kernel that can reproduce polynomials up to degree  $2N - 1$ . From the samples  $s_{j,k}$ , we compute the moments  $\tau_n$  of (5.8) by using the identities (5.4) and (5.5). To be more precise, the moments are given by

$$\tau_n = \sum_{\beta=0}^n \binom{n}{\beta} i^\beta \sum_j \sum_k c_{j,k}^{\alpha,\beta} s_{j,k} \quad \text{with} \quad \alpha = n - \beta, \quad (5.9)$$

where  $n = \{0, 1, \dots, 2N - 1\}$ , and using these moments we reconstruct the original Diracs. Therefore, we have the following result:

**Proposition 4.** *A set of  $N$  2-D Diracs  $g(x, y) = \sum_{l=1}^N a_l \delta(x - x_l, y - y_l)$  is uniquely determined from its samples  $s_{j,k} = \langle g(x, y), \varphi(x/T_x - j, y/T_y - k) \rangle$  provided that the sampling kernel  $\varphi(x, y)$  can reproduce polynomials up to degree  $2N - 1$  along both the Cartesian axes  $x$  and  $y$ .*

A simple simulation result for the global reconstruction of 2-D Diracs is illustrated in Figure 5.2. The input image  $g(x, y)$  of size  $3711 \times 3711$  pixels shown in Figure 5.2(b) contains  $N = 3$  Diracs with amplitudes 10, 20, and 30 located at pixel positions (1100, 1300), (1500, 900), and (1500, 1300) respectively. The Diracs are filtered by the B-spline sampling kernel  $\varphi(x, y) = \beta^5(x, y)$  (given in part (a)) of support  $379 \times 379$  pixels that can reproduce polynomials up to degree  $2N - 1 = 5$ . The filtered (or low resolution) version  $g(x, y) * \varphi(-x/T_x, -y/T_y)$  of part (c) is then uniformly sampled (with  $T_x = T_y = 63$  pixels) to obtain the set of  $50 \times 50$  samples  $s_{j,k} = \langle g(x, y), \varphi(x/T_x - j, y/T_y - k) \rangle$  as shown in part (d) (excluding some boundary samples). Since the B-spline kernel can reproduce polynomials up to degree  $2N - 1 = 5$ , the samples  $s_{j,k}$  are used to compute the simple complex-moments  $\tau_n$  up to order  $2N - 1 = 5$ . By using these moments in the annihilating filter method, the Diracs are reconstructed and the reconstruction is exact to machine precision.

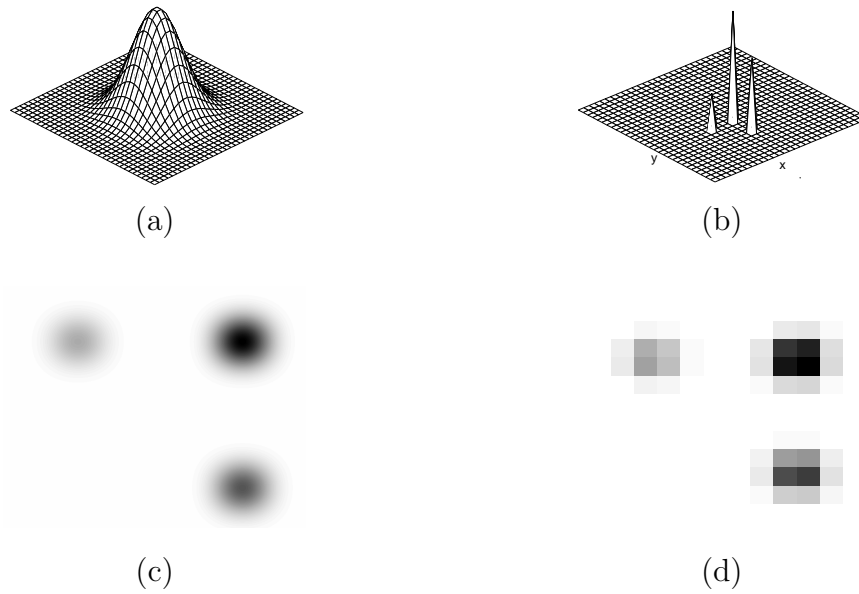


**Figure 5.2: Global reconstruction of 2-D Diracs:** (a) The B-spline sampling kernel  $\varphi(x, y) = \beta^5(x, y)$  of support  $379 \times 379$  pixels that can reproduce polynomials up to degree  $2N - 1 = 5$ . (b) The input image  $g(x, y)$  of size  $3711 \times 3711$  pixels contains  $N = 3$  Diracs with amplitudes 10, 20, and 30 located at pixel positions  $(1100, 1300)$ ,  $(1500, 900)$ , and  $(1500, 1300)$  respectively. (c) The low resolution version  $g(x, y) * \varphi(-x/T_x, -y/T_y)$  of the Diracs obtained by the convolution of  $g(x, y)$  with the smoothing kernel  $\varphi(x, y)$ . (d) The set  $50 \times 50$  of samples  $s_{j,k} = \langle g(x, y), \varphi(x/T_x - j, y/T_y - k) \rangle$  obtained by the uniform sampling of the low resolution version of part (c), where the sampling intervals  $T_x = T_y = 63$  pixels.

### Quadrature domains:

Finally, we consider a class of algebraic planar domains in the complex plane  $z = x + iy$ . Formally, a quadrature domain is a bounded planar domain of closure  $\Omega$  such that for any regular analytic function  $h(z)$  in  $\Omega$ , it satisfies [60]

$$\int \int_{\Omega} h(z) dx dy = \sum_{k=1}^m \sum_{j=0}^{\nu_k-1} a_{k,j} h^{(j)}(\gamma_k), \quad (5.10)$$

where  $\gamma_k \in \Omega$  are the quadrature nodes, and for  $1 \leq k \leq m$   $N = \nu_1 + \nu_2 + \dots + \nu_m$  is the order of the domain. The simplest example of the quadrature domain is the circle of radius  $r$  centered at the origin satisfying the quadrature identity:  $\int \int_{\Omega} h(z) dx dy = \pi r^2 h(0)$ .

In general, a quadrature domain  $\Omega$  has real algebraic boundary determined by a polynomial equation:  $\Omega = \{z \in \mathbb{C}; P(z, z^*) < 0\}$ , where  $P(z, z^*)$  is a polynomial of degree less than or equal to  $N$  in each variable, and  $N$  denotes the order of the quadrature domain [60]. Note that the circles and ellipses are the first order quadrature domain (with  $N = 1$ ), where as cardioids and lemniscates are the domains with  $N = 2$ . For further details on quadrature domains, we refer to [34, 69].

In particular, consider a quadrature domain  $g(x, y) \subset \Omega$  whose boundary is expressed by the algebraic equation

$$P(x, y) = P(z, z^*) = 0, \quad \text{with} \quad x = \frac{z + z^*}{2}, \quad y = \frac{z - z^*}{2i}. \quad (5.11)$$

In [34], it was shown that the domain  $g(x, y)$  satisfying (5.11) can be uniquely reconstructed from its finite complex-moments  $\tau_{\alpha, \beta}$ ,  $\alpha, \beta \leq N$  as defined in (5.2), where  $N$  is the order of the domain  $g(x, y)$ . The exact reconstruction algorithm for such domain is given in [60]. The reconstruction algorithm involves complex mapping of the moments  $\tau_{\alpha, \beta}$ ,  $\alpha, \beta \leq N$  into other complex numbers  $b_{\alpha, \beta}$ ,  $\alpha, \beta \leq N$  using the following form of exponential transform

$$1 - \exp\left(-\frac{1}{\pi} \sum_{\alpha=0}^{\infty} \sum_{\beta=0}^{\infty} \tau_{\alpha, \beta} X^{\alpha+1} Y^{\beta+1}\right) = \sum_{\alpha=0}^{\infty} \sum_{\beta=0}^{\infty} b_{\alpha, \beta} X^{\alpha+1} Y^{\beta+1}, \quad (5.12)$$

where  $X$  and  $Y$  are unknowns.

The new complex numbers  $b_{\alpha, \beta}$  are then used to derive the annihilating filter  $A[l]$ ,  $l = 0, 1, \dots, N$  such that its coefficients produce a polynomial

$$p(z) = A[0]z^N + A[1]z^{N-1} + \dots + A[N]z^0. \quad (5.13)$$

The polynomial  $p(z)$ , in turn, is used to form the product

$$R(z, z^*) = p(z) (p(z))^* \left( 1 - \sum_{\alpha=0}^{N-1} \sum_{\beta=0}^{N-1} b_{\alpha,\beta} \frac{1}{z^{\alpha+1} (z^*)^{\beta+1}} \right). \quad (5.14)$$

Finally, the product  $R(z, z^*)$  is manipulated to identify a polynomial  $P(z, z^*)$  that does not contain negative powers of  $z$  or  $z^*$ , that is,

$$R(z, z^*) = P(z, z^*) + \mathcal{O}(z^{-1}, (z^*)^{-1}). \quad (5.15)$$

The equation  $P(z, z^*) = 0$  represents the minimal defining equation for the boundary of the quadrature domain  $g(x, y)$  characterized by Equation (5.11).

Moreover, any bounded planar domain can be approximated by a sequence of quadrature domains, and therefore can be approximated by a finite number of moments [60].

Since it is possible to obtain the moments of  $g(x, y)$  from its samples  $s_{j,k}$ , Proposition 3 can be extended for the quadrature domain of order  $N$  provided that the sampling kernel  $\varphi(x, y)$  can reproduce polynomials at least up to degree  $N$  along  $x$  and  $y$  directions. In support of the sampling assertion and for the sake of clarity, we now present a simulations result for the simplest form of quadrature domain, that is, the circle. In particular, we show that it is possible to reconstruct a circle from its samples using a finite number of moments. However, rather than using the involved reconstruction algorithm discussed above, we retrieve the free parameters (center and radius) from the first order moments directly [39, 75]. This is explained in the following discussion. A similar approach can be used for the case of ellipses [43, 65].

As shown in Figure 5.3(a), consider a bilevel circle  $g(x, y)$  with center  $z_c = x_c + iy_c$  and radius  $r$  in the complex plane. Note that the number of degrees of freedom for a circle in the complex plane is two (i.e.  $z_c$  and  $r$ ). Since the circle is a quadrature domain of order 1, we use the sampling kernel



**Figure 5.3: Reconstruction of the circle: (a) The original circle  $g(x, y)$  with center  $(x_c, y_c)$  and radius  $r$ . (b) The samples  $s_{j,k} = \langle g(x, y), \varphi(x/T_x - j, y/T_y - k) \rangle$  obtained by the kernel  $\varphi(x, y)$  that can reproduce polynomials up to degree one.**

$\varphi(x, y)$  that can reproduce polynomials up to degree one to obtain the samples  $s_{j,k} = \langle g(x, y), \varphi(x/T_x - j, y/T_y - k) \rangle$  as shown in Figure 5.3(b). From the samples  $s_{j,k}$ , using the sample-moment connection (5.4) and (5.5), we compute the simple complex-moments

$$\tau_0 = \int \int_{\Omega} g(x, y)(x + iy)^0 dx dy = \sum_j \sum_k c_{j,k}^{0,0} s_{j,k} = \sum_j \sum_k s_{j,k}, \quad (5.16)$$

and

$$\tau_1 = \int \int_{\Omega} g(x, y)(x + iy)^1 dx dy = \sum_j \sum_k (c_{j,k}^{1,0} + ic_{j,k}^{0,1}) s_{j,k}, \quad (5.17)$$

where  $c_{j,k}^{0,0} = 1$  for the normalized kernel  $\varphi(x, y)$ , and  $c_{j,k}^{1,0}$  and  $c_{j,k}^{0,1}$  are the pre-computed coefficients responsible for reproducing polynomials of degree 1 along  $x$  and  $y$  directions respectively.

The knowledge of the moments  $\tau_0$  and  $\tau_1$  allows us to retrieve the center  $z_c = x_c + iy_c$  and the radius  $r$  from the identities:

$$z_c = x_c + iy_c = \frac{\tau_1}{\tau_0}, \quad \text{and} \quad \pi r^2 = \tau_0. \quad (5.18)$$

It is straightforward to see that the parameters  $z_c$  and  $r$  are sufficient for the unique

reconstruction of  $g(x, y)$ .

## 5.5 Summary

In this chapter, we presented global reconstruction schemes for bilevel-convex polygons, 2-D Diracs, and quadrature domains. In the beginning, we provided a background on various types of moments and have drawn a sample-moment connection which we have utilized throughout the chapter. First, we showed that it is possible to reconstruct bilevel and convex polygons from their samples. In particular, we achieved the global reconstruction of the polygon by retrieving all the corner points at the same time using complex-moments and annihilating filter method. We then extended the global reconstruction scheme of bilevel-convex polygons to 2-D Diracs and quadrature domains.

## Chapter 6

# Radon Transform based Approach

### 6.1 Introduction

Before we present the last approach, we would like to mention that there are many interesting papers in computed tomography (CT) that exploit Radon transform for parametric and nonparametric estimation of multidimensional shapes and contours from noisy tomographic data (e.g. [32, 61, 72]). In particular, the approach of [72] considers estimation of polygonal and polyhedral corner points in Bayesian framework, where as the focus of [32] is on information-theoretic issues in nonparametric boundary estimation.

In this chapter, we utilize the link between Radon transform projections and moments [61] as well as the connection between directional derivatives and differences (refer to Appendix A) for sampling more general FRI signals. In particular, we show that, in addition to polygons and Diracs, it is possible to reconstruct 2-D polynomials with convex polygonal boundaries from their samples. The key feature of the proposed scheme is an annihilating-filter-based-back-projection (AFBP) algorithm.

## 6.2 Reconstruction of 2-D polynomials

### Radon transform:

Let  $g(x, y)$  be a 2-D square-integrable function within a compact region  $\Omega$  over the Euclidean space  $\mathbb{R}^2$ . Then, the conventional Radon transform projection of  $g(x, y)$  is defined as [24] (see Figure 6.1(b)):

$$R_g(t, \theta) = \int \int_{\Omega} g(x, y) \delta(t - x \cos(\theta) - y \sin(\theta)) dx dy, \quad (6.1)$$

where the projection angle  $\theta \in [0, \pi)$ , and  $l_{t, \theta} = \delta(t - x \cos(\theta) - y \sin(\theta))$  is a straight line of integration at an angle  $\theta + \frac{\pi}{2}$  with the  $x$ -axis and at a radial distance  $t$  away from the origin. The projections  $R_g(t, \theta)$  are square integrable 1-D functions with finite support. The original function  $g(x, y)$  can again be reconstructed from its projections  $R_g(t, \theta)$  using filtered back-projection (FBP) reconstruction [24].

### Annihilating filter based back-projection (AFBP) algorithm:

Consider a specific case, where  $g(x, y)$  is a 2-D polynomial of total degree  $R - 1$  inside a convex polygonal closure  $\Omega$  with  $N$  corner points. To be more precise,  $g(x, y) = \sum_{j=0}^{R-1} \sum_{k=0}^j b_{j,k} x^k y^{j-k}$  [9, 10]. In this case, we observe that

- (a) Each projection  $R_g(t, \theta)$  is a 1-D piecewise polynomial of maximum degree  $R$  and with at most  $N$  discontinuities. Therefore, the  $(R + 1)$ -order derivative of such projection leads to a stream of at most  $N$  differentiated Diracs:  $d_t^{(R+1)} [R_g(t, \theta)] = \frac{d^{R+1}}{dt^{R+1}} [R_g(t, \theta)] = \sum_{i=0}^{N-1} \sum_{r=0}^R a_{i,r} \delta^{(r)}(t - t_i)$ , where  $t_i$  are locations and  $a_{i,r}$  are weights. It means that  $d_t^{(R+1)} [R_g(t, \theta)]$  represents at most  $N$  Diracs with  $\hat{N} = N(R + 1)$  weights [27, 28]. A simple illustration of this scenario is given in Figure 6.1.

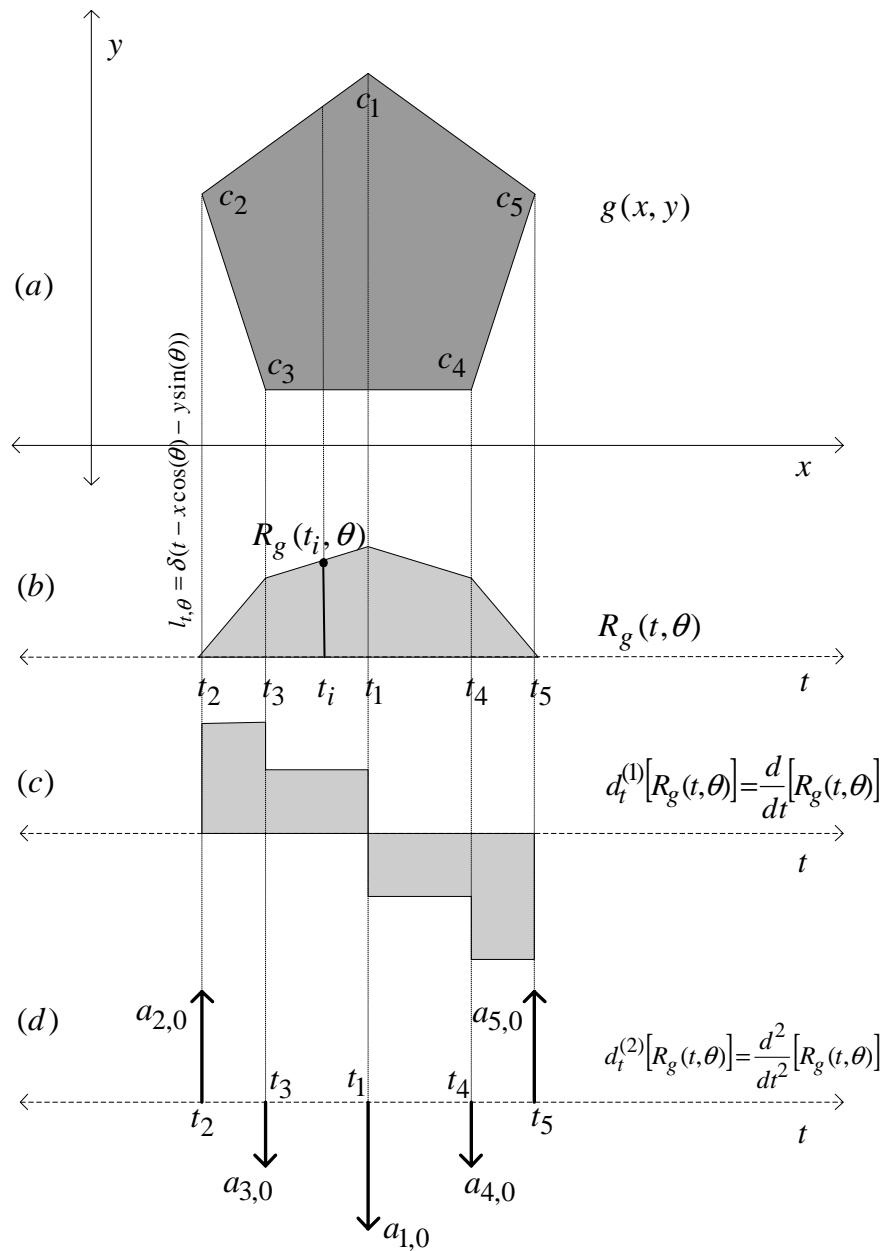


**Figure 6.1: AFBP reconstruction:** The polynomial  $g(x, y)$  of degree  $R - 1 = 0$  inside a convex polygon with  $N = 5$  corner points (i.e. bilevel pentagon) is shown in part (a). The Radon transform projection  $R_g(t, \theta)$  along an angle  $\theta = 0$  is shown in part (b). Note that  $R_g(t_i, \theta)$  is a single-valued line-integral at an arbitrary  $t = t_i$  within the support of  $R_g(t, \theta)$ . Since this projection  $R_g(t, \theta)$  is a piecewise polynomial of degree  $R = 1$ , the  $R + 1 = 2$ -nd order derivative can decompose it in a stream of differentiated Diracs  $d_t^{(2)}[R_g(t, \theta)]$  as shown in part (d). In this case  $d_t^{(2)}[R_g(t, \theta)]$  represents  $N$  Diracs with  $\hat{N} = N$  weights.

- (b) Moreover, following the connection between Radon projections and moments [61], the moments  $\mu_n$ ,  $n \in \mathbb{N}$  of the differentiated Diracs  $d_t^{(R+1)} [R_g(t, \theta)]$  are obtained by

$$\begin{aligned} \mu_n &= \int d_t^{(R+1)} [R_g(t, \theta)] t^n dt \\ &= \int \int_{\Omega} d_{\theta}^{(R+1)} [g(x, y)] (x \cos(\theta) + y \sin(\theta))^n dx dy \\ &= \sum_{\beta=0}^n \binom{n}{\beta} \cos^{\alpha}(\theta) \sin^{\beta}(\theta) \mu_{\alpha, \beta}, \quad \text{with } \alpha = n - \beta, \end{aligned} \quad (6.2)$$

where  $\mu_{\alpha, \beta} = \int \int_{\Omega} \frac{d^{R+1}}{d\theta^{R+1}} [g(x, y)] x^{\alpha} y^{\beta} dx dy$  are the geometric moments of the polynomial  $g(x, y)$  differentiated  $R + 1$  times along the direction  $\theta$ .

- (c) Since the projection  $d_t^{(R+1)} [R_g(t, \theta)]$  consists of at most  $N$  Diracs with  $\hat{N} = N(R + 1)$  weights, the  $2\hat{N} = 2N(R + 1)$  moments  $\mu_n, n = 0, 1, \dots, 2N(R + 1) - 1$  are sufficient to retrieve the locations  $t_i$  and weights  $a_{i,r}$  of the Diracs  $d_t^{(R+1)} [R_g(t, \theta)]$  (and therefore the piecewise polynomial signal  $R_g(t, \theta)$  itself) using annihilating filter method [27, 28].

- (d) By iterating the steps (a), (b), and (c) over  $N + 1$  distinct projection angles  $\theta_l, l = 0, 1, \dots, N$ , it is possible to retrieve the  $N + 1$  sets of Dirac locations  $t_i$ . By back-projecting the  $N + 1$  sets of Dirac locations  $t_i$ , the  $N$  corner points of the convex closure  $\Omega$  are uniquely determined, and therefore, the closure of  $g(x, y)$  itself [11, 54].

- (e) From the knowledge of closure  $\Omega$  and Radon projection  $R_g(t, \theta)$ , we have access to the single-valued line-integral  $R_g(t_i, \theta)$  for an arbitrary  $t = t_i$  within the support of  $R_g(t, \theta)$  (see Figure 6.1(b)). In fact,  $R_g(t_i, \theta) = \int_{l_{t_i, \theta}} g(x, y) dl = \int_{l_{t_i, \theta}} \left( \sum_{j=0}^{R-1} \sum_{k=0}^j b_{j,k} x^k y^{j-k} \right) dl$  is an equation with  $\hat{R} = R(R+1)/2$  unknown coefficients  $b_{j,k}$ . Clearly, the coefficients  $b_{j,k}$  can be determined by solving a system of  $\hat{R}$  such equations (i.e. a generalized Vandemonde system). Fortu-

nately, the theory of bivariate polynomial interpolation [9,10] assures a unique solution if at least  $R$  distinct projections  $R_g(t, \theta)$  are known.<sup>1</sup> Since  $N + 1$  projections are required for recovering the closure  $\Omega$ , and  $R$  projections are required for determining the coefficients  $b_{j,k}$ , we are sure that  $\max(N + 1, R)$  projections are sufficient for the unique reconstruction of  $g(x, y)$ .

To summarize, if  $g(x, y)$  is a 2-D polynomial of degree  $R - 1$  inside a convex polygonal closure  $\Omega$  with  $N$  corner points, then from the moments  $\mu_n$  we can retrieve the projection  $R_g(t, \theta)$  and from  $\max(N + 1, R)$  such projections we can retrieve the polygonal closure  $\Omega$  first and the coefficients  $b_{j,k}$  next. Notice that the crucial part of above reconstruction is the recovery of corner points. Since the retrieval of corner points is based on annihilating filter, we denote the proposed reconstruction as: annihilating filter based back-projection (AFBP) algorithm.

Equipped with the Radon-moment connection (6.2) and the AFBP algorithm, it is possible to show that many FRI signals such as 2-D polynomials with convex polygonal boundaries, 2-D Diracs, and bilevel-convex polygons<sup>2</sup> are perfectly reconstructed from their samples. Moreover, since the Radon transform is multi-dimensional, the AFBP algorithm can be extended for Diracs and bilevel-convex polytopes in higher dimensions (i.e. in 3-D and above). However, for simplicity, we concentrate on sampling of 2-D polynomials with convex polygonal boundaries in the following discussion.

### Sampling result:

Assume that  $g(x, y) = \sum_{j=0}^{R-1} \sum_{k=0}^j b_{j,k} x^k y^{j-k}$  is a 2-D polynomial of degree  $R - 1$  with at most  $\hat{R}$  coefficients  $b_{j,k}$  inside a convex polygonal closure  $\Omega$

---

<sup>1</sup> In fact,  $R$  projections  $R_g(t, \theta)$  are exploited to obtain  $\hat{R} = R(R + 1)/2$  line-integrals  $R_g(t_i, \theta)$  using arithmetic progression [9]. It is straightforward to obtain a unique (but suboptimal) solution by directly using  $\hat{R}$  distinct projections  $R_g(t, \theta)$  [35].

<sup>2</sup> In many cases, AFBP algorithm can also be tailored for bilevel-convex polygons with convex polygonal voids.

with  $N$  corner points. We observe the samples  $s_{j,k}$  of  $g(x, y)$  given by  $s_{j,k} = \langle g(x, y), \varphi(x/T_x - j, y/T_y - k) \rangle$ , where  $\varphi(x, y)$  is the sampling kernel that can reproduce polynomials up to certain degree  $n$  along  $x$  and  $y$  directions.

Recall that in order to retrieve the corner points of the closure  $\Omega$ , we need to compute the moments  $\mu_n$  of the differentiated projections  $d_t^{(R+1)} [R_g(t, \theta)]$  from the moments  $\mu_{\alpha, \beta}$  of the differentiated polynomial  $d_\theta^{(R+1)} [g(x, y)]$  as given in (6.2). Nevertheless, from lattice theory, it is possible to show that there exists a direction vector  $\vec{v} = [v_x, v_y]$  along a chosen projection angle  $\theta = \tan^{-1}(\frac{v_y}{v_x})$ ,  $v_x, v_y \in \mathbb{Z}$  such that the discrete domain directional differences  $\mathcal{D}_\theta^{(R+1)} [s_{j,k}]$  and the continuous domain directional derivatives  $d_\theta^{(R+1)} [g(x, y)]$  are related by (see Appendix A):

$$s'_{j,k} = \mathcal{D}_\theta^{(R+1)} [s_{j,k}] = \left\langle d_\theta^{(R+1)} [g(x, y)], \zeta_\theta(x/T_x - j, y/T_y - k) \right\rangle. \quad (6.3)$$

The new set of samples  $s'_{j,k} = \mathcal{D}_\theta^{(R+1)} [s_{j,k}]$ , obtained by the  $(R+1)$ -order directional differences on the original set of samples  $s_{j,k}$ , is equivalent to one produced by the inner products between the differentiated polynomial  $d_\theta^{(R+1)} [g(x, y)]$  and the modified (directional) kernel  $\zeta_\theta(x, y)$ . The kernel  $\zeta_\theta(x, y)$  is produced by  $R+1$  successive convolutions of zero-th order 1-D B-spline  $\beta_\theta^0(x, y)$  with the original sampling kernel  $\varphi(x, y)$  in the direction of  $\vec{v}$ . More precisely,  $\zeta_\theta(x, y) = |v|^{(R+1)} (\varphi(x, y) * \beta_\theta^R(x, y))$ .

It is important to note that the directional kernel also satisfies the polynomial reproduction property of (3.21). In particular, if the sampling kernel  $\varphi(x, y)$  can reproduce polynomials up to degree  $n$  along  $x$  and  $y$ , then the directional kernel  $\zeta_\theta(x, y)$  can reproduce polynomials up to degree  $n + R + 1$  along  $\theta$ .

In the light of link (6.3), Equations (6.2) and (5.5) enable us to obtain the moments  $\mu_n$  of the projection  $d_t^{(R+1)} [R_g(t, \theta)]$  using linear combinations of samples

$s'_{j,k}$  and coefficients  $c_{j,k}^{\alpha,\beta}$  as given by

$$\mu_n = \sum_{\beta=0}^n \binom{n}{\beta} \cos^\alpha(\theta) \sin^\beta(\theta) \left( \sum_j \sum_k s'_{j,k} c_{j,k}^{\alpha,\beta} \right), \quad \text{with } \alpha = n - \beta, \quad (6.4)$$

where  $c_{j,k}^{\alpha,\beta}$  are the coefficients associated with the kernel  $\zeta_\theta(x, y)$ .

Since  $d_t^{(R+1)} [R_g(t, \theta)]$  consists of at most  $N$  Diracs with  $\hat{N} = N(R+1)$  weights, the directional kernel  $\zeta_\theta(x, y)$  must allow us to retrieve  $2\hat{N} = 2N(R+1)$  moments  $\mu_n, n = 0, 1, \dots, 2N(R+1) - 1$ , and thus it follows that

$$n + R + 1 \geq 2N(R+1) - 1 \quad \Rightarrow \quad n \geq (2N-1)(R+1) - 1. \quad (6.5)$$

Therefore, a sampling kernel  $\varphi(x, y)$  that reproduces polynomial of degree  $n$  (with  $n$  satisfying (6.5)) allows us to obtain the  $2N(R+1)$  moments of each of  $\max(N+1, R)$  differentiated projections  $d_t^{(R+1)} [R_g(t, \theta_l)], l = 0, 1, \dots, \max(N+1, R) - 1$  from the samples  $s'_{j,k} = \mathcal{D}_{\theta_l}^{(R+1)} [s_{j,k}]$  using (6.4). Then following the steps (c) and (d) of the AFBP algorithm, we retrieve the convex polygonal closure  $\Omega$  of  $g(x, y)$ . Finally, from step (e), we determine the coefficients  $b_{j,k}$  of the polynomial of degree  $R-1$  inside  $\Omega$ , and thus the 2-D polynomial signal  $g(x, y)$  itself. In summary, we have:

**Proposition 5.** *Assume that  $g(x, y)$  is a 2-D polynomial of total degree  $R-1$  inside a convex polygonal closure  $\Omega$  with  $N$  corner points. A set of samples  $s_{j,k} = \langle g(x, y), \varphi(x/T_x - j, y/T_y - k) \rangle$  is sufficient to determine  $g(x, y)$  uniquely, if the sampling kernel  $\varphi(x, y)$  can reproduce polynomials at least up to degree  $(2N-1)(R+1) - 1$  along both the coordinate axes  $x$  and  $y$ .*

For the sake of completeness, we now show with a pseudo-algorithm how the reconstruction scheme operates. Given a valid set of samples  $s_{j,k} = \langle g(x, y), \varphi(x/T_x - j, y/T_y - k) \rangle$ , the reconstruction of 2-D polynomial  $g(x, y) = \sum_{j=0}^{R-1} \sum_{k=0}^j b_{j,k} x^k y^{j-k}$  of degree  $R-1$  inside the convex polygonal closure  $\Omega$  with  $N$  corner points follows the following steps:

**Algorithm 3. AFBP reconstruction of 2-D polynomial**

1. For a chosen angle  $\theta = \tan^{-1}(\frac{v_y}{v_x})$ ,  $v_x, v_y \in \mathbb{Z}$ , compute the difference  $s'_{j,k} = \mathcal{D}_\theta^{(R+1)} [s_{j,k}]$  given by (6.3).
2. Using (6.4), compute the first  $2N(R+1)$  moments  $\mu_n, n = 0, 1, \dots, 2N(R+1) - 1$  of the projection  $d_t^{(R+1)} [R_g(t, \theta)]$  from the new set of samples  $s'_{j,k}$  [recall step (b) of the AFBP algorithm on page 93].
3. From moments  $\mu_n$ , using annihilating filter method, obtain the exact locations  $t_i, i = 1, 2, \dots, N$  of the  $N$  Diracs of  $d_t^{(R+1)} [R_g(t, \theta)]$ , and thus, the projection  $R_g(t, \theta)$  itself [step (c)].
4. Iterate steps 1, 2, and 3 for  $N+1$  distinct projection angles  $\theta_l, l = 0, 1, \dots, N$ , and then by back-projecting  $N+1$  sets of Dirac locations  $t_i$ , retrieve the convex polygonal closure  $\Omega$  of  $g(x, y)$  [step (d)].
5. From the knowledge of the closure  $\Omega$  and Radon projections  $R_g(t, \theta_l), l = 0, 1, \dots, R-1$ , determine the coefficients  $b_{j,k}$  of the polynomial  $g(x, y)$  by solving a system of  $\hat{R}$  linear equations [step (e)].
6. Since the closure  $\Omega$  and the coefficients  $b_{j,k}$  are known, it is straightforward to reconstruct the 2-D polynomial  $g(x, y)$ .

A simple simulation result is shown in Figure 6.2. In this case,  $g(x, y)$  is a 2-D polynomial of degree  $R-1=0$  (i.e.  $g(x, y) = b_{0,0}$ ) inside a convex polygonal closure  $\Omega$  with  $N=3$  corner points. In part (a), the original polynomial  $g(x, y)$  is shown with the reconstructed corner points (marked with +). The samples  $s_{j,k} = \langle g(x, y), \varphi(x/T_x - j, y/T_y - k) \rangle$  are shown in part (b), where  $\varphi(x, y)$  is a B-spline sampling kernel that can reproduce polynomials up to degree  $n = (2N-1)(R+1) - 1 = 9$  along  $x$  and  $y$  directions, and therefore, the associated directional kernels  $\zeta_{\theta_l}(x, y)$ , with  $l = 0, 1, 2, 3$  can reproduce polynomials up to degree  $n + R + 1 = 11$  along  $\theta_l$ . The sets of differentiated samples  $s'_{j,k} = D_{\theta_l}^2 [s_{j,k}]$  along four distinct angles

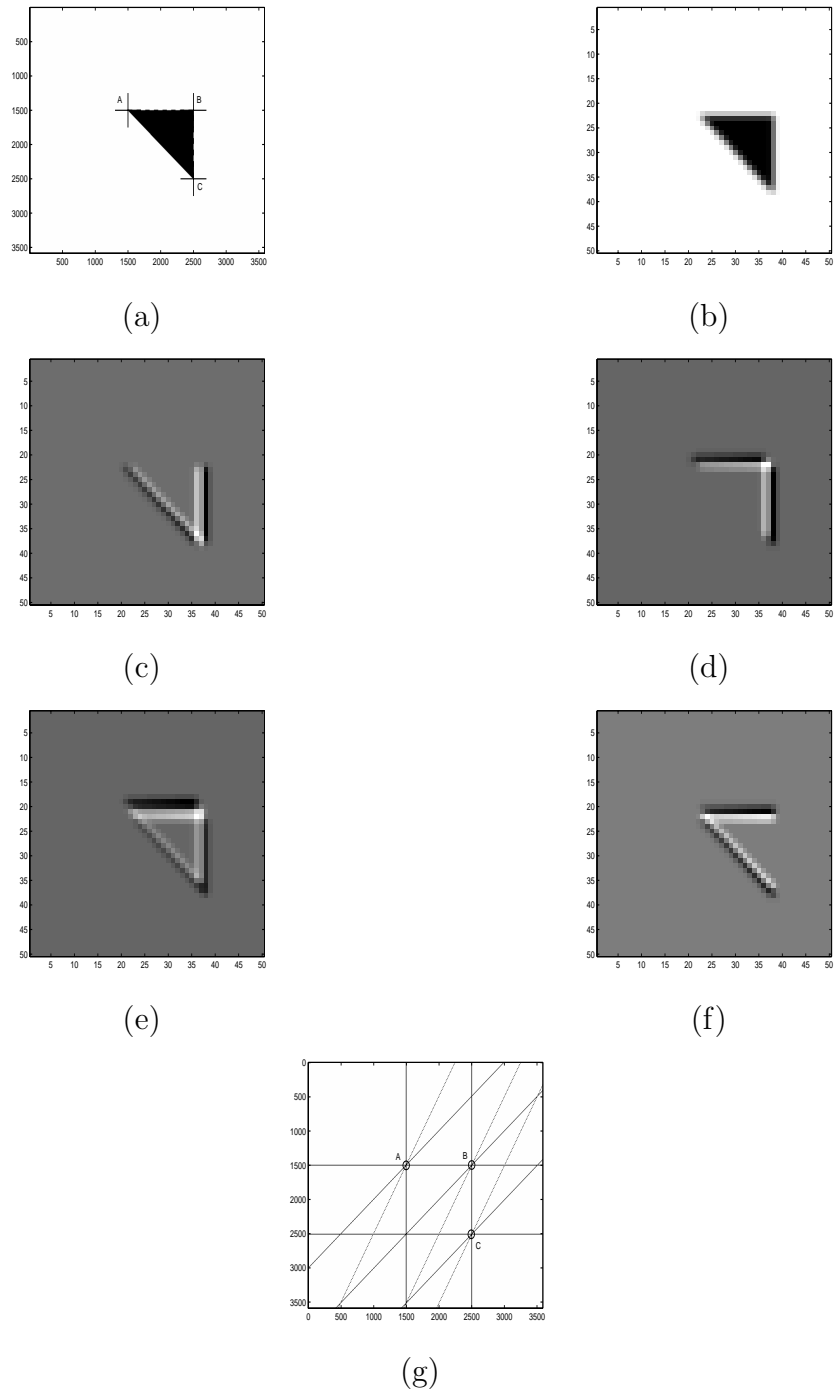


**Figure 6.2: Simulation:** The original 2-D polynomial  $g(x, y)$  of degree  $R - 1 = 0$  and the reconstructed corner points  $A$ ,  $B$ , and  $C$  (marked with  $+$ ) are given in part (a). The set of samples  $s_{j,k}$  produced by the B-spline sampling kernel  $\beta^9(x, y)$  is given in part (b). The  $N + 1 = 4$  sets of differentiated samples  $s'_{j,k} = D_{\theta}^{(2)}[s_{j,k}]$  along four angles  $\theta = 0, \frac{\pi}{4}, \tan^{-1}(2)$ , and  $\frac{\pi}{2}$  are given in parts (c), (d), (e), and (f). The AFBP reconstruction of the corner points  $A$ ,  $B$ , and  $C$  is illustrated in part (g).

$\theta_0 = 0, \theta_1 = \frac{\pi}{4}, \theta_2 = \tan^{-1}(2)$  and  $\theta_3 = \frac{\pi}{2}$  are shown in parts (c), (d), (e), and (f). The AFBP reconstruction of the corner points (marked with  $\circ$ ) using  $N + 1 = 4$  back-projections is shown in part (g), which is exact to machine precision. These corner points can uniquely recover the convex closure  $\Omega$ . From the knowledge of  $\Omega$  and any one projection  $R_g(t, \theta_l)$ , we can uniquely retrieve the coefficient  $b_{0,0}$ , and thus the polynomial  $g(x, y)$  itself.

In this case, the benefit of reconstructing more general signals comes with the price of higher computational cost. For instance, for a 2-D polynomial of degree  $R - 1 = 0$  inside a convex polygon with  $N$  corner points, the computational cost is of the order of  $\mathcal{O}(N^4)$ . This is due to the fact that the cost of finding the roots of each Radon projection is  $\mathcal{O}(N^3)$  and we need  $\mathcal{O}(N)$  projections to reconstruct the polynomial.

### 6.3 Real image experiment

Finally, we close this chapter by presenting an illustrative experiment<sup>3</sup> that demonstrates the potential of corner reconstruction algorithm for real images (e.g. a ‘Remote control’ image of Figure 6.3(a) in this case). In this experiment, we model a simple ‘Remote control’ object as a four-sided bilevel polygon (rectangle) with its sides parallel to coordinate axis  $x$  and  $y$ . The aim is to retrieve the corner points of the object with high precision from a small set of samples by employing AFBP algorithm. The experiment and the results are discussed as follows:

As shown in Figure 6.3(a), the ‘Remote control’ image (with illumination/background variations) of size  $2592 \times 1944$  pixels (along  $x$  and  $y$  directions respectively) is sampled using B-spline kernel  $\beta^3(x, y)$  of order 3 that can reproduce polynomials up to degree 3 along both  $x$  and  $y$  directions, where the size (support)

---

<sup>3</sup>This experiment was realized during undergraduate project supervision [19].

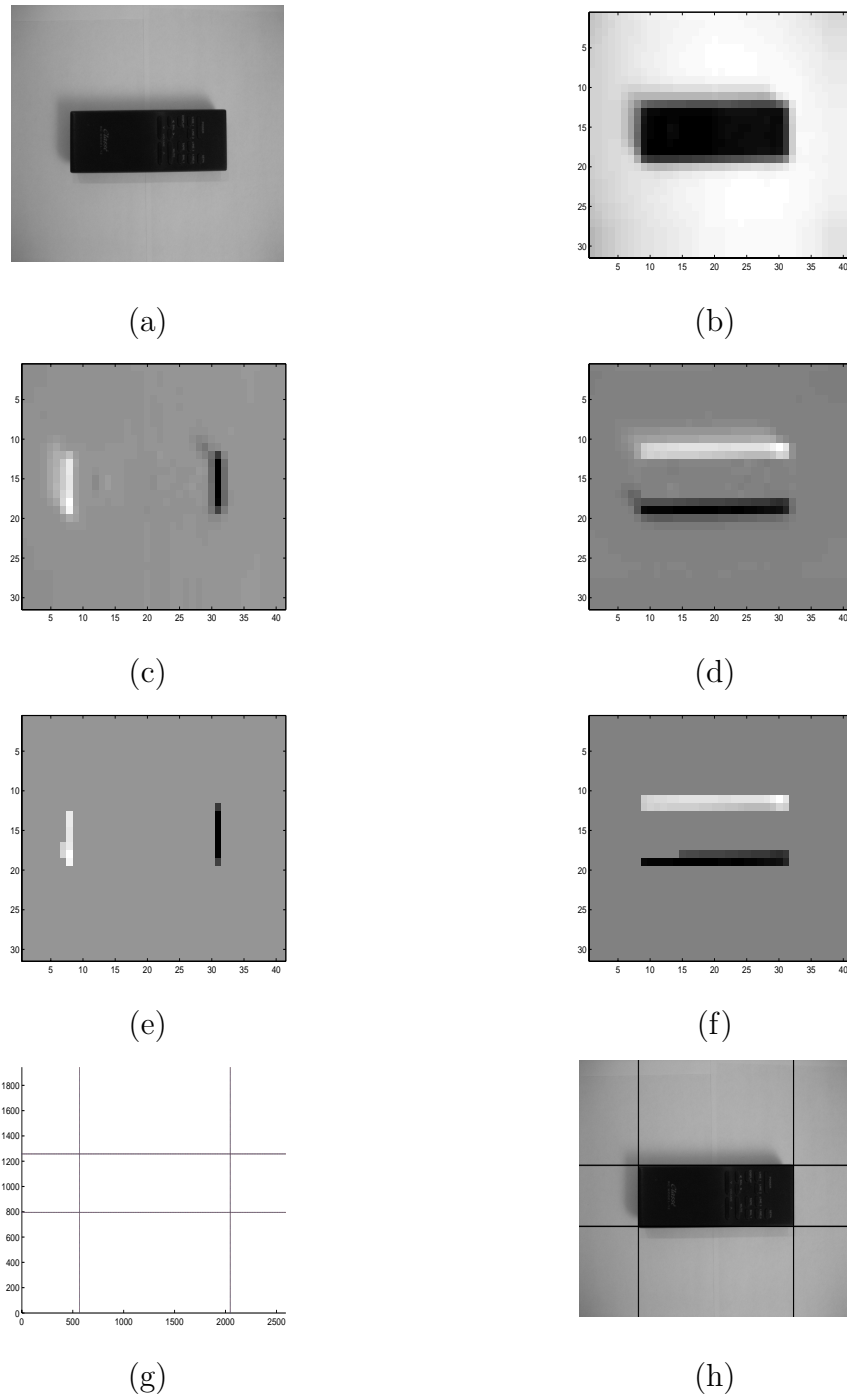


**Figure 6.3: A real image experiment:** As shown in part (a), the original 'Remote control' image  $g(x, y)$  of size  $2592 \times 1944$  pixels (along  $x$  and  $y$  directions respectively) is sampled using B-spline kernel  $\beta^3(x, y)$  of order 3 and support  $190 \times 190$  pixels. The raw set of  $41 \times 31$  samples  $s_{j,k}$  shown in part (b) is used to compute the 1st-order difference samples  $s'_{j,k} = \mathcal{D}_\theta^{(1)}[s_{j,k}]$  along  $\theta = 0$  and  $\frac{\pi}{2}$  as given in parts (c) and (d). Parts (e) and (f) contain the modified samples  $s'_{j,k} = \text{Thresh}(s'_{j,k})$  after properly thresholding the raw difference samples  $s'_{j,k}$ . Finally, the back-projection reconstruction of the corner points is given in part (g) and is super-imposed on the original image in part (h). The accuracy of the reconstruction is within  $\pm 5$  pixels.

of the kernel  $\beta^3(x, y)$  is  $190 \times 190$  pixels. The raw set of  $41 \times 31$  samples  $s_{j,k}$  shown in part (b) is used to compute the 1st-order difference samples  $s'_{j,k} = \mathcal{D}_\theta^{(1)}[s_{j,k}]$  along  $\theta = 0$  and  $\frac{\pi}{2}$  as given in parts (c) and (d). The difference samples  $s'_{j,k} = \mathcal{D}_\theta^{(1)}[s_{j,k}]$  are appropriately thresholded to reduce the effect of background/illumination variations and of noise, and are shown in parts (e) and (f). These modified samples are then used in the AFBP algorithm to achieve the back-projection reconstruction of the corner points as shown in part (g), which is super-imposed on the original image in part (h). The accuracy of the reconstruction is within  $\pm 5$  pixels.

## 6.4 Summary

In this chapter, we have proposed a global scheme for sampling more general FRI signals such as 2-D polynomials with convex polygonal boundaries. The reconstruction is based on annihilating filter based back projection (AFBP) algorithm which utilizes: 1) The link between Radon projections and moments [61]; 2) The results of 1-D and 2-D FRI sampling [28, 54]; 3) The connection between directional derivatives and differences (given in Appendix A); and 4) The theory of bivariate polynomial interpolation [9, 10].

In particular, by using the AFBP algorithm, we showed that it is possible to obtain the moments of the Radon projections (and thus the projections themselves) from the samples of 2-D polynomial signal. From a finite number of such moments and projections, we then retrieve the convex polygonal closure first and the polynomial inside the closure next. Moreover, since the Radon transform is multidimensional, it is straightforward to extend the AFBP algorithms for Diracs and bilevel-convex polytopes in higher dimensions (i.e. in 3-D and above). Finally, we conducted a real image experiment and demonstrated an application of AFBP algorithm in reconstructing the corner points of a simple ‘Remote control’ object

with high precision.

# Chapter 7

## Conclusion

We have considered the problem of sampling and perfect reconstruction of nonbandlimited signals known as signals with finite rate of innovation (FRI) [28,87]. In this thesis, we have extended the results of 1-D FRI sampling [28] into higher dimensions using kernels that reproduce polynomials. In particular, we offer local and global reconstruction approaches with varying complexities as summarized in Table 7.1.

**Table 7.1: Comparative summary**

Approach	Signals	Merits	Computational cost	Limitations
Directional derivatives (Local)	Planar polygons.	Local reconstruction, local complexity.	$\mathcal{O}(N)$ for polygon with $N$ corner points.	Finite orientations of polygonal sides, i.e. $\tan(\theta) \in \mathbb{Q}$ .
Complex-moments (Global)	Convex and bilevel polygons, Quadrature domains (e.g. ellipses, cardioids), and 2-D Diracs.	Reconstruction of corner points with any coordinates.	$\mathcal{O}(N^3)$ for bilevel-convex polygon with $N$ corner points.	Numerically unstable for closely spaced corner points.
Tomographic (Global)	2-D polynomials with polygonal boundaries, $n$ -D Diracs, and $n$ -D bilevel-convex polytopes.	Multidimensional.	$\mathcal{O}(N^4)$ for 2-D polynomial of degree $R - 1 = 0$ inside convex polygon with $N$ corner points.	Numerical instability in computation of higher order moments with directional kernels.

In the following section, we briefly summarize the content of each chapter and recall the key results. In Section 7.2, we highlight some issues that arise in applying this

work to real problems. Finally, we close the thesis by highlighting the future scope in Section 7.3.

## 7.1 Thesis summary

In the introduction, we explained the importance of sampling and identified the problem of sampling multidimensional FRI signals. We provided the background on sampling by reviewing the classical and FRI sampling theories in Chapters 2 and 3 respectively. In particular, in Section 3.3, we established the multidimensional framework for sampling higher dimensional FRI signals. Using the multidimensional framework of Section 3.3, we then presented novel local (Directional derivatives based) and global (Complex-moments and Radon transform based) reconstruction approaches in Chapters 4, 5, and 6 for various FRI signals such as planar and bilevel-convex polygons, 2-D Diracs, quadrature domains (e.g. circles, ellipses, cardioids), 2-D polynomials with convex polygonal boundaries, and higher dimensional Diracs and bilevel-convex polytopes. In particular:

In Chapter 4, we proposed local reconstruction algorithms for sampling 2-D Diracs and planar polygons. By utilizing the connection between directional derivatives and differences, we showed that it is possible to perfectly reconstruct planar polygons from their samples using lower order kernels that satisfy partition of unity. The directional derivatives based approach has local complexity irrespective of the number of corner points in a given polygon.

In Chapter 5, we presented a complex-moments based approach for the global reconstruction of convex-bilevel polygons, 2-D Diracs, and quadrature domains that are capable of approximating arbitrary planar shapes with closed boundaries. Implicitly, we provided a sampling perspective to the ‘shape from moments method’ of [30, 60].

In Chapter 6, we developed an ‘annihilating filter based back-projection’ (AFBP) algorithm which utilizes the link between Radon transform projections and moments [61]. By using the AFBP algorithm, we achieved the global reconstruction of more general FRI signals such as 2-D polynomials with convex polygonal boundaries. Since the Radon transform is multidimensional, it is straightforward to extend the AFBP algorithm for sampling bilevel-convex polytopes and Diracs in higher dimensions (i.e. in 3-D and above). Finally, a simple experiment using a real image is presented to highlight the potential of this approach for corner reconstruction.

## 7.2 Discussion on practical issues

The core of this thesis is fundamental in nature and proposes novel theoretical results in sampling and perfect reconstruction of multidimensional FRI signals. However, it is usual for practicing engineers and developers to see how practical issues such as noise, model mismatch, and numerical instability (or ill-conditioning) of algorithms affect the ideal performance. These issues are discussed as follows:

- *Noise*: The proposed reconstruction algorithms rely on continuous (and unperturbed) moments computed from the observed samples. If we consider the case when the observed samples are corrupted by the noise,<sup>1</sup> it is clear that the computed moments are perturbed<sup>2</sup> and hence proposed algorithms cannot achieve perfect reconstruction. However, the accuracy of reconstruction is influenced by the amount of noise and selected reconstruction approach. For instance, in case of ‘directional derivatives based approach’, where reconstruction algorithm is local (i.e. one corner point at a time) and uses low order moments (i.e. 0th and 1st), the effect of noise is less severe. On the con-

---

<sup>1</sup>The usual noise model is additive, white, and Gaussian. The input FRI signal is assumed to be noiseless and the noise is introduced by the acquisition device at the time of sampling.

<sup>2</sup>The higher order moments are more affected.

trary, in case of ‘complex-moments’ and ‘Radon transform’ based approaches, the reconstruction algorithms are global, which use higher order moments and thus are more sensitive to noise.

In principle, one can employ the techniques used in array processing [30] and spectral estimation [73] for estimating a signal from its noisy moments. Moreover, the recent result in 1-D FRI sampling shows that the effect of noise in computed moments can be reduced by oversampling and averaging [28]. On average, oversampling by a factor  $M$  reduces the MSE of the reconstruction by factor  $M$  [28]. It may be interesting to explore similar method for the multidimensional case.

- *Model mismatch*: The proposed reconstruction schemes are parametric and model based. In other words, the input signals (e.g. polygons) and sampling kernels (e.g. B-splines) have predefined characteristics. Now, if one considers an arbitrary input signal that is not an FRI signal or a sampling kernel that does not reproduce polynomials then a range of model mismatches are possible. In such situation, proposed algorithms do not provide perfect reconstruction. However, the reconstruction error depends on the degree of model mismatch, and in many cases, the error can be reduced by best-fit solutions. For instance, in case of ‘directional derivatives based approach’, the polygonal sides oriented at non-rational tangents may be approximated by the nearest rational tangents. Similarly, the problem of sampling a bounded smooth shape using Gaussian kernel may be approximated to the problem of sampling multiple-sided-polygon (or an appropriate quadrature domain) using a higher order B-spline and considering a complex-moments based approach. In general, the proposed reconstruction schemes consider signals (or shapes) that have constant background (or are prior segmented) and are under uniform illumination. However, it is possible to reduce the effect of background and illumination vari-

ations by thresholding the background samples as highlighted in the real image experiment of Section 6.3.

- *Numerical instability:* The numerical precision, in computation of quantities such as coefficients  $c_{j,k}^{\alpha,\beta}$  associated with the sampling kernel or in computation of (geometric or complex) moments,<sup>3</sup> plays important role in perfect reconstruction. The local approaches (that require first order moments) are numerically more stable. However, the global reconstruction algorithms are based on annihilating filter method that involves matrix inversion and root finding components. These components are numerically unstable in some cases, for example, in reconstructing polygons with large number of corner points or sets of closely spaced Diracs. Moreover, such cases require computation of higher order moments that are vulnerable to numerical precision. A particular example is the computation of higher order moments using directional kernels in the Radon transform based approach. One can reduce the numerical instability by centering the signal at the origin, normalizing the moments, and by employing more stable algorithms such as matrix pencils based method of [33].

Finally, note that some of the above mentioned issues (e.g. noise and numerical instability) are rather general practical issues that affect many signal/image processing techniques.

## 7.3 Future scope

- The sampling results of this thesis have been promisingly explored for image super-resolution [2] and for distributed sampling and compression in camera sensor networks [31]. In particular, the novel work on image super-resolution algorithms [2]

---

<sup>3</sup>Recall Equations (3.21) and (3.23) for instance.

aims is to achieve a high resolution image of the real-scene from several low resolution images (or sampled versions) using low cost multiple cameras. By modeling the camera lens with polynomial reproducing kernels (e.g. cubic B-splines), one can achieve enough continuous moments so that the disparity between different camera images can be retrieved accurately up to affine transformations. Thus, the continuous moments allow accurate super-resolved registration of various low resolution camera images. Moreover, the moment based approach of registration eliminates the traditional stages of control point extraction and correspondence which are less efficient while working with very low resolution images. Further details of the moment based super-resolution algorithm that operates on real images is given in [2]. Similarly, the work on distributed sampling and compression in the network of digital cameras exploits the FRI sampling schemes for deriving minimum number of cameras for perfect reconstruction of the scene as well as in establishing novel rate-distortion behavior using practical distributed coding approach [31]. Finally, the proposed schemes might find their applications in vectored graphics, computer animations, and machine vision.

- While working with the real images, it might be useful to concentrate on selected regions of interest (ROI). The ROI consideration is potentially suitable for local feature extraction and reconstruction. In particular, it would be of interest to investigate the use of the corner (or orientation) reconstruction algorithms for super-resolution feature extraction with applications in modern photogrammetry/videogrammetry.
- From an academic point of view, we notice that the complex-moments based approach is limited to 2-D FRI signals. This is due to the fact that the annihilating filter method in the existing form cannot annihilate hyper-complex numbers (e.g. quaternions [36] in 3-D and 4-D). It would be interesting to see whether it is possible to design the annihilating filter for hyper-complex numbers.

- Since the objective of this research was to develop novel sampling and perfect reconstruction schemes, the issues of noise, model mismatch, and numerical instability are still open for further investigation- in particular, for quantitative analysis.
- Finally, discovering other higher dimensional FRI signals and developing more efficient transformations and reconstruction algorithms remains a challenging sparse representation problem.<sup>4</sup>

---

<sup>4</sup>One such attempt in different context is compressive sampling [18] (or compressed sensing [26]) which concentrates on sparse representation of discrete/digital signals through random measurements and probabilistic reconstruction algorithms.

# Appendix A

## Directional kernel

Consider the set of samples  $s_{j,k} = \langle g(x, y), \varphi(x/T_x - j, y/T_y - k) \rangle$  of the given planar polygon  $g(x, y)$ , where  $\varphi(x, y)$  is the sampling kernel, and let the sampling intervals  $T_x = T_y = 1$ .

### Connecting directional differences to the derivatives: Equation (4.8)

Now, as illustrated in Figure 4.4, apply a pair of finite differences  $\mathcal{D}_{\theta_1}^{(1)}[\cdot]$  and  $\mathcal{D}_{\theta_2}^{(1)}[\cdot]$  on samples  $s_{j,k}$ , first along the lattice direction  $\vec{v}_1 = [v_{1,1}, v_{1,2}]$  and then along  $\vec{v}_2 = [v_{2,1}, v_{2,2}]$ . The pair of directional differences  $\mathcal{D}_{\theta_1}^{(1)}[\cdot]$  and  $\mathcal{D}_{\theta_2}^{(1)}[\cdot]$  modifies the original set of samples  $s_{j,k}$  into a new set of samples  $s'_{j,k}$  as given by

$$\begin{aligned}
 s'_{j,k} &= \mathcal{D}_{\theta_2}^{(1)} \left[ \mathcal{D}_{\theta_1}^{(1)} [s_{j,k}] \right] \\
 &= \left\{ s_{(j+v_{2,1}+v_{1,1}), (k+v_{2,2}+v_{1,2})} - s_{(j+v_{2,1}), (k+v_{2,2})} \right\} - \left\{ s_{(j+v_{1,1}), (k+v_{1,2})} - s_{j,k} \right\} \\
 &= \left\langle g(x, y), \right. \\
 &\quad \left. \left\{ \varphi(x - (j + v_{2,1} + v_{1,1}), y - (k + v_{2,2} + v_{1,2})) - \varphi(x - (j + v_{2,1}), y - (k + v_{2,2})) \right\} \right. \\
 &\quad \left. - \left\{ \varphi(x - (j + v_{1,1}), y - (k + v_{1,2})) - \varphi(x - j, y - k) \right\} \right\rangle.
 \end{aligned}$$

Using Parseval's identity, it follows that

$$\begin{aligned}
s'_{j,k} &= \frac{1}{4\pi^2} \left\langle \hat{g}(\omega_x, \omega_y), \hat{\varphi}(\omega_x, \omega_y) \cdot e^{-i(j\omega_x + k\omega_y)} \cdot \right. \\
&\quad \left. \left( \left\{ e^{-i((v_{2,1}+v_{1,1})\omega_x + (v_{2,2}+v_{1,2})\omega_y)} - e^{-i(v_{2,1}\omega_x + v_{2,2}\omega_y)} \right\} - \left\{ e^{-i(v_{1,1}\omega_x + v_{1,2}\omega_y)} - 1 \right\} \right) \right\rangle \\
&= \frac{1}{4\pi^2} \left\langle \hat{g}(\omega_x, \omega_y), \hat{\varphi}(\omega_x, \omega_y) \cdot e^{-i(j\omega_x + k\omega_y)} \cdot \right. \\
&\quad \left. \left( e^{-i(v_{1,1}\omega_x + v_{1,2}\omega_y)} - 1 \right) \cdot \left( e^{-i(v_{2,1}\omega_x + v_{2,2}\omega_y)} - 1 \right) \right\rangle,
\end{aligned}$$

where  $i = \sqrt{-1}$ , and  $\hat{g}(\omega_x, \omega_y)$  and  $\hat{\varphi}(\omega_x, \omega_y)$  are the 2-D Fourier transforms of  $g(x, y)$  and  $\varphi(x, y)$  respectively. After multiplying and dividing by the same factors, we have that

$$\begin{aligned}
s'_{j,k} &= \frac{1}{4\pi^2} \left\langle \hat{g}(\omega_x, \omega_y), \right. \\
&\quad \hat{\varphi}(\omega_x, \omega_y) \cdot e^{-i(j\omega_x + k\omega_y)} \cdot \left( i(v_{1,1}\omega_x + v_{1,2}\omega_y) \right) \cdot \left( i(v_{2,1}\omega_x + v_{2,2}\omega_y) \right) \cdot \\
&\quad \left. \frac{\left( e^{-i(v_{1,1}\omega_x + v_{1,2}\omega_y)} - 1 \right) \left( e^{-i(v_{2,1}\omega_x + v_{2,2}\omega_y)} - 1 \right)}{\left( i(v_{1,1}\omega_x + v_{1,2}\omega_y) \right) \left( i(v_{2,1}\omega_x + v_{2,2}\omega_y) \right)} \right\rangle. \tag{A.1}
\end{aligned}$$

Now recall that  $\hat{\beta}^0(\omega) = \frac{1-e^{-i\omega t}}{i\omega}$  is a frequency domain representation of the zero-th order 1-D B-spline  $\beta^0(t)$ . This representation can be extended for 1-D directional B-spline in 2-D plane and is given by

$$\hat{\beta}_{\theta_1}^0(\omega_x, \omega_y) = \frac{(1 - e^{-i(v_{1,1}\omega_x + v_{1,2}\omega_y)})}{i(v_{1,1}\omega_x + v_{1,2}\omega_y)}, \quad \hat{\beta}_{\theta_2}^0(\omega_x, \omega_y) = \frac{(1 - e^{-i(v_{2,1}\omega_x + v_{2,2}\omega_y)})}{i(v_{2,1}\omega_x + v_{2,2}\omega_y)}, \tag{A.2}$$

where  $\hat{\beta}_{\theta_1}^0$  and  $\hat{\beta}_{\theta_2}^0$  are the 1-D B-splines of order zero in 2-D plane along orientations  $\theta_1 = \tan^{-1} \left( \frac{v_{1,2}}{v_{1,1}} \right)$  and  $\theta_2 = \tan^{-1} \left( \frac{v_{2,2}}{v_{2,1}} \right)$  respectively. For simplicity, let

$$\hat{\xi}_{\theta_1, \theta_2}(\omega_x, \omega_y) = \hat{\varphi}(\omega_x, \omega_y) \hat{\beta}_{\theta_1}^0(\omega_x, \omega_y) \hat{\beta}_{\theta_2}^0(\omega_x, \omega_y). \tag{A.3}$$

Replacing (A.2) and (A.3) in the formulation of (A.1) and then multiplying and

dividing by a factor  $|v_1||v_2|$ , we have

$$s'_{j,k} = \frac{|v_1||v_2|}{4\pi^2} \left\langle \hat{g}(\omega_x, \omega_y), \hat{\xi}_{\theta_1, \theta_2}(\omega_x, \omega_y) \cdot e^{-i(j\omega_x + k\omega_y)} \cdot \left\{ (i\omega_x)^2 \frac{v_{1,1} v_{2,1}}{|v_1||v_2|} + (i\omega_x)(i\omega_y) \frac{(v_{1,1} v_{2,2} + v_{1,2} v_{2,1})}{|v_1||v_2|} + (i\omega_y)^2 \frac{v_{1,2} v_{2,2}}{|v_1||v_2|} \right\} \right\rangle.$$

Using the identities  $v_{1,1} = |v_1| \cos(\theta_1)$ ,  $v_{1,2} = |v_1| \sin(\theta_1)$ ,  $v_{2,1} = |v_2| \cos(\theta_2)$ ,  $v_{2,2} = |v_2| \sin(\theta_2)$ ,  $|\det(V_\Lambda)| = |v_{1,1} v_{2,2} - v_{1,2} v_{2,1}|$ , and  $|v_1||v_2| = \frac{|\det(V_\Lambda)|}{|\sin(\theta_2 - \theta_1)|}$  in the righthand side of the above equation, we have

$$s'_{j,k} = \frac{|\det(V_\Lambda)|}{4\pi^2 |\sin(\theta_2 - \theta_1)|} \left\langle \hat{g}(\omega_x, \omega_y), \hat{\xi}_{\theta_1, \theta_2}(\omega_x, \omega_y) \cdot e^{-i(j\omega_x + k\omega_y)} \cdot \left\{ (i\omega_x)^2 \cos(\theta_1) \cos(\theta_2) + (i\omega_x)(j\omega_y) \sin(\theta_1 + \theta_2) + (i\omega_y)^2 \sin(\theta_1) \sin(\theta_2) \right\} \right\rangle.$$

Using Parseval's identity, we have

$$s'_{j,k} = \frac{|\det(V_\Lambda)|}{|\sin(\theta_2 - \theta_1)|} \left\langle g(x, y), \left\{ \cos(\theta_1) \cos(\theta_2) \frac{\partial^2}{\partial x^2} (\xi_{\theta_1, \theta_2}(x - j, y - k)) + \sin(\theta_1 + \theta_2) \frac{\partial}{\partial y} \left( \frac{\partial}{\partial x} (\xi_{\theta_1, \theta_2}(x - j, y - k)) \right) + \sin(\theta_1) \sin(\theta_2) \frac{\partial^2}{\partial y^2} (\xi_{\theta_1, \theta_2}(x - j, y - k)) \right\} \right\rangle.$$

Comparing the righthand side of the above equation with the continuous directional derivative model given in Equation (4.7), it follows that

$$\begin{aligned} \frac{s'_{j,k}}{|\det(V_\Lambda)|} &= \frac{1}{|\sin(\theta_2 - \theta_1)|} \left\langle g(x, y), \frac{\partial}{\partial \theta_2} \left( \frac{\partial}{\partial \theta_1} (\xi_{\theta_1, \theta_2}(x - j, y - k)) \right) \right\rangle \\ &\stackrel{(a)}{=} \left\langle \frac{\partial}{\partial \theta_2} \left( \frac{\partial}{\partial \theta_1} (g(x, y)) \right), \frac{1}{|\sin(\theta_2 - \theta_1)|} \xi_{\theta_1, \theta_2}(x - j, y - k) \right\rangle \\ &= \left\langle \frac{\partial}{\partial \theta_2} \left( \frac{\partial}{\partial \theta_1} (g(x, y)) \right), \zeta_{\theta_1, \theta_2}(x - j, y - k) \right\rangle, \end{aligned} \quad (\text{A.4})$$

where equality (a) is obtained using integration by parts, and  $\zeta_{\theta_1, \theta_2}(x, y) = \frac{\xi_{\theta_1, \theta_2}(x, y)}{|\sin(\theta_2 - \theta_1)|} = \frac{(\varphi(x, y) * \beta_{\theta_1}^0(x, y)) * \beta_{\theta_2}^0(x, y)}{|\sin(\theta_2 - \theta_1)|}$  is the modified directional kernel.

# Bibliography

- [1] Y. S. Abu-Mostafa and D. Psaltis. Recognitive aspects of moment invariants. *IEEE Transactions on Pattern Analysis and Machine Intelligence*, 6(6):698–706, November 1984.
- [2] L. Baboulaz and P. L. Dragotti. Distributed acquisition and image super-resolution based on continuous moments from samples. In *Proc. of IEEE International Conference on Image Processing (ICIP)*, Atlanta, GA, USA, October 2006.
- [3] S. Bandyopadhyay, Q. Tian, and E. J. Coyle. Spatio-temporal sampling rates and energy efficiency in wireless sensor networks. *IEEE/ACM Transactions on Networking*, 13(6):1339–1352, December 2005.
- [4] J. J. Benedetto. Frames, sampling, and seizure prediction. In K. S. Lau, editor, *Advances in Wavelets*, pages 1–15. Springer-Verleg, NY, 1998.
- [5] J. J. Benedetto and P. J. S. G. Ferreira, editors. *Modern Sampling Theory: Mathematics and Applications*. Applied and Numerical Harmonic Analysis Series. Birkhauser, Boston, 2001.
- [6] J. Berent and P. L. Dragotti. Perfect reconstruction scheme for sampling piecewise sinusoidal signals. In *Proc. IEEE International Conference on Acoustic, Speech and Signal Processing (ICASSP)*, Toulouse, France, May 2006.
- [7] R. E. Blahut. *Theory and practice of Error Control Codes*. Addison-Wesley, 1983.
- [8] T. Blu and M. Unser. Approximation errors for quasiinterpolators and (multi-) wavelet expansions. *Applied and Computational Harmonic Analysis*, 6(2):219–251, March 1999.
- [9] B. Bojanov and I. K. Georgieva. Interpolation by bivariate polynomials based on Radon projections. *Studia Mathematica*, 162(2):141–160, 2004.
- [10] B. Bojanov and Y. Xu. Reconstruction of a polynomial from its Radon projections. *SIAM Journal on Mathematical Analysis*, 37(1):238–250, September 2005.

- 
- [11] Y. Bresler. *Model based estimation techniques for 3-D reconstruction from projections*. PhD thesis, Stanford University, Stanford, CA, USA, 1985.
- [12] J. L. Brown. Multi-channel sampling of lowpass signals. *IEEE Transactions on Circuits and Systems*, 28(2):101–106, February 1981.
- [13] W. M. Brown. Optimal prefiltering of sampled data. *IEEE Transactions on Information Theory*, 7(4):269–270, October 1961.
- [14] J. L. Brown Jr. and S. D. Cabrera. On well-posedness of the Papoulis generalized sampling expansion. *IEEE Transactions on Circuits and Systems*, 38(5):554–556, May 1991.
- [15] J. L. Brown Jr. and K. Sa-ngsari. Sampling reconstruction of N-dimensional band-limited images after multilinear filtering. *IEEE Transactions on Circuits and Systems*, 36(7):1035–1038, July 1989.
- [16] P. L. Butzer. A survey of the Whittaker-Shannon sampling theorem and some of its extensions. *Journal of Mathematical Research Exposition*, 3:185–212, 1983.
- [17] P. L. Butzer and R. L. Stens. Sampling theory for not-necessarily band-limited functions: A historical overview. *SIAM Review*, 34(1):40–53, March 1992.
- [18] E. Candes, J. Romberg, and T. Tao. Robust uncertainty principles: Exact recovery from highly incomplete frequency information. *IEEE Transactions on Information Theory*, 52(2):489–509, February 2006.
- [19] Varit Chaisinthop. Radon transform based super-resolution algorithm for shape reconstruction. Final year undergraduate project report, Department of Electrical and Electronic Engineering, Imperial College London, 2006.
- [20] J. H. Conway and N. J. A. Sloane. *Sphere Packing, Lattices and Groups*. Springer-Verlag, 1998.
- [21] R. G. Cornell. A method for fitting linear combinations of exponentials. *Biometrika*, 18(1):104–113, March 1962.
- [22] I. Daubechies. *Ten Lectures on Wavelets*. SIAM, PA, 1992.
- [23] P. J. Davis. Triangle formulas in the complex plane. *Mathematics of Computation*, 18(88):569–577, October 1964.
- [24] S. R. Deans. *The Radon Transform and Some of Its Applications*. John Wiley, 1983.
- [25] I. Djokovic and P. P. Vaidyanathan. Generalized sampling theorems in multiresolution subspaces. *IEEE Transactions on Signal Processing*, 45(3):583–599, March 1997.

- [26] D. L. Donoho. Compressed sensing. *IEEE Transactions on Information Theory*, 52(4):1289–1306, April 2006.
- [27] P. L. Dragotti, M. Vetterli, and T. Blu. Exact sampling results for signals with finite rate of innovation using Strang-Fix conditions and local kernels. In *Proceedings of IEEE International Conference on Acoustics, Speech and Signal Processing (ICASSP)*, Philadelphia, USA, March 2005.
- [28] P. L. Dragotti, M. Vetterli, and T. Blu. Sampling moments and reconstructing signals with finite rate of innovation: Shannon meets Strang-Fix. *IEEE Transactions on Signal Processing*, 55(5):1741–1757, May 2007.
- [29] S. A. Dudani, K. J. Breeding, and R. B. McGhee. Aircraft identification by moment invariants. *IEEE Transactions on Computers*, 26(1):39–45, January 1977.
- [30] M. Elad, P. Milanfar, and G. H. Golub. Shape from moments- an estimation theory perspective. *IEEE Transactions on Signal Processing*, 52(7):1814–1829, July 2004.
- [31] N. Gehrig and P. L. Dragotti. Distributed sampling and compression of scenes with finite rate of innovation in camera sensor networks. In *Proceedings of Data Communication Conference (DCC)*, Snowbird, Utah, USA, March 2006.
- [32] A. Goldenshluger and V. Spokoiny. Recovering convex edges of an image from noisy tomographic data. *IEEE Transactions on Information Theory*, 52(4):1322–1334, April 2006.
- [33] G. H. Golub, P. Milanfar, and J. Varah. A stable numerical method for inverting shape from moments. *SIAM Journal on Scientific Computing*, 21(4):1222–1243, December 1999.
- [34] B. Gustafsson, C. He, P. Milanfar, and M. Putinar. Reconstructing planar domains from their moments. *Inverse Problems*, 16(4):1053–1070, August 2000.
- [35] H. Hakopian. Multivariate divided differences and multivariate interpolation of Lagrange and Hermite type. *Journal of Approximation Theory*, 34(3):286–305, 1982.
- [36] W. R. Hamilton. On quaternions. *Proceedings of the Royal Irish Academy*, 3:1–16, 1847.
- [37] Y. Hao, P. Marziliano, M. Vetterli, and T. Blu. Compression of ECG as signal with finite rate of innovation. In *27th Annual International Conference of the IEEE Engineering in Medicine and Biology Society*, Shanghai, China, September 2005.

- [38] J. R. Higgins. Five short stories about the cardinal series. *Bulletine of American Mathematical Society*, 12(1):45–89, 1985.
- [39] M. K. Hu. Visual pattern recognition by moment invariants. *IRE Transactions on Information Theory*, 8:179–187, February 1962.
- [40] A. A. Istratov and O. F. Vyenko. Exponential analysis in physical phenomena. *Review of Scientific Instruments*, 70(2):1233–1257, February 1999.
- [41] A. J. Jerry. The Shannon sampling theorem- its various extensions and applications: A tutorial review. *Proceedings of IEEE*, 65(11):1565–1596, November 1977.
- [42] I. Jovanović and B. Beferull-Lozano. Oversampled A/D conversion and error-rate dependence of nonbandlimited signals with finite rate of innovation. *IEEE Transactions on Signal Processing*, 54(6):2140–2154, June 2006.
- [43] A. Kavianpore, N. Bagherzadeh, and S. Shoari. Finding elliptical shapes in an image using a pyramid architecture. In *Proc. of International Symposium on Speech, Image Processing and Neural Networks (ISSIPNN)*, Hong Kong, pages 445–448, April 1994.
- [44] J. Konrad and P. Agniel. Subsampling models and anti-alias filters for 3-D automultiscopic displays. *IEEE Transactions on Image Processing*, 15(1):128–140, January 2006.
- [45] V. A. Kotel’nikov. On the transmission capacity of ‘ether’ and wire in electrocommunications. *Izd. Red. Upr. Svyazzi RKKA (Moscow)*, 1933.
- [46] V. A. Kotel’nikov. Reprint: On the transmission capacity of ‘ether’ and wire in electrocommunications. In J. J. Benedetto and P. J. S. G. Ferreira, editors, *Modern Sampling Theory: Mathematics and Applications*. Birkhauser, Boston, 2000.
- [47] J. Kusuma. *Economic Sampling of Parametric Signals*. PhD thesis, Massachusetts Institute of Technology, Cambridge, MA 02139, USA, August 2006.
- [48] D. A. Linden. A discussion of sampling theorems. *Proceedings of IRE*, 47:1219–1226, 1959.
- [49] Y. Lu and M. N. Do. A geometrical approach to sampling signals with finite rate of innovation. In *Proc. IEEE International Conference of Acoustic, Speech and Signal Processing (ICASSP)*, Montreal, Canada, May 2004.
- [50] H. D. Luke. The origins of the sampling theorem. *IEEE Communications Magazine*, 37(4):106–108, April 1999.

- [51] S. Mallat. Multiresolution approximation and wavelet orthogonal bases of  $l^2(r)$ . *Transactions of American Mathematical Society*, 315(1):69–87, 1989.
- [52] F. A. Maravasti, editor. *Nonuniform Sampling: Theory and Practice*. Information Technology: Transmission, Processing and Storage. Springer, NY, 2001.
- [53] I Maravic. *Sampling Methods for Parametric Non-bandlimited Signals: Extensions and Applications*. PhD thesis, Audio Visual Communication Laboratory, Swiss Federal Institute of Technology (EPFL), Laussane, Switzerland, 2004.
- [54] I. Maravić and M. Vetterli. A sampling theorem for the Radon transform of finite complexity objects. In *Proc. of IEEE International Conference on Acoustics, Speech and Signal Processing (ICASSP)*, pages 1197–1200, Orlando, Florida, USA, May 2002.
- [55] I. Maravić and M. Vetterli. Exact sampling results for some classes of parametric nonbandlimited 2-D signals. *IEEE Transactions on Signal Processing*, 52(1):175–189, January 2004.
- [56] I. Maravić and M. Vetterli. Sampling and reconstruction of signals with finite rate of innovation in the presence of noise. *IEEE Transactions on Signal Processing*, 53(8):2788–2805, August 2005.
- [57] R. J. Marks II. *Introduction to Shannon Sampling and Interpolation Theory*. Springer-Verleg, 1993.
- [58] P Marziliano. *Sampling Innovations*. PhD thesis, Audio Visual Communication Laboratory, Swiss Federal Institute of Technology (EPFL), Laussane, Switzerland, 2001.
- [59] Meijering. A chronology of interpolation: from ancient astronomy to modern signal and image processing. *Proceedings of IEEE*, 90(3):319–342, March 2002.
- [60] P. Milanfar, M. Putinar, J. Varah, B. Gustafsson, and G. Golub. Shape reconstruction from moments: theory, algorithms, and applications. *Proceedings of SPIE*, 4116:406–416, November 2000.
- [61] P. Milanfar, G. Verghese, W. Karl, and A. Willsky. Reconstructing polygons from moments with connections to array processing. *IEEE Transactions on Signal Processing*, 43(2):432–443, February 1995.
- [62] H. Nyquist. Certain topics in telegraph transmission theory. *Trans. Amer. Inst. Elect. Eng.*, 47:617–644, 1928.
- [63] A. V. Oppenheim and R. W. Schaffer. *Discrete-Time Signal Processing*. Prentice-Hall, 1989.

- [64] A. Papoulis. Generalized sampling expansion. *IEEE Transactions on Circuits and Systems*, 24:652–654, November 1977.
- [65] L. Rocha, L. Velho, and Paulo Cezar P. Carvalho. Motion reconstruction using moments analysis. In *Proc. of 17th Brazilian Symposium on Computer Graphics and Image Processing*, IEEE Computer Society, pages 354–361, Brazil, October 2004.
- [66] D. Seidner, M. Feder, D Cubanski, and S. Blackstock. Introduction to vector sampling expansion. *IEEE Signal Processing Letters*, 5(5):115–117, May 1998.
- [67] C. E. Shannon. Communication in the presence of noise. *Proceedings of IRE*, 37(1):10–21, January 1949.
- [68] C. E. Shannon. Classic paper: Communication in the presence of noise. *Proceedings of IEEE*, 86(2):447–457, February 1998.
- [69] H. S. Shapiro. *The Schwartz function and its generalization to higher dimensions*. Wiley, New York, 1992.
- [70] P. Shukla and P. L. Dragotti. Sampling schemes for 2-D signals with finite rate of innovation using kernels that reproduce polynomials. In *Proc. of IEEE International Conference on Image Processing (ICIP)*, Genova, Italy, September 2005.
- [71] P. Shukla and P. L. Dragotti. Tomographic approach for sampling multidimensional signals with finite rate of innovation. In *Proc. of IEEE International Conference on Image Processing (ICIP)*, Atlanta, USA, October 2006.
- [72] C. Soussen and A. Mohammad-Djafari. Polygonal and polyhedral contour reconstruction in computed tomography. *IEEE Transactions on Image Processing*, 13(11):1507–1523, November 2004.
- [73] P. Stoica and R. Moses. *Introduction to Spectral Analysis*. Prentice-Hall, Englewood Cliffs, NJ, 2000.
- [74] G. Strang and Fix. G. Fourier analysis of the finite element variational method. *Constructive Aspects of Functional Analysis, Rome, Italy*, pages 796–830, 1971.
- [75] C. Teh and R. T. Chin. On image analysis by the methods of moments. *IEEE Transactions on Pattern Analysis and Machine Intelligence*, 10(4):496–513, July 1988.
- [76] G. Thomas. A comparison of motion-compensated interlace-to-progressive conversion methods. *Signal Processing Image Communication*, 12(3):209–229, June 1998.

- [77] M. Unser. Splines - a perfect fit for signal and image processing. *IEEE Signal Processing Magazine*, 16(6):22–38, November 1999.
- [78] M. Unser. Sampling—50 Years after Shannon. *Proceedings of the IEEE*, 88(4):569–587, April 2000.
- [79] M. Unser. Cardinal Exponential Splines: Part II- think analogue, act digital. *IEEE Transactions on Signal Processing*, 53(4):1439–1449, April 2005.
- [80] M. Unser and A. Aldroubi. A general sampling theory for nonideal acquisition devices. *IEEE Transactions on Signal Processing*, 42(11):2915–2925, November 1994.
- [81] M. Unser and T. Blu. Cardinal Exponential Splines: Part I- theory and filtering algorithms. *IEEE Transactions on Signal Processing*, 53(4):1425–1438, April 2005.
- [82] M. Unser and J. Zerubia. A generalized sampling without bandlimiting constraint. *IEEE Transactions on Circuits and Systems*, 45(8):959–969, August 1998.
- [83] H. Ur and D. Gross. Improved resolution from subpixel shifted pictures. *CVGIP: Graphical Models and Image Processing*, 54(2):181–186, March 1992.
- [84] P. P. Vaidyanathan. Generalizations of the sampling theorem: Seven decades after Nyquist. *IEEE Transactions on Circuits and Systems- I*, 48(9):1094–1109, September 2001.
- [85] V. Velisavljevic, B. Beferull-Lozano, M. Vetterli, and P. L. Dragotti. Directionlets: Anisotropic multi-directional representation with separable filtering. *IEEE Transactions on Image Processing*, 15(7):1916–1933, July 2006.
- [86] M. Vetterli and Kovacevic J. *Wavelets and Subband Coding*. Prentice-Hall, Englewood Cliffs, NJ, 1995.
- [87] M. Vetterli, P. Marziliano, and T. Blu. Sampling signals with finite rate of innovation. *IEEE Transactions on Signal Processing*, 50(6):1417–1428, June 2002.
- [88] J. M. N. Vieira and P. J. S. G. Ferreira. Interpolation, spectrum analysis, error-control coding and fault-tolerant computing. In *Proc. of IEEE Conference on Acoustic, Speech and Signal Processing (ICASSP)*, Munich, Germany, 1997.
- [89] A. J. Weiss, A. S. Willsky, and B. C. Levy. Eigenstructure approach for array-processing with unknown intensity coefficients. *IEEE Transactions on Acoustics, Speech, and Signal Processing*, 36(10):1613–1617, October 1988.

- 
- [90] E. T. Whittaker. On the functions which are represented by the expansion of interpolating theory. *Proc. Royal Society of Edinburgh*, 35:181–194, 1915.
- [91] J. M. Whittaker. The Fourier theory of the cardinal functions. *Proc. Mathematical Society of Edinburgh*, 1:169–176, 1929.
- [92] J. L. Yen. On the nonuniform sampling of bandwidth limited signals. *IRE Transactions on Circuit Theory*, 3(4):251–257, December 1956.
- [93] A. I. Zayed. *Advances in Shannon's Sampling Theory*. CRC Press, 1993.